



Preliminary Design of the Northern Breakwater-Quay from the Project: “Reconstruction and Modernization of Fishing Harbor Sarafovo”

MASTER'S THESIS

submitted for the degree of

“MASTER OF SCIENCE”

Master's programme

Infrastructure Planning and Management

submitted by

Stefina Dimitrova

Matriculation number 0927914

under the supervision of

Prof. John Fenton

Ao.Univ.Prof. Dipl.-Ing. Dr.techn. Norbert Krouzecky

Assoc. Prof. Dr. Eng. Ignat Ignatov

Sofia, October 2014



MASTER'S THESIS ASSIGNMENT
of
Stefina Dimitrova
Matriculation number 0927914
Master's programme
Infrastructure Planning and Management

Preliminary Design of the Northern Breakwater-Quay
from the Project: "Reconstruction and Modernization
of Fishing Harbor Sarafovo"

Develop a preliminary design of the northern breakwater-quay from the project:
"Reconstruction and modernization of Fishing Port Sarafovo", including:

1. Calculation of wind wave parameters and their transformation from deep water to the breakwater-quay including refraction and diffraction by using 2 methods
2. Analysis and comparison of the obtained results
3. Construction of the northern breakwater-quay with combined functions composed of an attached rubble-mound breakwater and a steel sheet pile quay wall including detailed drawings of the facility in layout, longitudinal and cross sections, details
4. Stability check of the wave protective structure
5. Technological sequence of operations during construction

A bathymetric map and geodetic survey data are presented in Appendix 1. of the Master's Assignment.

Supervisors:

Prof. John Fenton

Ao.Univ.Prof. Dipl.-Ing. Dr.techn. Norbert Krouzecky

Assoc. Prof. Dr. Eng. Ignat Ignatov

Sofia, October 2011

Table of contents

1	INTRODUCTION	4
1.1	Location of Fishing Harbor Sarafovo and scope of the project for reconstruction and modernization	5
1.1.1	Specifications	8
1.1.2	Navigation conditions	8
2	COASTAL HYDRAULIC PHENOMENA. DEFINITION OF WATER WAVE PARAMETERS	9
2.1	Introduction	9
2.2	Basic definitions and concepts	9
2.3	Classification of waves	10
2.3.1	Classification after wave period	10
2.3.2	Classification according to wave height	11
2.3.3	Classification according to water depth	11
2.3.1	Classification according to wave height, wavelength and water depth	12
2.4	Waves of short period	14
2.5	Waves of long period	19
2.6	Tidal motion	20
2.7	Storm surge	20
2.8	Currents	21
3	STUDY OF WAVE PROPERTIES IN DEEP WATER	23
3.1	Wind properties	23
3.1.1	Wind influence	23
3.1.2	Sources of information	24
3.1.3	Determining the wind properties	25
3.1.4	Wind frequency from the 8 main directions	26
3.1.5	Wind velocity from the 8 main directions	27
3.1.6	Wind duration from the 8 main directions	29
3.2	Wave properties	30
3.2.1	Reference period of meteorological observations for the assessment of wave parameters	31
3.2.2	Wave height monthly distribution in deep water from the 4 main directions	33
3.2.3	Maximum water levels	39
3.3	Wave properties in deep water for E and SE	41
3.4	Transformation of the wave properties with directions E and SE from deep water to depth 35m and 12m using wave modeling software WAM and SWAN [1]	41

3.5	Determining of the wave properties – direction S	44
3.5.1	Wave properties in deep water:	44
3.5.2	Wave properties in shallow water	47
4	NUMERICAL MODELING OF WAVE TRANSFORMATION AND REFRACTION FROM E, SE AND S FROM 35M DEPTH TO THE SURF ZONE	48
4.1	Theoretical basis of the software COPLA-RD	48
4.2	Wave properties in shallow water	50
4.3	Results of the numerical wave modeling	51
4.3.1	Waves from East (E)	52
4.3.2	Waves from Southeast (SE)	61
4.3.3	Waves from South (S)	70
4.4	Analysis of the results obtained through numerical modeling	77
5	CALCULATION OF WAVE TRANSFORMATION AND REFRACTION FROM 12M DEPTH TO THE PROTECTIVE STRUCTURE ACCORDING TO THE "STANDARDS FOR LOADS AND IMPACTS OF HYDRAULIC STRUCTURES BY WAVES, ICE AND VESSELS" [2], VALID PRESENTLY IN BULGARIA	80
5.1	Wave properties at 12m depth	80
5.2	Plan of refraction	80
5.3	Wave properties in the surf zone – determining the critical breaker depth d_{cr}	83
5.3.1	Sequence for calculating the basic wave parameters in the surf zone [2]	83
5.3.2	Performed calculations for the particular project – subject of the Master’s thesis:	85
5.3.3	Results	88
6	DIFFRACTED WAVE HEIGHT EVALUATION IN THE SHADOW REGION	89
6.1	Wave diffraction – directions E and SE	89
6.2	Wave diffraction – direction S	90
6.2.1	Numerical modeling using Copla-RD	90
6.2.2	Graphical calculation using a method given in [6]	90
7	COMPARISON OF THE WAVE PROPERTIES OBTAINED BY APPLYING DIFFERENT METHODS OF CALCULATION	93
7.1	Wave height immediately in front of the harbor	93
7.2	Wave height inside the harbor after diffraction	94
8	CONSTRUCTION OF THE NORTHERN BREAKWATER-QUAY BY RECONSTRUCTING GROUYNE 7	95

8.1	Input data for the reconstruction	95
8.1.1	Topographic conditions	95
8.1.2	Hydrodynamic conditions	95
8.1.3	Geologic conditions	96
8.2	Construction of the northern breakwater-quay	99
8.3	Steel sheet pile wall design	101
8.3.1	Static system, loads and dimensions	101
8.3.2	Steel sheet pile cross sectional properties	103
8.3.3	Results	104
9	STABILITY CHECK OF THE WAVE PROTECTIVE STRUCTURE	110
9.1	Calculating the weight of the armor units on the breakwater slope	110
9.1.1	Armour unit weight in zone 1	110
9.1.2	Armour unit weight in zone 2	111
9.1.3	Armour unit weight in zone 3	112
9.1.4	Results summary	112
9.2	Calculation of the wave run-up on the breakwater slope according to the "Standards for loads and impacts of hydraulic structures by waves, ice and vessels" [2] Section V art. 57	113
9.2.1	Wave run-up height in zone 1	113
9.2.2	Wave run-up height in zone 2	115
9.2.3	Wave run-up height in zone 3	116
9.2.4	Summary of the results	116
10	TECHNOLOGICAL SEQUENCE OF OPERATIONS IN THE CONSTRUCTION OF THE NORTHERN MOLE-QUAY	117
11	LIST OF FIGURES	118
12	LIST OF TABLES	120
13	LIST OF DRAWINGS	122
14	SOURCES OF REFERENCE	123

1 Introduction

Fishing harbor Sarafovo has established itself naturally throughout the last few decades to meet the preferences of fishermen, suitable with its favorable location and the migration of fish resources as an area providing good draught and allowing better organization for fishermen in the area. In the water area north and south of Sarafovo are located nine pound nets, the draught from which is unloaded and sold at Fishing Harbor Sarafovo.

In addition to creating suitable conditions for the berthing and unloading of fishing vessels, first sale tendering and implementation of control and quality assessment of catches, last but not least is the significant social impact on the fishermen community in Bourgas and the region.

The focus of the present Master's thesis lies solely on the northern breakwater – the main wave protective structure of the harbor. Among the main goals of the present thesis is the assessment of the coastal hydraulic phenomena and the resulting impact on the protective harbor structure. The deepwater wave properties are obtained based on the wind data gathered from several meteorological observation stations in the Bourgas Bay region. The wave transformation from deep water to the shore is studied by applying both analytical and numerical approaches. Of great importance for the particular design is the assessment of the wave properties in immediate proximity to the protective structure, as well as the evaluation of the diffracted wave height inside the harbor area.

After analysis and comparison of the obtained results and taking into consideration the topographic and geologic conditions of the site, the design procedure is initiated. The type of the structure is predefined in the assignment – a quay-mole with combined functions composed of an attached rubble-mound breakwater and a steel sheet pile quay wall. The stability check includes armour unit weight calculation and determining of the wave run-up on the breakwater slope. An example of the steel sheet pile dimensioning is also included.

1.1 Location of Fishing Harbor Sarafovo and scope of the project for reconstruction and modernization

Sarafovo is located on the western coast of the Black Sea north of Bourgas – the fourth largest city in Bulgaria (Figure 1).

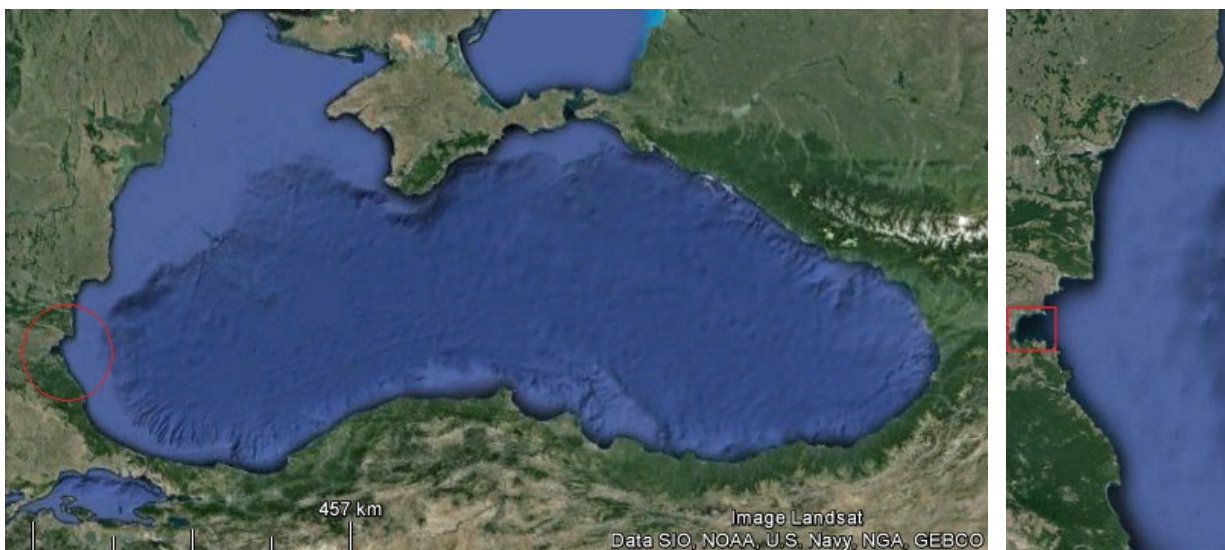


Figure 1: Aerial maps of Black Sea (left) and Bulgarian Black Sea coast (right); Source: Google Maps 4/10/2013



Figure 2: Aerial map of Bourgas Bay; Source: Google Maps 4/10/2013

The Bourgas Bay coastline between Cape Lahna and Bourgas is arch-shaped, concave to the shore and with a segmentation coefficient of 1.22 (Figure 2) [5].

The harbor lies between the two most southern coastal dykes built in 1994 (Figure 3). Their purpose is to control the activity of a cirque-type landslide which is located south of the harbor. The total harbored area is 46 097 m². Depth varies from 0 to 4.50 m.



Figure 3: Location of Fishing Harbor Sarafovo; Source: Google Maps 4/10/2013

The project for reconstruction and modernization of Fishing Harbor Sarafovo includes the reconstruction of groyne 8 into a Southern quay-mole and the reconstruction and elongation of groyne 7 into a Northern quay-mole with a with a bend towards the south of 23°. The present Master's Thesis is focused solely on the design of the Northern quay-mole of the harbor.

The foreseen number of berths in the harbor is 110, divided into 2 zones - with navigation depth (draught) 1.5m for 104 fishing boats with length up to 8m and 3.0m for 6 fishing ships with length up to 20m.

Fishing harbor Sarafovo has established itself naturally throughout the last few decades to meet the preferences of fishermen, suitable with its favorable location and the migration of fish resources as an area providing good draught and allowing better organization for fishermen in the area. In the water area north and south of Sarafovo are located nine pound nets, the catch from which is unloaded and sold at Fishing Harbor Sarafovo [1].

In addition to creating suitable conditions for the berthing and unloading of fishing vessels, first sale tendering and implementation of control and quality assessment of catches, last but not least is the significant social impact on the fishermen community in Bourgas and the region.

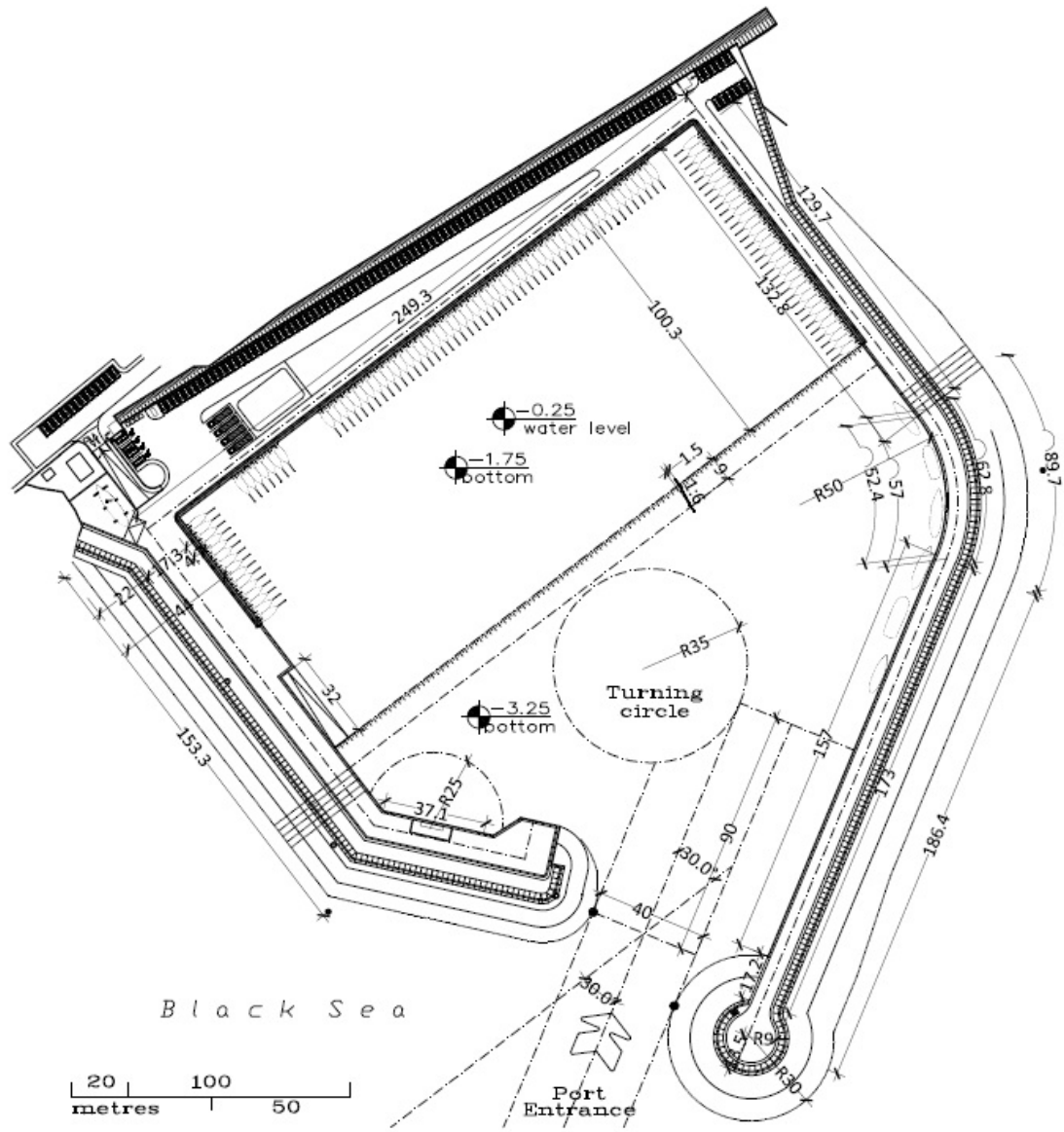


Figure 4: Navigation plan of the harbor

Two areas for catch unloading have been foreseen. In the northwestern part of the harbor, in immediate proximity to the catch sorting and processing, is situated the area for unloading of fishing vessels with length up to 8m. The unloading of fishing ships with length up to 20m is done in the southwestern corner of the harbor next to the bunker zone. An open site for unloading, sorting and first processing of the catch, handling nets and other fishing gear is also foreseen. It is located close to the storage rooms and the first sale area.

Adjacent to the area for catch unloading and sorting, there is a service and office building and a sheltered market for the first sale of the catch (20 tables). Drawing 1 is a detailed drawing of the harbor facilities and zones.

1.1.1 Specifications

Harbored area – 46 097 m²

Facility area (on land) – 19 296 m²

Pier length after reconstruction – 250 m

Breakwaters length:

Southern breakwater – 210 m

Northern breakwater – 400 m

Ratio between territory and water surface area – 1 : 2.39

Ratio between water surface area (m²) and pier length (m) – 184.4:1

Harbor entrance width – 40 m

Navigation depth:

Zone A: depth - 1.50 m

Zone B: depth - 3.00 m

Inner turning circle radius – 35 m

Turning circle radius at tanker area - 25 m

Number of boat stands – 110

1.1.2 Navigation conditions

Harbor entrance

The harbor entrance is the deepest part of the harbor area. Its width has to meet two basic requirements – comfort and safe entry to and exit from the harbor area and minimum diffracted wave height. The harbor entrance width of 40m provides diffracted waves with the smallest height [9]. The angle between the shoreline and the vessel axis entering the harbor should not be too small in order not to be thrown ashore in strong wind. The planned angle is 30° (Figure 4).

Harbor basin dimensions and depth

The dimensions and the depth of the harbor basin determine the terminal capacity of the harbor itself. The harbor basin depth depends on the vessel draught and the necessary safety reserve for sediment deposition, wave height reserve etc. The basin has been divided into two zones according to the water depth. Adjacent to the quay front shoreside the water depth is -1.5m (zone A). At the harbor entrance the water depth is -3.0m (zone B). The greater depth is consistent with the mooring of fishing vessels with a draught up to two meters, while the lesser is suitable for vessel draught from 0.7 up to 1.0m. The so planned depth zones ensure a safety reserve of 1m in order to avoid bottom dredging.

The harbor basin size is determined by the requirements for safe entry, maneuvering in the navigation roadsteads, approaching the quay front and waiting in the internal raids.

The navigation roadstead at the harbor entrance is 50m wide and 80m long. The inner turning circle radius is 35m, while the one at the tanker area has a radius of 25m. The turning circles radii are calculated

based on the maximum design vessel length of 20m for the fishing harbor [31].

2 Coastal hydraulic phenomena. Definition of water wave parameters

2.1 Introduction

In a calm state the water surface depends on the direction of the gravitational forces acting on it. If these forces are uniformly distributed and parallel to one another, the surface is planar. If they are directed to a single point, the surface is spherical. When the equilibrium state is disturbed by an external force, the individual water particles receive oscillations expressed on the surface as visible undulation. This movement of the sea water surface is called wave motion and can be the result of various causes [19]. Some of them are: wind, vessel traffic, water hammer from torrents flowing into the sea and rapid local changes in atmospheric pressure. Other causes for wave generation are: gravitational pull between the Earth and the moon responsible for tide and ebb motion, and underwater tectonic movements (earthquakes, volcanic eruptions and sea bed landslides) whose shock wave spreads radially from the epicenter and hits the nearest shore with great force.

The biggest wave movement of sea water masses with huge force and size, spread over vast areas are generated by wind. The wind wave motion is a source of great dynamic and static load on coastal structures and is one of the main factors affecting sea coast formation.

2.2 Basic definitions and concepts

A periodic surface gravity wave of permanent form propagating over a horizontal bottom (Figure 5) is fully characterized by the:

Wave height – H (h);

Wave length – L (λ)

Average water depth - d - distance from the bottom to the mean water level (MWL).

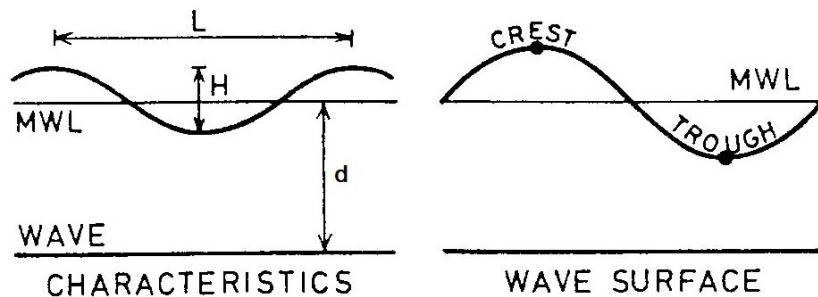


Figure 5: Basic parameters of ocean waves; Source: [34]

The MWL is so defined that the area under the wave *crest* equals that over the wave *trough*. These expressions are also used for the highest and the lowest points of the wave profile (Figure 5). The crest height is the distance from the MWL to the top of the wave (*positive amplitude*). The trough depth represents the *negative wave amplitude*.

The time interval between the passages of two successive crest points at a fixed station is denoted as *wave period* T . At such a fixed station the *phase* or *phase angle* is zero under the crest point; it then increases by 360° during the wave period. Thus the phase of a trough point is 180° .

If wave motion is considered in a horizontal plane, we can distinguish a *wave front* which is a *curve of constant phases* [34].

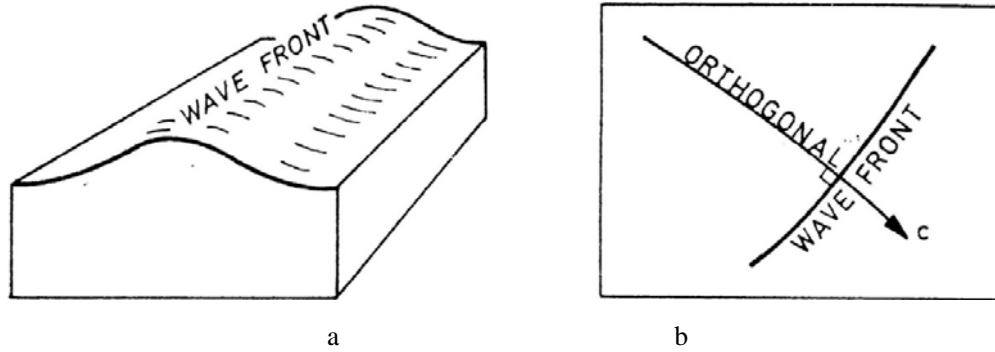


Figure 6: Wave front and wave ray (orthogonal); Source: [34]

Less general but easier to visualize, a wave front is a curve in a horizontal plane through adjacent crest points (Figure 6 a). The direction of wave propagation is described by the *wave rays* (orthogonals) which are orthogonal trajectories of the wave front (Figure 6 b).

The wave front propagates with the *phase velocity C* (wave *celerity*) in the orthogonal direction.

A progressive wave transports energy and momentum, but not necessarily mass. Whether it does or not can only be settled if we look at individual particle motion.

The *wave steepness S* is defined as the ratio between wave height and length, i.e. $S=H/L$.

2.3 Classification of waves

2.3.1 Classification after wave period

The water level fluctuations in the coastal zone can be subdivided into three categories according to their period (Table 1).

Table 1 Wave classification according to their period; Source: [34]

Phenomenon	Cause	Period (time scale)
Wind waves	Shear stress due to wind	< 15 s
Swell	Wind waves	< 30 s
Surf beat	Wave groups	1 to 5 minutes
Seiche	Changes in wind intensity and direction	2 to 40 minutes
Harbor resonance	Tsunami, surf beat	2 to 40 minutes
Tsunami	Earthquake	5 to 60 minutes
Ebb and tide	Gravity force of the Sun and the moon	Ca. 12 and 24 hours
Storm surge	Shear stress due to wind; pressure drop	1 to 30 days

Figure 7 is an illustration of classification by period or frequency given by Kinsman (1965). The figure shows the relative amount of energy contained in ocean waves having a particular frequency.

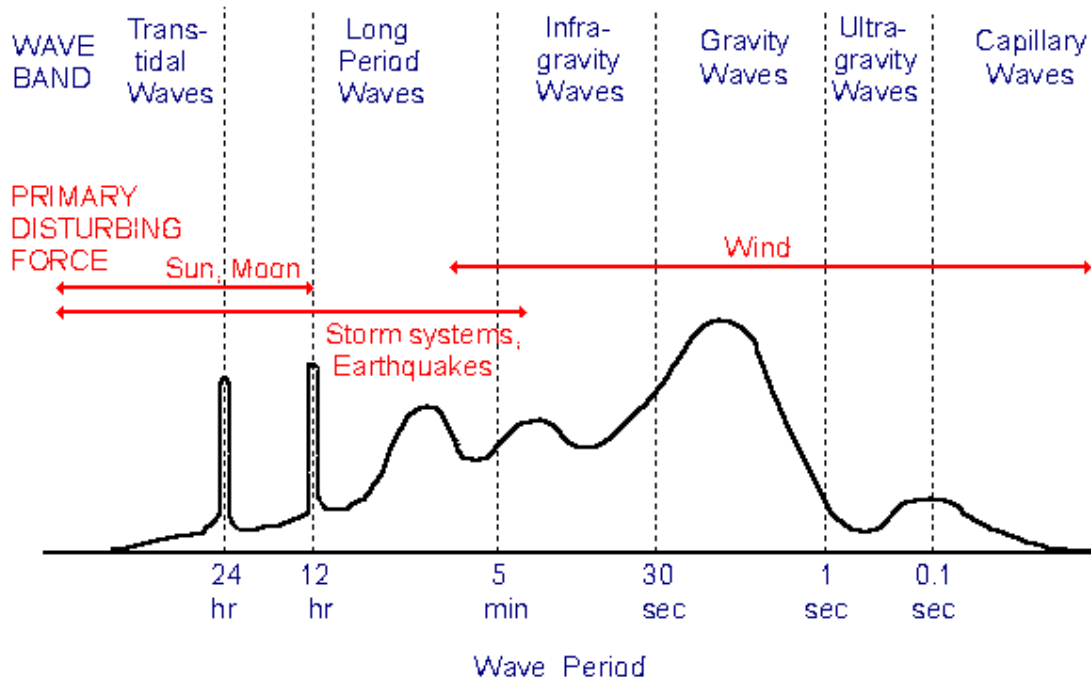


Figure 7: Qualitative wave power spectrum; Source: [33]

2.3.2 Classification according to wave height

If the wave height is infinitesimal, e.g. $H/L \rightarrow 0$ and $H/d \rightarrow 0$, linear wave theory can be used, also referred to as Airy theory or first-order Stokes theory.

Surface gravity waves are non-linear in nature. Very often, the nonlinearity does not manifest itself. However, if it does, these are *waves with finite amplitude* (height). Examples of this type of waves are those described by the second or higher order Stokes theory or cnoidal wave theory. The waves with finite amplitude are not necessarily very high. If the wave height is comparable with the water depth, i.e., $H = 0(d)$, these waves are called *high waves*.

2.3.3 Classification according to water depth

The following definitions are normally used.

Shallow water $d/L < 1/20$

Intermediate depth $1/20 < d/L < 1/2$

Deep water $1/2 < d/L$

Entering more shallow water the wave “starts to *feel*” the bottom when the water depth becomes about one half of the wave length $d < L/2$.

For small waves the particle orbits are *closed curves*. In deep water ($d/L > 1/2$) the particles move in circles, while in shallow water ($d/L < 1/2$), they move in ellipses (Figure 8).

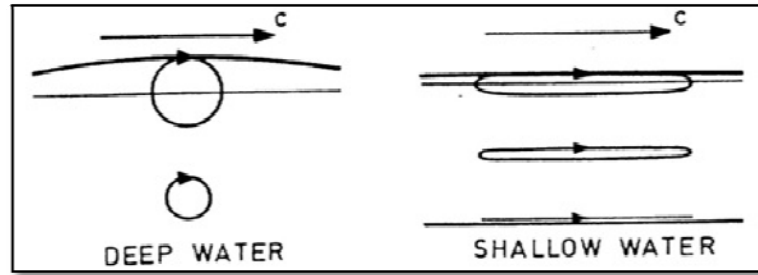


Figure 8: Water particle orbits in deep and in shallow water; Source: [34]

The waves are hereafter slowed, shortened and steepened, as they travel into more shallow water. This process is called *shoaling*. In this area energy dissipation – and so wave height reduction – due to bottom friction becomes important. Internal viscous dissipation is insignificant at any depth, and is therefore also very much smaller than the dissipation in the bottom boundary layer. Percolation losses in a permeable sea are normally of less significance than those caused by the bottom friction.

2.3.1 Classification according to wave height, wavelength and water depth

As long as a wave train propagates over a horizontal sea bed, it can be defined uniquely by three physical dimensions: wave crest-to-trough height H , wavelength L and mean depth d . It is natural to expect that a dimensionless complex exists, which is important in distinguishing between the different wave motion cases. This is the so called “*Ursell parameter*”, sometimes also called “*Stokes parameter*” [35].

$$U = \frac{HL^2}{d^3} \quad (2.1)$$

Various analytical theories exist for describing trains of regular waves. Two main theories are known to describe steady waves. Stokes theory is most suitable for waves that are not very long relative to the water depth, while cnoidal theory is best applicable for the opposite limit where the waves are long [40].

A limitation to the use of both Stokes and cnoidal theories has been that they are not accurate for all waves.

The following assumptions have been made in developing the linear wave theory:

- The fluid is homogeneous and incompressible; therefore, the density ρ is a constant.
- Surface tension can be neglected.
- Coriolis effect due to the earth's rotation can be neglected.
- Pressure at the free surface is uniform and constant.
- The fluid is ideal or inviscid
- The particular wave being considered does not interact with any other water motions. The flow is irrotational so that water particles do not rotate (only normal forces are important and shearing forces are negligible).
- The bed is a horizontal, fixed, impermeable boundary, which implies that the vertical velocity at the bed is zero.
- The wave amplitude is small and the waveform is invariant in time and space.

- Waves are plane or long-crested (two-dimensional).

Long and high waves in shallow water have high values of the Ursell parameter. The boundary between linear and Stokes' higher-order theories at $H/L = 1/25$, chosen for deepwater conditions, has been assumed to apply even in some intermediate water depths, although cnoidal theory replaces both once $HL^2/d^3 > 40$. The upper limit for H/L as a function of U is also shown.

For a highly accurate description of wave properties, it is necessary to resort to a numerical solution of the governing equations. In this case, a Fourier approximation method may be used. Fenton [39] describes this approach, and he compares some results from his presentations of Stokes' and cnoidal theories with the Fourier solutions. In particular, he uses the integral from the sea-bed to the water surface of the wave-induced horizontal fluid velocity under the crest (the instantaneous discharge under the crest in the absence of a current) as the basis for assessing the accuracy of the analytical theories.

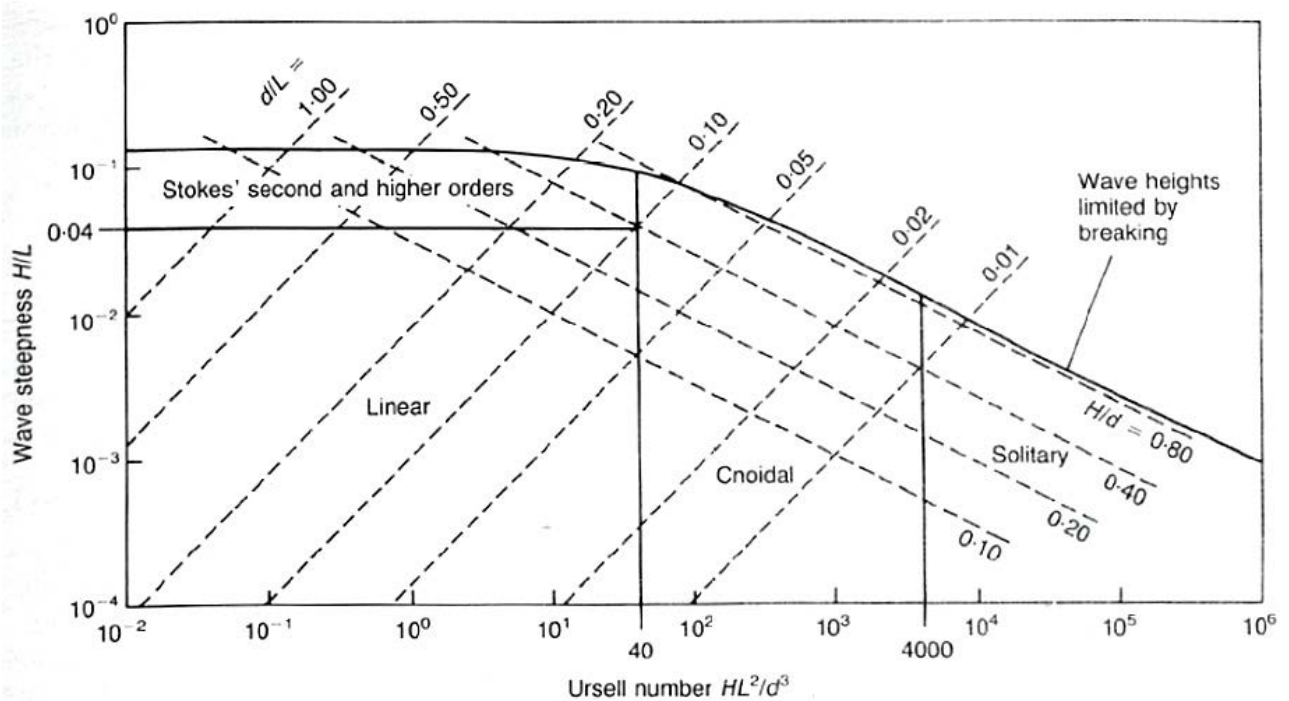


Figure 9: Approximate regions of validity of analytical wave theories; Source: [40]

Figure 10 depicts contours of the errors in the predicted discharges. It can be seen that both Stokes' theory (for short waves) and cnoidal theory (for long waves) are capable of providing results which are generally within about 5% of the more accurate Fourier values. It may also be seen that the proposed demarcation line between Stokes' and cnoidal theories, $U = 40$, is satisfactory, except possibly for the very steepest waves.

It should be noted that Stokes waves and cnoidal waves are not phenomena but are different ways of describing surface waves of constant shape on a horizontal seabed.

In addition to considering the validity of the theories on purely theoretical grounds, it also seems prudent to check them against laboratory measurements. Silvester (1974) has compared some measurements of water-particle velocities (Le mehaute et al., 1968) with the values given by various wave theories. His main conclusion was that linear theory appeared to predict the velocities quite well throughout the whole range of intermediate water depths ($0.5 < d.L < 0.04$). This was in spite of the fact that the wave steepnesses used in the tests were up to $1/16$ and the Ursell number had values up to about

400. Comparisons by Grace (1976, 1978) of measured and predicted sub-surface pressures and velocities also support the view that linear wave theory may satisfactorily predict some wave properties over a wider region than that shown in Figure 9.

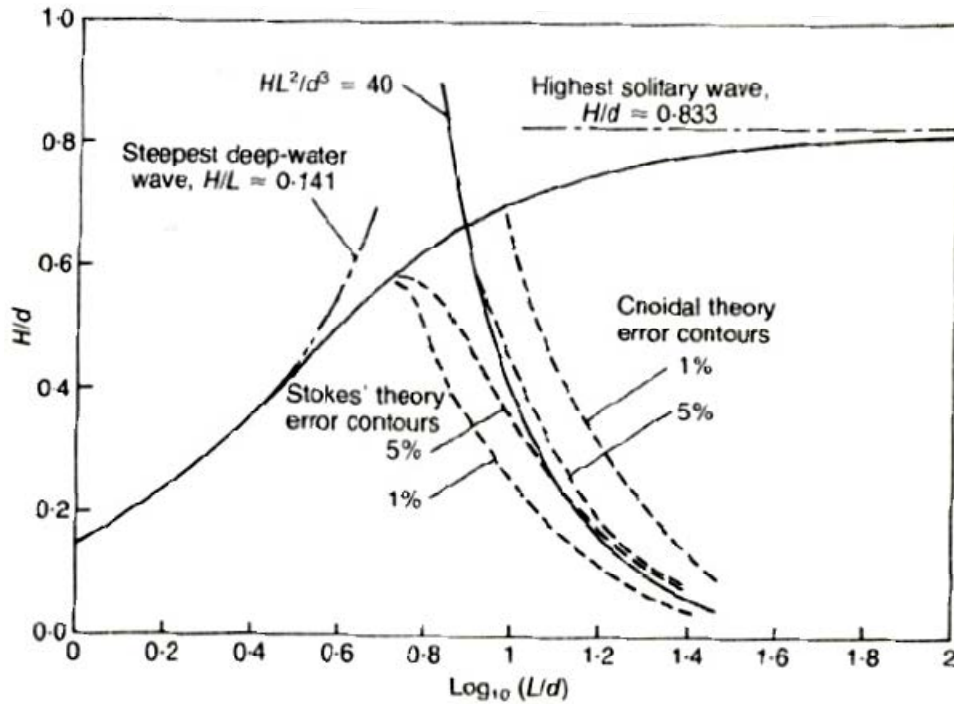


Figure 10: Limits of application of the Stokes and Cnoidal wave theories, together with proposed demarcation line between both theories, adapted from Fenton 1990; Source: T.S. Hedges, 1995 [40]

2.4 Waves of short period

As mentioned before, these are waves with a period shorter than 30 seconds, i.e. these are the so called seas and swell.

In this section we will follow these waves from the moment of their generation to their breaking upon the coastal slope. These waves are defined with the presence of a bottom boundary layer (Figure 11).

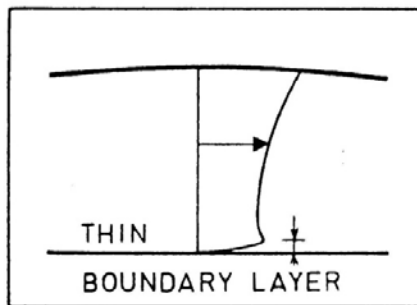


Figure 11: Thin boundary layer scheme; Source: [34]

Wind waves originate offshore when the wind velocity close to the water surface exceeds the critical value of about 1 m/s. At this early stage ripples with length 5-10 cm and a height of 1-2 cm form on the surface. Gradually the waves grow both in height and in length and period up to a certain maximum

value (Figure 12). This value depends on the wind speed, the length of the water surface on which the wind acts, called "fetch" and the water depth.

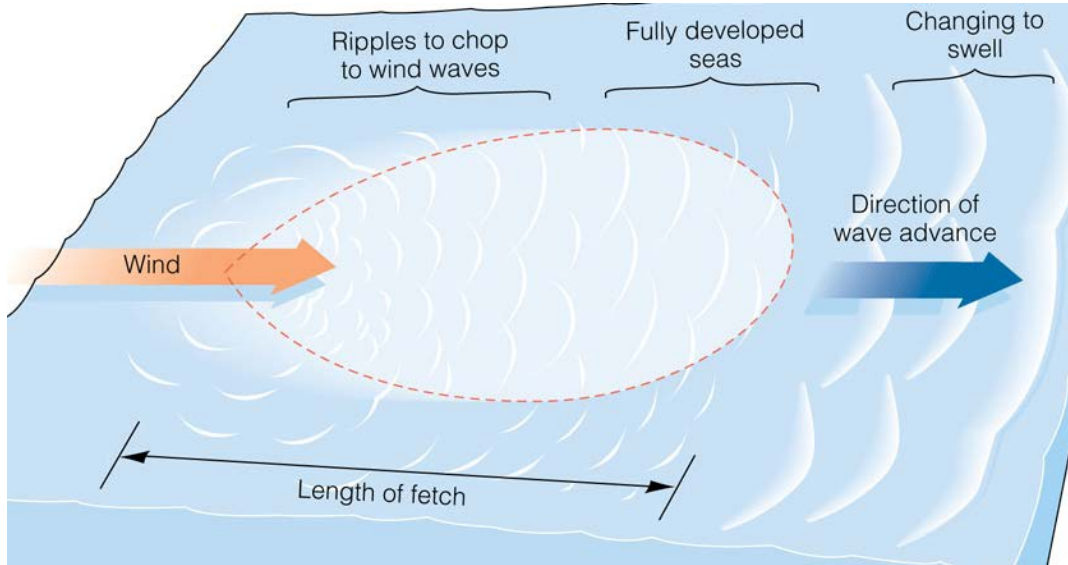


Figure 12: Wind fetch; Source: Brooks/Cole – Thomson (2005)

When the wind blows for a sufficiently long period of time in a given direction, the waves develop into a *fully developed sea*. This process is not deterministic, which means that the height, length, direction and periods of subsequent one after the other waves are not equal. These parameters follow statistical laws. For example, wave heights tend to follow quite well the Rayleigh normal distribution [34].

When the waves leave the area where wind acts, they continue their movement under the action of gravitational forces. This type of waves are called *free waves* or *swell* (Figure 12). They are characterized by more regular and longer periods.

While the waves propagate in deep water, energy dissipation occurs mainly at the expense of the so called "whitecaps", which are obtained by breaking of the wave crest under the effect of the wind.

After entering shallow water, where the depth becomes smaller than a half wavelength, waves begin to "feel the bottom". As a consequence the waves slow down the velocity of their movement, reduce their length and increase their steepness. This process is called *transformation*. In this zone energy dissipation is predominant, thus lowering the wave height as a result of the *bottom friction* (Figure 13).

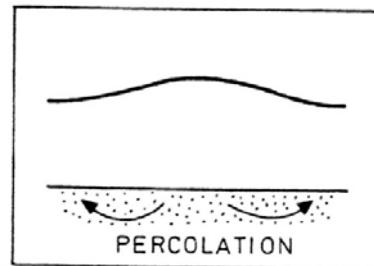


Figure 13: Bottom friction caused by wave action; Source: [34]

The internal damping from the viscous forces is insignificant at any depth, and is significantly less than in the bottom boundary layer, where it is relevant for it to be introduced. In permeable bottom the energy losses also much smaller than the one resulting from bottom friction.

At the instance that the wave front in shallow water meets a bottom contour at an angle, the direction of travel is changed (Figure 14). This process of *refraction* is due to the fact that water waves propagate more slowly in shallower than in deeper water and therefore wave front tends to become aligned with the bottom contours. This is obvious at any beach. Changes of phase velocity can also be caused by currents, resulting in *current refraction*.

Waves are also observed in regions, which are sheltered by breakwaters or similar structures (Figure 15). These disturbances are caused by the bending of incident waves around obstacles into “shadow zone”. This phenomenon is called *diffraction*.

If an obstacle does not dissipate all the energy of the wave, *reflection* takes place (Figure 16). Through porous structures *transmission* of wave energy can be seen (Figure 17)

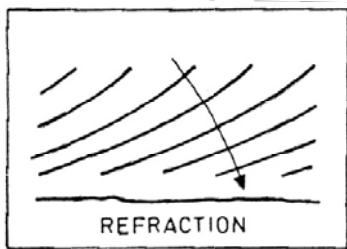


Figure 14: Refraction

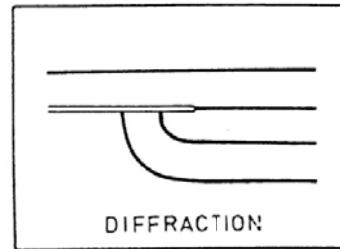


Figure 15: Diffraction

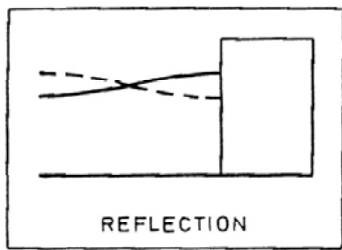


Figure 16: Reflection

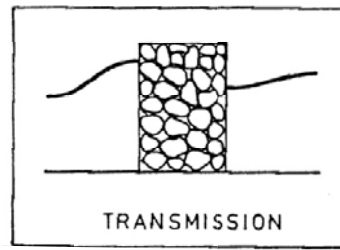


Figure 17: Transmission; Source: [34]

When the water depth becomes progressively shallower, the effect of the bottom slope increases, which eventually leads to a pronounced asymmetry or *deformation* of the wave profile. Before the wave breaks, a slight depression of the mean water level can also be observed (Figure 18).

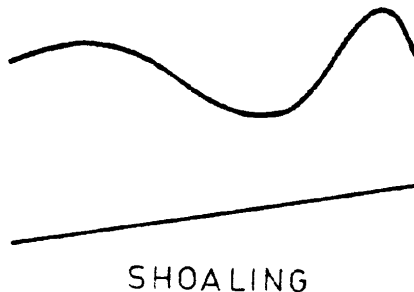


Figure 18: Wave shoaling; Source: [34]

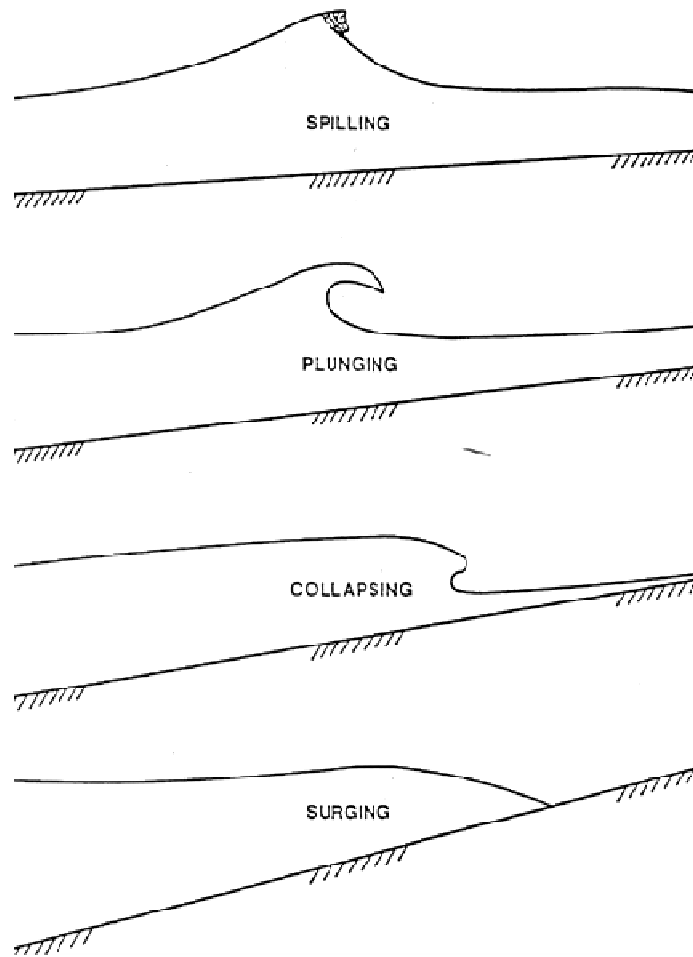


Figure 19: Breaker type classification; Source: [30]

Near shore, where the wave height becomes commensurate with the water depth, the wave is no longer stable and breaking sets in. In the *surf zone*, which is limited between the outmost breaker and the limit of wave uprush, four main types of wave breaking can be found (Figure 19).

Steep waves over flat beaches will end their lives as spilling breakers. This is a gradual type of breaking, which takes place over 6-7 wave lengths. The counterpart of this is the surging breaker, which is the fate of flatter waves on steeper beaches. In the case, the lower part of the wave surges up on the beach face, and there is no real surf zone. On steep slopes reflection can be large.

In between these two types we find the most dramatic breaking phenomenon, plunging, in which the wave curls over and loses considerable amount of energy in one big “splash”. The width of the surf zone is there typically just one wave length. Breaking, although being the most obvious and spectacular of all wave processes, is still only poorly understood [6].

The reduction of wave height through the surf zone causes a rather large rise in the mean water level; this is called *wave set-up*. At the very shoreline the waves *creep* onto the slope of a beach or a dyke, as this event is characterized by the *creep height*. The varying wave height in a wave group (low waves followed by high waves) causes long-period oscillations of the wave set-up, called *surf beat*. Near shore we also find edge waves travelling along the shore, with front normal to the coastline. The height of such a wave decreases rapidly seaward. By the definitions of Table 1 an edge waves can be short- or

long-periodic. The wave and wind induced water level variations determine to a high degree the circulation of water in nearshore areas. If the waves break at an angle to the bottom contours, the momentum of the wave motion generates a longshore current (or littoral current) parallel to the coastline.

Most of the mentioned phenomena do not occur separately in nature, but manifest as a result of their combination. Modeling and analysis of isolated processes is only possible in hydraulic laboratories. The complex situation which can be met in a nearshore region is sketched in Figure 20, while Figure 21 illustrates diffraction and reflection of waves at the entrance and in the harbor of Port of Bourgas.

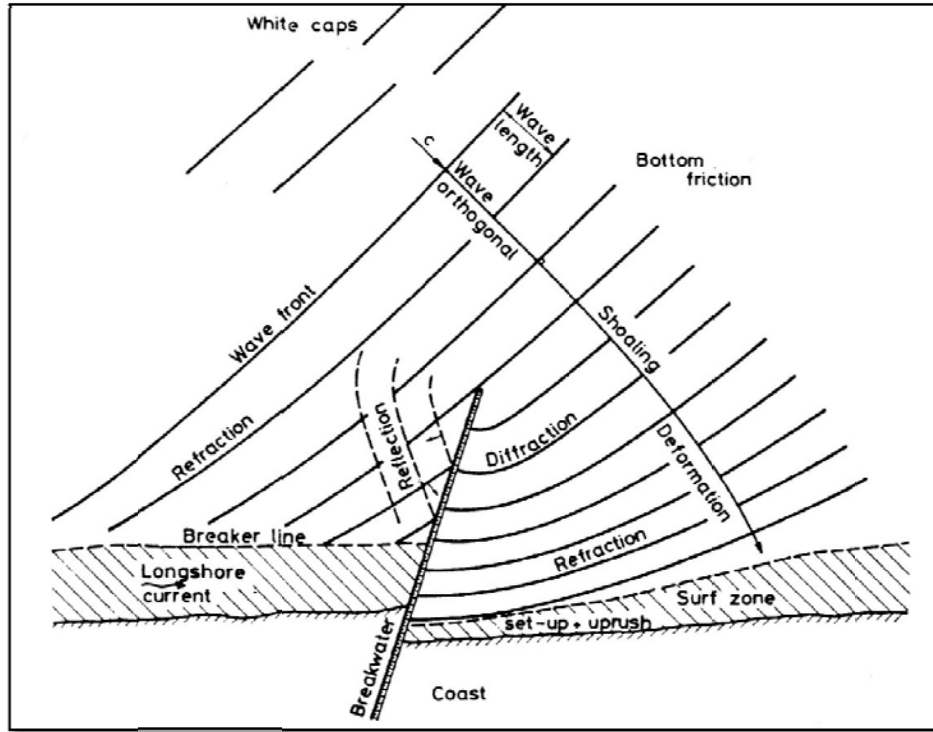


Figure 20: Shoaling, refraction, diffraction and reflection of waves in a nearshore region; Source: [34]



Figure 21: Aerial photo of Port of Bourgas; Source: Google Earth 06/15/2012

2.5 Waves of long period

Waves with a period of 30 s to several hours are too lengthy to be perceived as periodic events by a casual observer. Their length varies, typically from several kilometers in the coastal zone to more than 100 km in the oceans and their height is not more than a few decimeters in oceans as well as in the coastal zone.

Exceptions are tsunami waves which are caused by seismic activity under the seabed. These waves can cross oceans and seas without being noticed. In certain regions the topographic conditions are such that shoaling, refraction and reflection transform the initial small in one with a considerable height and destructive force. This is particularly true for the Asia Pacific coast, where seismic activity is very intense. For example, on the shores of Japan, Hawaii and the Russian Far East were observed seismic waves with a height of more than 10 m, which have caused thousands of deaths in the past. The average frequency of their occurrence is approximately 10 years.

Tectonic waves (tsunami) in the Black Sea are observed very rarely, the most vivid example is the earthquake of 1901 with an epicenter east of Cape Kaliakra (Figure 22) and 7.2 magnitude on the Richter scale. The 4 m high tsunami had a devastating effect on the northern Bulgarian coast as separate sandbanks were shifted by the wave motion. Destructive waves of seismic origin, the height of which

reached 4 meters along the coasts of the Caucasus, the Crimean Peninsula and Bulgaria in 20, 101, 543 and 1427 AD are mentioned in legends and historical records [27].



Figure 22: Kaliakra Cape; Source: inews.bg, author: Zdravko Doychev

Another example of long-period waves is the *wave resonance in harbor areas*, which is forced oscillations of water in closed basins. The generating wave (for instance tsunami) usually has a small height (1 dm) which is continuously amplified by the resonance mechanism. The velocities and accelerations resulting from these fluctuations can often be dangerous for the vessels bound in that area.

Water levels in closed basins such as lakes can oscillate with periods coinciding with those of their own fluctuations. This phenomenon can be caused by a rapid change of the wind climate, but mostly they are free oscillations called *seiches* [10].

2.6 Tidal motion

Tides and ebbs are a result from gravitational and centrifugal forces upon rotation of the moon around the earth and the earth around the sun. This movement of water in the oceans is transformed and amplified by the bottom topography and the local resonance effects in bays and estuaries, and mostly by the Coriolis acceleration. Due to the fact that the main driving forces are periodic with two components with periods respectively 12 and 24 hours, the tides are with the same period and can be regarded as a long periodic wave motion. The wavelength with a period of 12 hours is ca. 8000 km, and even in the North Sea, which has a depth of merely 100 m, the wave length reaches 1000 km. In the open ocean the height of the tidal wave is only a few decimeters. Large tidal heights observed in some locations are the result of amplification due to the local topography and Coriolis acceleration. In small enclosed seas such as the Black Sea this phenomenon barely occurs because the ocean tides hardly penetrate them. In some funnel-shaped bays due to the narrowing and the depth reduction tidal waves can grow in height exceeding 10 m. Examples of this are certain bays along the French coast near the English Channel and the Bristol Channel in Western England, where the height of the tidal wave reaches 14 m and spreads in the nearby Severn river in the form of tidal bore. The highest tidal wave in the world is the Fundy Bay, Nova Scotia, Canada [36].

2.7 Storm surge

Storm surge occurs as a result of wind action (wind surge) and the decrease in atmospheric pressure in storm conditions. Wind surge is caused by shear stress created by the wind on the water surface, which

is sometimes intensified by the dynamic effects of rapidly changing wind direction and velocity when crossing the center of the cyclone. Extreme values of storm surge usually last no longer than a few hours, but if they coincide with high tide, they can cause extremely devastating floods. Wind surge values grow with decrease of depth, i.e. on steep underwater slope this phenomenon is barely observed.

Storm surge, like tides, is a large-scale movement of water masses in shallow water. Both phenomena are described by the same equations. For the conditions of the Bourgas Bay storm surge can reach maximum values of 70-80 cm [22].

2.8 Currents

The currents in the sea can be classified in a variety of ways. One way is to distinguish between currents related to short-period waves, tidal currents, currents related to wind action of relatively short duration, and major ocean currents (Wiegel 1964) [36]. These last large scale flows are associated with long duration winds ('climatic').

When short-period waves approach the coast, refraction tends to align the wave fronts with the underlying bottom contours. However, the waves will normally break at an angle with the coast, and the momentum of the breaking wave in connection with the mass transport of the waves will then generate a current parallel to the shoreline. This is called a *long-shore current* (or a littoral current), and it is responsible for the development of many sandy coasts, since it transports that sediment along the coast which is brought into suspension by the particle motion near the seabed in the surf zone. Figure 23 shows the main features of this nearshore phenomenon.

A pure longshore current does not constitute a stable system, however, and at intervals along the coast water returns seawards in the form of strong narrow currents denoted rip currents (Figure 23). These are easily seen from the air, but can be difficult to detect from land. According to Wiegel (1964), "A ground observer usually can distinguish a rip by a stretch of relatively unbroken water in the breaker line and patches of foam and discolored water offshore".

Rip currents are the greatest cause of drowning for inexperienced swimmers [38]. They also occur for normal wave incidence on the beach, i.e. without refraction. The water area between two subsequent rips is termed a *nearshore circulation cell*. The spacing between rip currents is usually two to eight times the width of the surf zone. Longshore currents may attain velocities in excess of 2.5 m/s, while rip current velocities in excess of 1.5 m/s have been measured. The strength of a rip current can be increased by the return flow of water piled up by an onshore wind.

In the surf zone, measurements have indicated a seaward flow near the bottom of a sloping beach, *undertow*, exceeding 0.4 meters per second [38].

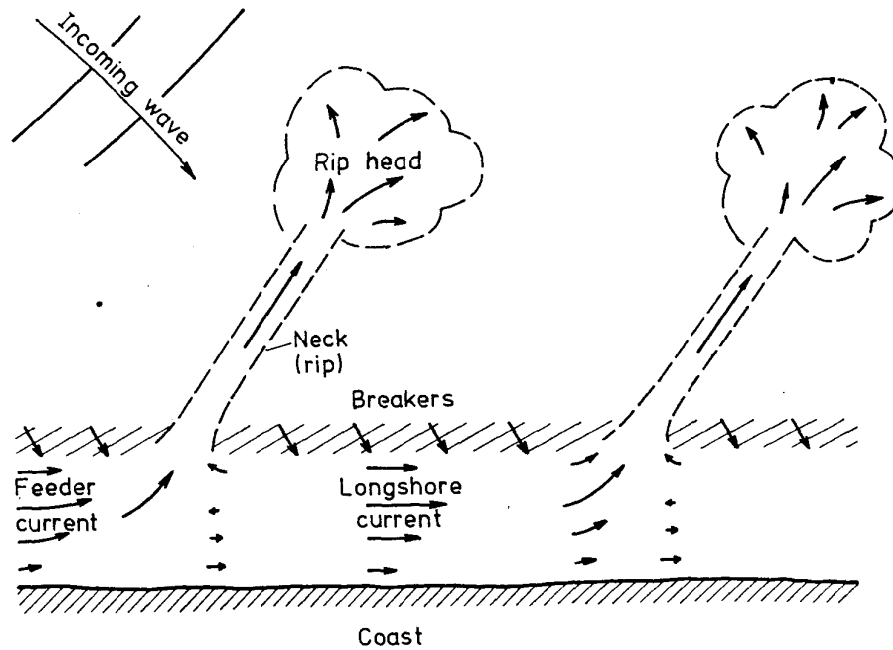


Figure 23: Rip currents; Source: [34]

Another wave induced current motion, which also exists over a horizontal bed, however, is the so-called *wave-induced current*. In a pure wave motion (zero net mass transport) water particles will be transported in the direction of wave travel in the upper layers, with a return flow below. This is a second order effect, and so increases rapidly with wave height. A tidal current distinguishes itself from the just described short-period phenomena, in that it actually is the particle motion itself in a tidal wave. In coastal waters such a flow has all the features of a quasi-steady turbulent flow.

The cause of the *wind drift* current lies in the name. In deep water this is a pure surface process which penetrates downwards because of turbulent mixing. In shallow open regions the effect of the wind is to 'drag' the fluid with it, so that a 'one-way' velocity profile develops over the whole depth of water. In more or less confined areas, the effect of the boundaries on mass conservation can result in a return flow in the lower parts of the water. In such areas, the return flow can also take place through possible deep regions.

Indirectly the wind can generate strong currents in narrow straits, if these connect basins the surfaces of which are 'tilted' because of the wind, giving a wind set-up at one end of the strait, and a set-down at the other. Also an inflow of water into one of the basins, due to a storm surge, will give this effect.

The currents described in this section seldom — if ever — occur alone. For this reason field measurements of currents are not easy to analyse.

3 Study of wave properties in deep water

3.1 Wind properties

The design and construction of marine and coastal structures requires a significant volume of research related to wave phenomena, which in turn are directly dependent on wind conditions at open sea, as well as in the particular area, in this case – the northern part of Bourgas Bay. The specific coast outline and the absence of wind measurements at high seas impose wind properties to be developed for the conditions of the coastal stations. The primary source of information for the wind conditions is the 1982 reference book published by the National Institute of Meteorology and Hydrology at Bulgarian Academy of Sciences – volume IV – Wind [7]. In this reference book the wind properties are developed based on data for the period 1931 – 1970. The published work proves that the study results for the mentioned period do not differ significantly from these for a 20-year period within the 40-year period.

3.1.1 Wind influence

Bourgas Bay lies predominantly under the influence of the atmospheric transport which is distinctive for the moderate European climate zone. Along with this, tropical air transfer from lower latitudes is observed, while during the cold half-year cold air is transported from higher latitudes. Consequently, a moderate climate with two atmospheric circulation influences is formed: European continental influence from NW and NE and Mediterranean influence from SW. The penetration of Arctic air masses during the winter months is distinguished by a high frequency, strong intensity and severe frosts.

Air mass transport to temperate latitudes is observed throughout the whole year. Usually warm continental air masses enter temperate latitudes during the warm months and their formation is associated with the transformation and warming of cold air under the influence of solar radiation. Air masses at moderate latitude with ocean origin are relatively warm at winter, while in the summer they are perceived as cold.

Warm air masses at moderate latitude (oceanic and continental) push indirectly through the Mediterranean basin or directly in the rear parts of polar-front cyclones. When the rush is indirect, the air masses transformed over the Mediterranean Sea are perceived as warm during the cold half-year, causing rainfall and warm spell. The rushing of those air masses during summer is associated with their rapid overheating, imparting them typically continental features.

Penetration of cold air currents with ocean origin is observed predominantly from NW and less frequently from SW and NE. Usually rushes from SW are accompanied by violent weather phenomena, torrential rainfall and short-term warm spells. The penetration of cold ocean air masses from NE into temperate latitudes causes significant rainfall.

Tropical air mass transport, though observed throughout the year, is far more uncommon than the air mass transport from temperate latitudes, thus keeping its climatic significance minor. Tropical air currents transported to this area have both ocean and continental origin. In most cases they rush in from the Mediterranean. Their formation happens in the Atlantic Ocean and within the boundaries of Northern Africa and Anatolia (Asia Minor). Having received the reflection of the covering surfaces in these areas, the so formed tropical air masses pass over the Mediterranean Sea and head towards the Bourgas Bay. During the summer months continental tropical air currents push in from NE and E. These currents originate from central Asia and in rare cases from the southern part of Eastern Europe, as with the overheating of local air masses they are significantly transformed.

Air mass transport depends primarily on the directions in which cyclones and anticyclones move. Their diverse activity in Europe and the complex interactions between them are a prerequisite for significant differentiation of the paths, directions and character of air masses. The Atlantic area near the southwest of Iceland is a constant source of cyclone generation, while seasonal genesis of cyclones is observed over the western part of the Mediterranean. The region of the Azores is a source of anticyclone generation all year round. Moreover, other regions where anticyclones originate have a seasonal baric display - Eastern Europe, Scandinavia and a significant part of Asia - Siberia. Mediterranean cyclones and east European anticyclones occur mainly during the cold half. In Bourgas the solar irradiance is 560 J/cm^2 per year. The average annual sunlight duration is 2239 hours [7].

3.1.2 Sources of information



Figure 24: Meteorological observation stations in the Bourgas Bay region; Source Google Maps 4/10/2013

The sources of information used are the 1982 reference book published by the National Institute of Meteorology and Hydrology at Bulgarian Academy of Sciences – volume IV – Wind [7], additional data from wind studies conducted in relation to other facilities near Sarafovo [13], as well as data from meteorological observations at the stations Emine, Obzor, Pomorie, Burgas and Sozopol, the location of which is shown in the aerial photo on Figure 24. The selection of those stations is based on both the analysis of the available data and the ability to draw parallels between these station based on previous research. The location of the stations covers adequately the area of examination - the large Bourgas Bay.

3.1.3 Determining the wind properties

For the determination of the wind properties the following sequence of structuring and processing the data was used:

For each station and for each of the 8 main wind directions two time series (samples) are formed, respectively from the maximum wind speed and from the number of cases of wind speed greater than 5 m/s. These samples can be conditionally labeled as type A;

For station Burgas two additional samples are prepared, which have contain the wind speed for each of the eight directions and the observed wind duration. These samples were developed only for the observations outside the time series and for wind speeds greater than 14 m/s, which corresponds to the objective conditions for wind data collecting. These samples can be conditionally labeled as samples type B;

For samples type A the wind rose is calculated by relative frequency and for 100% is adopted the overall number of cases with wind speed greater than 5 m/s, which for the individual stations are as follows:

- Emine - 11696 cases;
- Burgas - 7148 cases;
- Sozopol - 7326 cases.

From the given number of cases it follows, that at Emine station, in 53.38% of the maximum possible 21912 cases, a wind speed greater than 5 m/s was observed, while at Bourgas it is in 32.62 % of the cases, and in Sozopol - 33.43 %. This goes to show that the wind activity at Emine is approximately 20 % greater than in Burgas and Sozopol. Probably the main reason for this is the configuration of the coastline and the terrain, as well as the specifics of atmospheric circulation. For all samples of type A the probability of exceedance curves for the annual maximum wind speed are calculated with the help of the following statistical methods:

- the empirical probability of exceedance is calculated using a Weibull distribution, which has certain advantages to Alekseev's formula when studying extreme events and processes, since the latter requires centeredness of the sample with respect to the total. This advantage also applies when studying the distribution curves where more than 1 annual maximum is included in the sample [1];
- approximations to the empirical distribution are analyzed using the following theoretical density of probability distribution curves: two-parameter gamma distribution, generalized gamma distribution, Pearson type III distribution, log Pearson type III distribution, Weibull distribution and log-normal distribution. The Cramér–von Mises criterion is used to judge the goodness of fit in choosing the most suitable distribution curve type. The distribution curve parameters are determined in compliance with the available solutions from the moment methods, the maximum likelihood and the conditional maximum likelihood. In fact, 6 to 12 probability of exceedance curves are computed for each station and

wind direction and 1 of them is chosen for each wind direction. It is important to note that for the Sozopol station a data replenishment is conducted for the annual maximum wind speed by means of regression analysis using the Bourgas station data, as well as extrapolation of the theoretical curves for Sozopol, computed for wind velocity lower than 20m/s and other methods. As end results can be adopted those values, which comply to dependencies with the smallest statistical imprecision.

- for samples type B (8 samples) were determined the average, maximum and minimum wind duration for the station in Bourgas. Analyses were also conducted to establish a correlation between wind velocity and wind duration for the separate wind directions, but there have not been established reliable statistical dependencies and therefore they are not applicable. The following tendency should be noted – with increase of the wind velocity, the wind duration decreases.

Table 2 Mean monthly and annual wind velocity [m/s]; Source: [7]

Station / Month	I	II	III	IV	V	VI	VII	VIII	IX	X	XI	XII	Year
Obzor	5.2	4.8	4.5	3.9	4.0	3.8	4.2	4.4	4.7	5.3	4.8	5.3	4.6
Nessebar	3.7	3.0	3.1	2.2	2.0	2.2	2.1	2.3	2.7	3.1	3.4	3.4	2.7
Pomorie	4.5	4.6	4.5	4.1	3.9	3.7	3.8	3.7	4.0	4.1	4.1	4.1	4.1
Bourgas	3.0	3.5	4.4	3.6	3.3	3.1	3.3	3.7	3.9	3.5	3.3	2.9	3.4
Sozopol	3.7	3.4	3.2	2.0	1.7	1.9	2.0	2.2	2.7	2.9	3.3	3.5	3.7

Table 3 Mean monthly and annual wind velocity [m/s] by direction for station Pomorie [15]

Direction / Month	I	II	III	IV	V	VI	VII	VIII	IX	X	XI	XII
N	6.5	6.4	6.0	4.8	4.7	4.6	4.8	4.3	4.9	5.0	5.5	6.0
NE	5.1	4.6	5.7	4.9	5.4	4.3	4.5	4.7	4.8	5.5	5.8	5.1
E	4.4	4.3	4.2	4.4	4.5	4.3	4.2	4.3	4.5	4.1	5.1	4.2
SE	4.4	3.7	4.2	4.7	4.5	4.1	4.6	4.2	4.2	3.8	4.3	5.7
S	4.5	6.1	4.5	3.9	3.8	4.6	3.3	3.2	3.5	4.3	4.6	6.6
SW	4.5	4.7	4.3	4.6	3.9	3.6	3.7	3.8	3.6	4.5	3.8	3.9
W	4.3	5.0	4.2	4.6	4.1	4.2	3.8	3.8	4.5	3.8	3.4	3.9
NW	4.7	4.9	5.9	4.2	3.6	3.8	4.5	4.4	4.0	4.7	4.1	4.0

3.1.4 Wind frequency from the 8 main directions

Table 4 Relative wind frequency [%] by velocity gradient for station Pomorie [15]

Wind velocity [m/s]	I	II	III	IV	V	VI	VII	VIII	IX	X	XI	XII	Year
0-1	20.8	21.4	18.3	19.3	18.6	18.3	19.5	21.7	18.5	21.7	19.4	20.3	19.8
2.0-5.0	57	54.9	59.3	63.7	66.4	69.8	67.7	65.6	66.1	60.5	63.1	63.1	63.2
6.0-9.0	14.2	15.5	15	13.3	12.4	10.6	11.5	11.1	12.6	14.3	12.6	11.6	12.8
10.0-13.0	4.8	5.6	5.1	2.8	1.8	1.1	1	1.4	2.2	2.5	3.3	3.5	2.9
14-17	1.7	1.6	1.9	0.8	0.6	0.1	0.2	0.2	0.4	0.7	0.8	1.9	0.9
18-20	0.6	0.6	0.3	0.1	0.2		0.1	0.1	0.2	0.2	0.6	0.4	0.3
>20	0.8	0.6	0.1			0.1	0.1			0.2	0.2	0.2	0.2

Data regarding the relative wind frequency by direction and speed gradient - $V > 5 \text{ m/s}$ for stations Emine, Bourgas and Sozopol are presented in the following tables.

Table 5 Relative frequency [%] for wind with $V > 5 \text{ m/s}$ for station Emine [20]

V [m/s]	N	NE	E	SE	S	SW	W	NW	Frequency by velocity
5 - 10	18.78	8.56	1.50	1.48	4.03	8.41	11.11	4.77	58.66
10 - 15	17.07	5.44	0.38	0.32	1.76	2.91	4.79	2.60	35.27
15 - 20	1.62	0.70	0.06	0.00	0.11	0.17	0.12	0.12	2.90
> 20	1.91	0.62	0.06	0.10	0.13	0.10	0.10	0.15	3.17
Frequency by direction	39.38	15.34	2.00	1.90	6.03	11.59	16.12	7.64	100.00

Table 6 Relative frequency [%] for wind with $V > 5 \text{ m/s}$ for station Bourgas [18]

V [m/s]	N	NE	E	SE	S	SW	W	NW	Frequency by velocity
5 - 10	9.81	18.44	23.91	2.06	0.99	5.36	5.81	5.97	72.35
10 - 15	4.66	10.98	7.29	0.28	0.29	0.67	0.41	0.62	25.20
15 - 20	0.39	0.69	0.08	0.00	0.08	0.10	0.00	0.01	1.35
> 20	0.26	0.64	0.08	0.00	0.07	0.04	0.00	0.00	1.09
Frequency by direction	15.12	30.75	31.36	2.34	1.44	6.17	6.22	6.60	100.00

Table 7 Relative frequency [%] for wind with $V > 5 \text{ m/s}$ for station Sozopol [21]

V [m/s]	N	NE	E	SE	S	SW	W	NW	Frequency by velocity
5 - 10	15.00	16.58	12.94	5.58	1.95	2.73	5.92	14.66	75.36
10 - 15	5.54	3.38	0.97	0.70	0.52	0.49	0.22	1.66	13.48
15 - 20	1.50	1.00	0.41	0.12	0.10	0.05	0.03	0.25	3.46
> 20	3.68	1.66	0.11	0.18	0.45	0.85	0.04	0.73	7.70
Frequency by direction	25.72	22.62	14.43	6.58	3.02	4.12	6.21	17.30	100.00

3.1.5 Wind velocity from the 8 main directions

The wind velocity V [m/s] from the 8 main directions is studied by the method described above. Results from the study such as probability of exceedance and recurrence are presented in the tables below. For hydraulic or numerical modeling of wave processes in large Bourgas Bay it is recommended to use the wind data as follows: Station Emine for wave motion from NE, Bourgas for waves of E and Sozopol for SE waves [11].

Table 8 Maximum wind velocity [m/s] of different probability of exceedance – station Emine; Source: [7]

Probability of exceedance p [%]	Recurrence once every ... years	Direction							
		N	NE	E	SE	S	SW	W	NW
		Wind velocity [m/s]							
1.0	100	40.5	35.1	28.8	23.5	27.2	25.3	23.9	29.1
2.0	50	37.7	33.3	25.1	21.8	25.7	24.6	22.8	27.7
5.0	20	33.9	30.8	20.8	19.5	23.6	23.6	21.2	25.8
10.0	10	31.0	28.8	17.8	17.7	21.9	22.7	19.9	24.2
20.0	5	28.0	26.7	15.1	15.7	19.9	21.5	18.4	22.4
50.0	2	23.7	23.5	11.5	12.5	16.4	19.1	15.9	19.1
80.0	1.25	21.1	21.1	9.3	10.1	13.3	16.3	13.9	16.1
90.0	1.11	20.3	20.2	8.5	9.1	11.9	14.7	12.9	14.7

Table 9 Maximum wind velocity [m/s] of different probability of exceedance – station Bourgas; Source: [7]

Probability of exceedance p [%]	Recurrence once every ... years	Direction							
		N	NE	E	SE	S	SW	W	NW
		Wind velocity [m/s]							
1.0	100	29.0	39.5	35.1	15.9	31.2	29.2	14.4	18.2
2.0	50	27.7	35.3	30.8	15.1	28.7	26.9	13.9	17.1
5.0	20	25.6	30.3	25.1	13.8	25.2	23.7	13.3	15.7
10.0	10	23.9	26.8	21.4	12.8	22.3	21.1	12.7	14.5
20.0	5	22.0	23.4	18.1	11.6	19.1	18.2	12.0	13.3
50.0	2	18.7	18.7	14.3	9.6	13.9	13.3	10.4	11.3
80.0	1.25	15.7	15.6	12.1	7.8	9.7	9.5	8.6	9.7
90.0	1.11	14.3	14.3	11.3	6.9	7.9	7.8	7.6	9.1

Table 10 Maximum wind velocity [m/s] of different probability of exceedance – station Sozopol; Source: [7]

Probability of exceedance p [%]	Recurrence once every ... years	Direction							
		N	NE	E	SE	S	SW	W	NW
		Wind velocity [m/s]							
1.0	100	28.9	33.6	28.8	34.3	33.7	32.9	24.0	34.2
2.0	50	27.8	31.9	26.4	31.1	31.8	31.0	22.2	31.8
5.0	20	26.3	29.5	23.2	26.8	28.8	28.2	21.5	28.4
10.0	10	24.9	27.5	20.6	23.3	26.2	25.6	17.7	25.6
20.0	5	23.3	25.2	18.0	19.6	23.0	22.4	15.4	22.5
50.0	2	20.5	21.2	14.0	14.0	17.1	16.6	11.5	17.2
80.0	1.25	18.0	17.9	11.5	10.0	11.6	11.6	8.4	12.8
90.0	1.11	16.7	16.4	10.6	8.5	9.0	9.3	7.1	10.9

Table 11 Maximum wind velocity [m/s] from all directions of different probability of exceedance – station Pomorie; Source: [7]

	Recurrence once every ... years							
	1	5	10	15	20	25	50	100
p [%]	100	20	10	6.7	5	4	2	1
V [m/s]	23	29	30	32	34	35	37	40

Table 12 Frequency of the prevailing wind (% of the number of cases with wind) by direction - station Pomorie; Source: [7]

	I	II	III	IV	V	VI	VII	VIII	IX	X	XI	XII	Ann.
Direction	NW32	N3	N20	NE13	NE21	NE11	NE7	NE18	N34	N22	N5	NW30	N24
Frequency [%]	49	47.2	49.3	49.8	44.4	43.2	46.4	49.8	53.6	52.8	43.1	45.2	43.1

Note: "NW32" signifies 32 degrees clockwise from the NW direction.

The results obtained were compared to the probability of exceedance curves for the maximum wind speed published by P. Ivanov. In the probability of exceedance range of 1 to 10% of the maximum wind speed determined by the unconditional probability curves by direction shown in Table 9 (for Burgas) and the unconditional probability curve for the maximum wind speed published by P. Ivanov good compliance is observed:

Table 13 Comparison of the study results with probability of exceedance curves for V_{max} published by P. Ivanov

Probability of exceedance p [%]	1	2	5	10	50	90
Climate reference book 1982	45.0	42.0	39.0	34.0	29.0	27.0
P. Ivanov (1095 cases per year)	40.9	38.4	35.1	32.6	26.9	24.8
P. Ivanov (375 cases per year)	37.0	34.5	31.2	28.8	23.0	20.9
Present study	39.5	35.3	30.3	26.8	18.7	14.3

There are significant differences between the maximum wind velocity assessments in the range of greater probability of exceedance. Such disparities are due to differences between the methods used, as well as to insufficient knowledge of the phenomenon. It should be taken into account that the Beaufort scale for wind velocities greater than 20-23m / s describes such damage that is not observed in the Bourgas region every year.

3.1.6 Wind duration from the 8 main directions

The studies reveal that there is no reliable statistical relationship between wind speed and wind duration according to the data from station Bourgas. Characteristics for the duration of the strong winds are given in Table 14.

Due to the fact that no qualitative observations on the wind duration are conducted for the other stations, Table 14 is used for determining the wave height in the Bourgas Bay. This data can be used for determining the parameters of developed wind waves in deep water.

Table 14 Duration of the strong winds for station Burgas; Source: [7]

Direction	Frequency [%]	Duration [h]			$V_{\max 2\%}$ [m/s]
		min	av.	max	
N	15.12	0.15	3.50	12.17	28
NE	30.75	0.15	3.95	15.42	36
E	31.36	0.1	3.92	22.75	31
SE	2.34	0.33	2.66	6.67	16
S	1.44	0.15	4.00	8.83	29
SW	6.17	0.15	3.25	12.95	27
W	6.22	0.10	3.00	13.42	15
NW	6.60	0.25	2.00	4.67	18

Conclusions:

From the wind analysis performed for the large Bourgas Bay the following important conclusions can be drawn:

- For the region considered the prevailing wind directions are N, NE and E.
- The maximum wind velocity for deep water with recurrence once every 50 years for N and NE directions can be determined from the data for station Emine, for E – from station Burgas and for SE from station Sozopol.
- The maximum wind velocity for wave motion generated by local wind in the bay for S and SE directions is to be determined from the data for station Bourgas.
- With the exception of direction SE, the local wind duration in the Bourgas Bay is probable and sufficient for the formation of developed wind waves.

3.2 Wave properties

When designing coastal hydraulic structures, the assessment of wave conditions (wave climate) is of paramount importance. Wave climate - this is the time distribution of average wave conditions over the years. The joint distribution of wave heights, periods and direction for a given period of time defines the wave conditions. These conditions are the result of the wind action at the measuring point, the wind at high seas along the fetch, the duration of its impact on the water surface and the length of the fetch.

In the wave regime description, the extreme values of both wave-generating factors and wave properties need to be determined. These are the phenomena with low frequency (low probability of recurrence) and big parameters, such as the extreme squalls. As extreme are defined those events, whose occurrence is possible once in more than 50 or 100 years. In accordance with the requirements of [2] [art. 7, par. 1. Table 1], which are in essence a Bulgarian translation of [3], the design probability of exceedance in the system for wave height should be adopted 1% for vertical and sloped coastal structures and 5% when assessing the degree of protection of the harbor area, as for the wind velocity, the probability of exceedance for marine structures class I is adopted 2% (once every 50 years).

3.2.1 Reference period of meteorological observations for the assessment of wave parameters

Multiannual studies on wind and wave conditions show that the annual number of storms varies significantly through the years. In order to determine the regime features of wind and waves, very long period of continuous observations is required. Unfortunately, systematic multiannual observations on the wave regime in the Bourgas Bay have not been performed yet. Available are only individual registrations at “Stavrova” sand bank for several not too big squalls [24]. These measurements are primarily used for comparison. As a measure of storm activity we can adopt the number of cases (averaged over several years) when the wind velocity exceeds 15m/s. A year in which the number of cases of wind speed $V \geq 15$ m/s is greater than the average annual, is considered a year of increased storm activity. Multiannual research shows that there is a clear cyclic recurrence of storm activity, which is presented in [23]. With increased storm activity in the Black Sea are the years 1918 to 1930, 1944 to 1956, 1968 to 1977, and with reduced storm activity are 1907 to 1917, 1931 to 1943, 1957 to 1967. Disregarding storm activity when using short data series can lead to large errors in determining the extreme wave properties.

Data sources on wind velocity, based on which the wave parameters are determined, are the following:

- standard synoptic observations (every 3 hours) of the wind direction and velocity for the station on Cape Kaliakra;
- ship observations in areas close to the Bulgarian coast;
- pressure fields (every 3 hours) over the Black Sea for 58 storms in the period 1952 - 1968, when the wind velocity exceeds 15 m/s [25].

The most complete are the 10-year data series from station Kaliakra with wind direction and velocity measurements every 3 hours. Conducted by on other occasions calculations Waves in various areas of the western part of the Black Sea has been found that in terms of wind most representative is the data from Cape Kaliakra station. Wave calculations on other occasions in various areas of the Western Black Sea indicate that in terms of wind, most representative is the data from Cape Kaliakra. From the selected time period (1972 – 1981), the first 6 years (1972 - 1977) fall into a period of increased storm activity and the next 4 years (1978 - 1981) – in one with reduced storm activity. Ship measurements cover a longer period of time, but were taken on occasional basis - only when there was a vessel in the area. Barometric air pressure maps were used for the model calculations of wind waves for the specific shallow-water site in the Bourgas Bay.

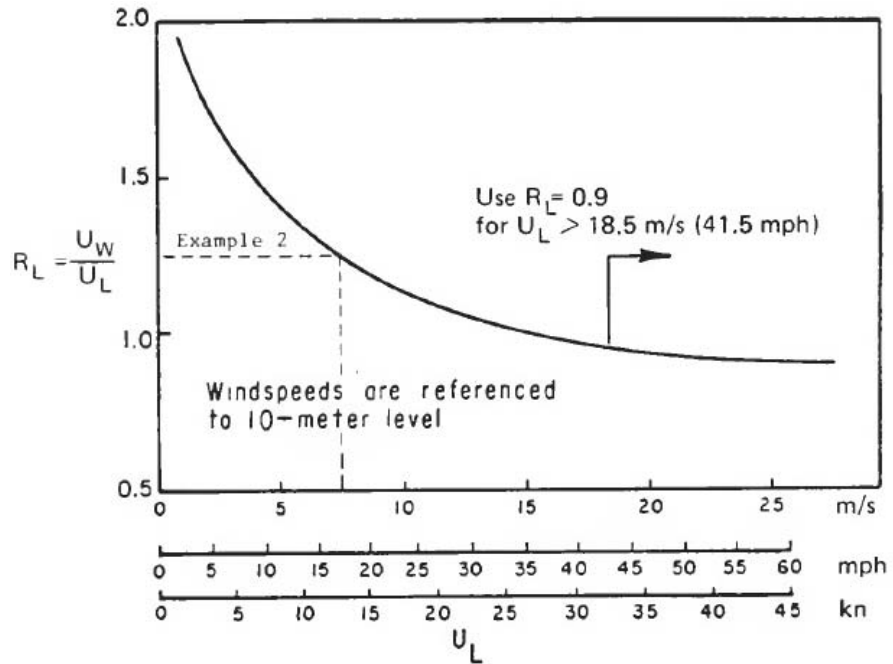


Figure 25: Wind velocity estimation; Source: [6]

For the assessment of the wave regime properties, the Kaliakra series is used. In order to avoid local effects, the relationship between the wind velocity over land and the ratio V_S/V_L (V_S - wind velocity over sea, V_L - wind velocity over land) is determined for the separate months (SPM, 1984). From the wind velocity data for Kaliakra and for high seas relationships of the kind $V_S/V_L=f(V_L)$ are obtained. Usually for velocities $V_L \geq 10$ m/s, the ratio $V_S/V_L < 1$, while for $V_L < 10$ m/s, $V_S/V_L > 1$ (Figure 25).

The figure clearly shows that for wind velocities $V_L \geq 15$ m/s the ratio V_S/V_L is close to 1 but never exceeds it. Therefore, in order to ensure being on the safe side, it is reasonable to apply for design purposes the wind velocity data from Table 14.

3.2.2 Wave height monthly distribution in deep water from the 4 main directions

The monthly distribution of wave heights in deep water is presented in the figures below, as only these directions are taken into consideration, from which the wave reaches the harbor range (NE, E, SE and S).

Table 15 Monthly distribution of wave heights in deep water from NE; Source: [1]

H_{av} [cm]	Jan	Feb	Mar	Apr	May	Jun	Jul	Aug	Sep	Oct	Nov	Dec
40	.1925	.3064	.9074	.9939	1.0332	1.0292	.9664	1.2964	1.0882	.8132	.5893	.2828
80	.1728	.3261	.3614	.2475	.3850	.2711	.4203	.5107	.4085	.3261	.2671	.1139
120	.1414	.1846	.3025	.1532	.1021	.1336	.1493	.2964	.2475	.2593	.0432	.1021
160	.1571	.1100	.1061	.0511	.0668	.0629	.0432	.0904	.0707	.1689	.0825	.0786
200	.0432	.0196	.0629	.0118	.0314	.0079	.0039	.0196	.0354	.0079	.0039	.0039
240	.0786	.0943	.0157	.0196	.0039	.0039	.0000	.0000	.0118	.0550	.0314	.0196
280	.0039	.0039	.0393	.0000	.0000	.0000	.0000	.0000	.0000	.0236	.0118	.0000
320	.0000	.0000	.0000	.0000	.0000	.0000	.0000	.0000	.0000	.0275	.0039	.0000

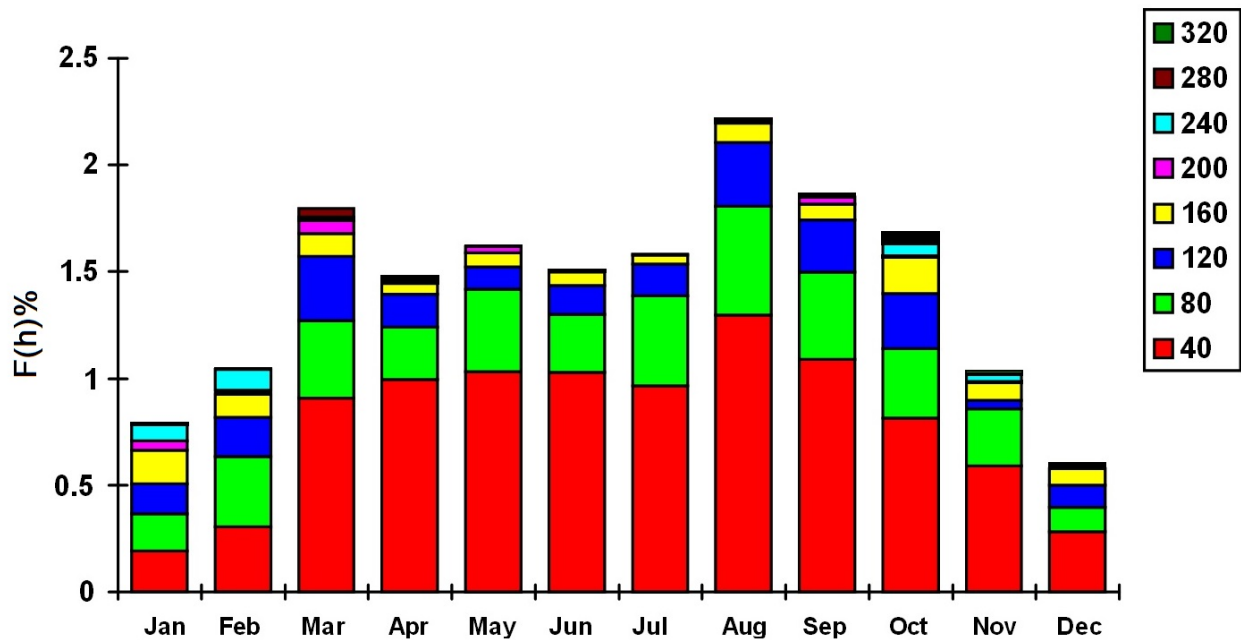


Figure 26: Mean wave height [cm] from NE for deep water; Source: [1]

Table 16 Monthly distribution of wave heights in deep water from E; Source: [1]

H _{av} [cm]	Jan	Feb	Mar	Apr	May	Jun	Jul	Aug	Sep	Oct	Nov	Dec
40	.1453	.1689	.4439	.4675	.6521	.4675	.3300	.3732	.6010	.4164	.2632	.2161
80	.0589	.1414	.0864	.1336	.1414	.0746	.1375	.1218	.1728	.1925	.1375	.0982
120	.1296	.0982	.0432	.0550	.0746	.0432	.0471	.0354	.0668	.0864	.0393	.0707
160	.1100	.0157	.0236	.0157	.0079	.0039	.0157	.0393	.0275	.0707	.0668	.0275
200	.0707	.0079	.0000	.0000	.0039	.0000	.0039	.0157	.0000	.0079	.0039	.0236
240	.0000	.0000	.0000	.0000	.0000	.0000	.0000	.0000	.0000	.0039	.0000	.0000
280	.0039	.0079	.0000	.0000	.0000	.0000	.0000	.0000	.0000	.0000	.0039	.0000
320	.0000	.0000	.0000	.0000	.0000	.0000	.0000	.0000	.0000	.0000	.0118	.0000

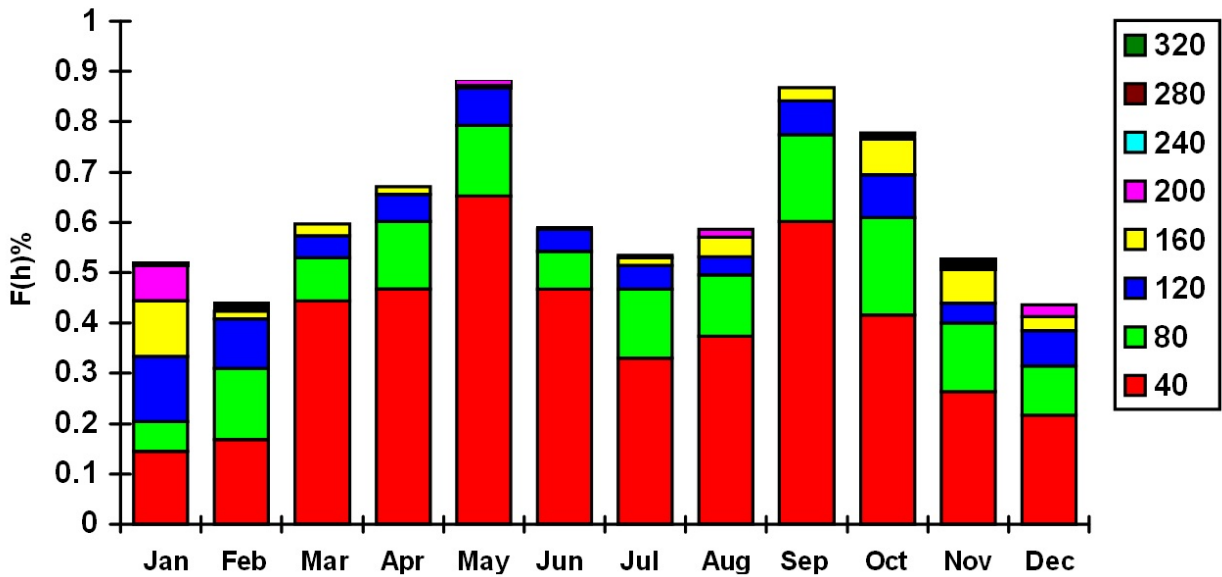


Figure 27: Mean wave height [cm] from E for deep water; Source: [1]

Table 17 Monthly distribution of wave heights in deep water from SE; Source: [1]

H _{av} [cm]	Jan	Feb	Mar	Apr	May	Jun	Jul	Aug	Sep	Oct	Nov	Dec
40	.1846	.1886	.3025	.4360	.4007	.4635	.4282	.3064	.3496	.3103	.0982	.1453
80	.1139	.2043	.0904	.0982	.1021	.1061	.0668	.0864	.0550	.1375	.0746	.1218
120	.0550	.0550	.0157	.0157	.0000	.0196	.0000	.0039	.0000	.0079	.0157	.0118
160	.0039	.0000	.0000	.0039	.0000	.0000	.0000	.0039	.0000	.0157	.0000	.0000
200	.0000	.0000	.0000	.0000	.0000	.0000	.0000	.0000	.0000	.0000	.0000	.0000
240	.0000	.0000	.0000	.0000	.0000	.0000	.0000	.0000	.0000	.0000	.0039	.0000
280	.0000	.0000	.0000	.0000	.0000	.0000	.0000	.0000	.0000	.0000	.0000	.0000
320	.0000	.0000	.0000	.0000	.0000	.0000	.0000	.0000	.0000	.0000	.0000	.0000

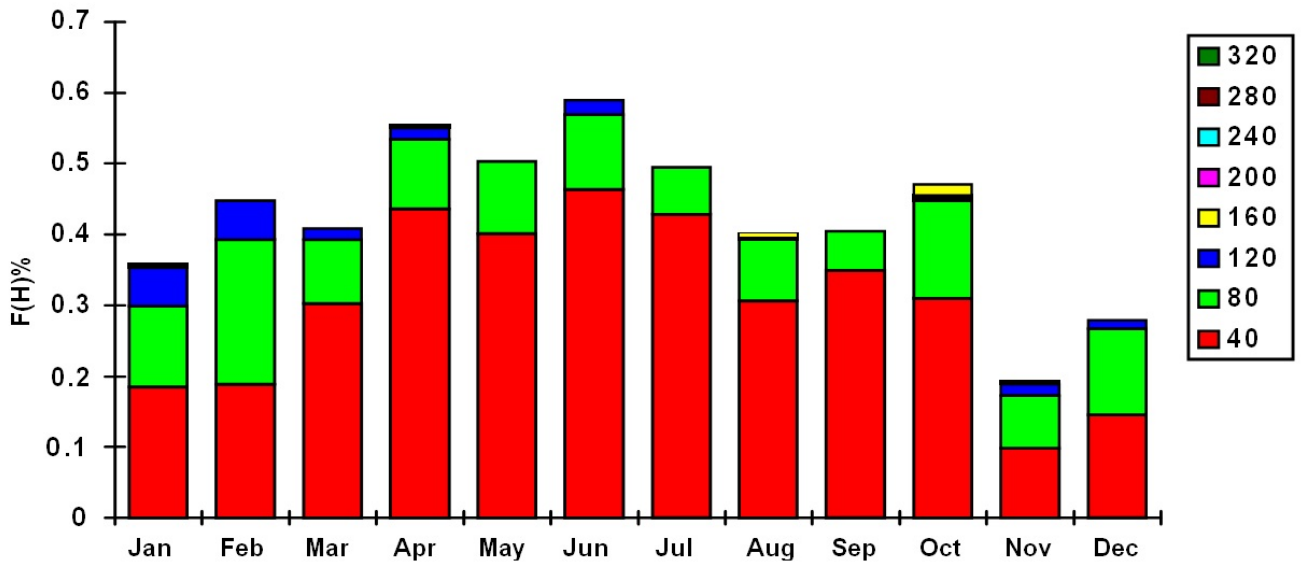


Figure 28: Mean wave height [cm] from SE for deep water; Source: [1]

Table 18 Monthly distribution of wave heights in deep water from S; Source: [1]

H _{av} [cm]	Jan	Feb	Mar	Apr	May	Jun	Jul	Aug	Sep	Oct	Nov	Dec
40	.3025	.2514	.3771	.6482	.6207	.8407	.8210	.5460	.4950	.6364	.2946	.4007
80	.4321	.3653	.3496	.3771	.2593	.2593	.3418	.1768	.2986	.5530	.5735	.4714
120	.0471	.0825	.0550	.0354	.0354	.0079	.0079	.0039	.0314	.0236	.1218	.1375
160	.0000	.0354	.0000	.0354	.0157	.0000	.0000	.0000	.0196	.0471	.0236	.0236
200	.0000	.0000	.0000	.0000	.0000	.0000	.0000	.0000	.0039	.0000	.0039	.0000
240	.0000	.0000	.0000	.0000	.0000	.0000	.0000	.0000	.0079	.0000	.0000	.0000
280	.0000	.0000	.0000	.0000	.0000	.0000	.0000	.0000	.0000	.0000	.0000	.0000
320	.0000	.0000	.0000	.0000	.0000	.0000	.0000	.0000	.0000	.0000	.0000	.0000

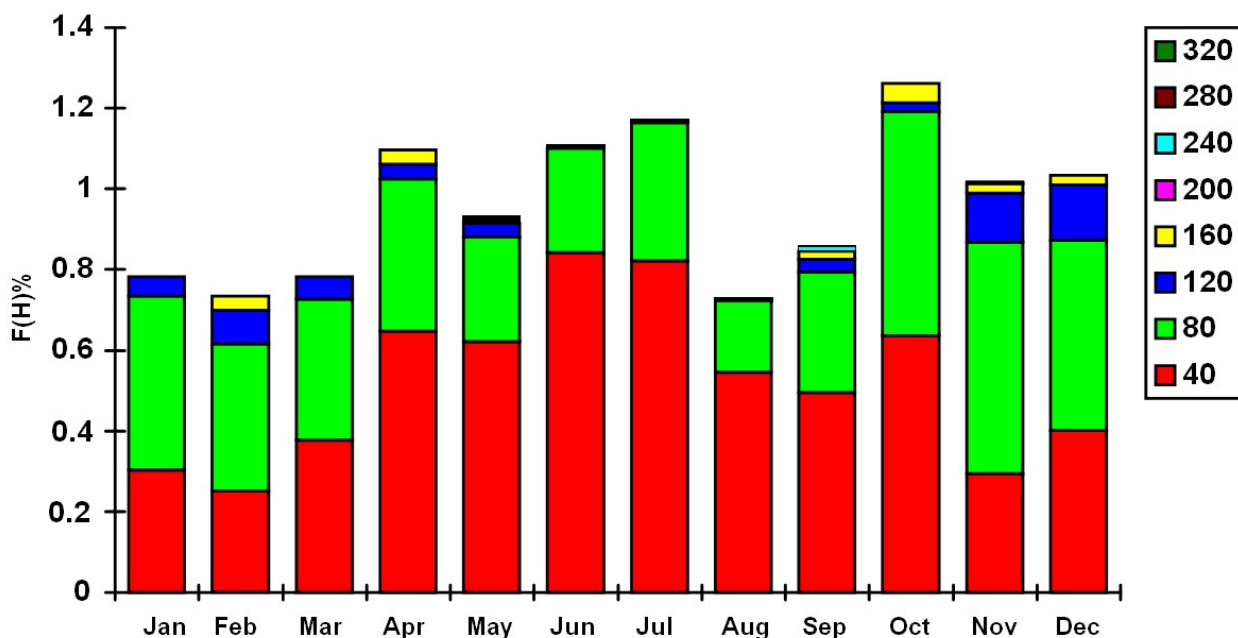


Figure 29: Mean wave height [cm] from S for deep water; Source: [1]

With the greatest recurrence are the lowest waves (with mean height up to 40 cm) during the warm half-year – from April to September. During the summer months (May-August) the mean wave height reaches 200 cm on very few occasions. Strong wave motion with height over 260 cm is observed from October until March. Regardless of the wave direction in deep water, in shallow water (eastern boundary with depth of about 35 m) waves spread in the sector 80 - 120 toward the North. Deep water waves from N and SE undergo the strongest transformation, which is also confirmed by the transformation calculations from deep water into shallow water in front of the Bourgas Bay. For all periodical observations on strong wind recurrence and duration, an analysis is performed for each of the hazardous wind directions by months:

Wind from N

$V > 15 \text{ m/s}$ ($H_{av} = 0.60 \text{ m}$)

January - probability of occurrence twice each year with an average duration 15 hours

February – once a year, average duration 10 hours;

March - once a year, average duration 10 hours;

September - once a year, average duration 6 hours;

October - once a year, average duration 9 hours;

November - once every 2 years, average duration 9 hours;

December - once a year, average duration 9 hours.

$V > 18 \text{ m/s}$ ($H_{av} = 0.70 \text{ m}$)

January - probability of occurrence once every 2 years with an average duration 10 hours;

September - once every 2 years, average duration 12 hours;

October - once every 5 years, average duration 9 hours;

December - once every 2 years, average duration 6 hours.

$V > 20 \text{ m/s}$ ($H_{av} = 0.90 \text{ m}$)

January - probability of occurrence once every 3 years with an average duration 6 hours

September - once every 3 years, average duration 9 hours;

October - once every 5 years, average duration 9 hours;

December - once every 5 years, average duration 6 hours.

Wind from NE

$V > 15 \text{ m/s}$ ($H_{av} = 1.20 \text{ m}$)

January - probability of occurrence once a year with an average duration 12 hours

February – once every 2 years, average duration 12 hours;

March - once a year, average duration 12 hours;

October - once every 3 years, average duration 12 hours;

November - once every 5 years, average duration 6 hours;

December - once every 5 years, average duration 10 hours.

$V > 18 \text{ m/s}$ ($H_{av} = 1.30 \text{ m}$)

January - probability of occurrence once every 3 years with an average duration 10 hours

March - once every 3 years, average duration 9 hours;

October - once every 5 years, average duration 15 hours.

$V > 20 \text{ m/s}$ ($H_{av} = 1.50 \text{ m}$)

January - probability of occurrence once every 10 years with an average duration 4 hours

March - once every 3 years, average duration 9 hours;

October - once every 10 years, average duration 15 hours;

November - once every 10 years, average duration 15 hours.

Wind from E

$V > 15 \text{ m/s}$ ($H_{av} = 1.30 \text{ m}$)

January - probability of occurrence once every 2 years with an average duration 6 hours

February – once every 5 years, average duration 10 hours;

December - once every 5 years, average duration 9 hours.

$V > 18 \text{ m/s}$ ($H_{av} = 1.50 \text{ m}$)

February – probability of occurrence once every 10 years with an average duration 10 hours

November - once every 5 years, average duration 9 hours.

For the stretch of the coast studied, hazardous wave directions are those from the E and SE quarters, as the strongest wave regimes from the E quarter occur during the period November – February. Although for the entire coast of Bulgaria the strongest wave modes come from NE, the exposure of the stretch in question does not imply examining the wave regime from this quarter due to of the wave shadow created by cape Emine and Pomorie.

Given the fact that the strongest winds are observed in winter and autumn, maximum wind waves are registered during these seasons. For the coast of Burgas region the most common are waves from E, followed by SE, S and SW [1].

Waves from E and SE play a decisive role for determining the hydromechanical properties in the bay for the given harbor layout and for the design of the wave protective facilities. The wave properties in the range of the considered facility are defined by the means of wave transformation and refraction calculation from deep water, taking into account the relief of the submerged coastal slope and the shoreline configuration.

3.2.3 Maximum water levels

Changes in the Black Sea water level and in particular in the coastal area are mainly due to changes in atmospheric pressure and the related wind structure. Thanks to the use of the collected data for over 60 years, the average water level is defined as H_{av} and the annual maximum - as H_{max} . In order to determine the maximum water levels (maximum high/low water levels above/below the average annual level) a series of 60 years is used (from 1928 to 1987 with a break in 1967 and 1968). The level gauge, equipped and maintained by GUGK, is located near the port of Bourgas. The registration is continuous with a chart pen gauge which filters wind waves and oscillations with a period shorter than 15-20 minutes [22].

Taking into account that the maximum levels are formed due to surge-drop impulse events, in the sequence of maxima are present in equal shares periods of increased and decreased storm activity. Most often the water level annual maxima series are non-stationary. Maximum water level variations are influenced by the following factors:

- multiannual variability of climatic and heliophysical processes manifesting in cyclic or unidirectional level variations,
- rise or subsidence of land caused by tectonic processes,
- disturbance of the water balance by changes in the water inflow.

The distribution functions for the maximum values are determined using the deviations of the maximum annual values H_{max} from the average annual values H_{av} are used [17].

$$H_{max} = H_{max} - H_{cp} \quad (3.1)$$

Stationarity of the multiannual series is achieved by using the maximum annual deviations H_{max} , excluding the influence of the different zero level readings, as well as the effect of local landslides in the area of the measuring point. The extreme values statistics are based on the double exponential law of the distribution function: $P = \exp(-e^y)$,

where $y = y(H_{max})$ is a translated variable function of the examined statistical variable H_{max} .

The method of least squares is employed for determining of the function. Maximum deviations from the average multiannual water level are obtained for a 95% confidence interval. The maximum deviations for different recurrence intervals are presented in Table 19.

Table 19 Maximum rise and decline from the average multiannual water level for the Black Sea west coast;

Source: [17]

Recurrence [years]	1	5	10	25	50	100
H_{max} [cm]	27.6	49.2	54.6	61.4	66.4	71.3
from-to [cm]	26.8-28.6	48.5-50.3	53.7-55.9	60.2-62.9	65.0-68.2	69.9-73.4
H_{min} [cm]	-25.7	-47.3	-52.6	-59.3	-64.3	-69.2
from-to [cm]	-(25.2-26.3)	-(46.7-47.80)	-(51.9-53.3)	-(58.4-60.2)	-(63.2-65.3)	-(68.0-70.4)

Apart from the water level rise due to wind set-up (storm surge), in the Bourgas Bay are observed tidal waves with low intensity. They have a clear time period of 12-13 hours and a height of 3-15cm. Typical for the bay are another four harmonic variations with a period between 95 and 150 minutes, average height 5-7 cm, maximum height 15-30cm with the longest steady state duration of 2-4 days.

At the Black sea west coast winds from E rise the sea level (storm surge), while winds from W decrease it (drop).

In Bourgas Bay the storm surge can reach a maximum height of 60cm. Seiches and standing waves which are generated by rapid local changes in air pressure, are rarely observed. Seiches cause rise and fall of the sea level with up to 1.5m from the average level with a period of ca. 30 minutes and complete damping of oscillations over several hours [23].

Multiannual level gauge reports in the region of Port Burgas show a slight increase of the average monthly sea level in late spring and early summer due to the large water inflows in those seasons running into the sea.

A set of factors have influence on sea level fluctuations – such with cyclic manifestation, others with a slow unidirectional development and such of random nature. The latter are usually identified with storm surge or extremely long waves generated by an explosion or an earthquake. The data on the maximum increase or decrease of the average annual water level shown in Table 19 is based on sufficiently long series of observations (60 years) and it is safe to assume that increases in sea level of random nature are recorded Not explicit enough is, however, the question of simultaneous occurrence of different events with small probability or recurrence. In this regard calculations were performed for wind surge in the bay as a result of continuous wind impact from NE, E and SE with wind velocities 25, 30 and 35 m/s for each direction. The maximum values of the storm surge for wind velocities with return period once every 100 years are lower than the observed water level rise with the same return period. Therefore, the question arises: Is it possible that the occurrence of waves with return period 50 years coincides with a water level rise in Table 19 with the same return period? It is more logical beside the wave motion with a certain probability of exceedance, defined as a design value, to add only the storm surge. But since this issue has neither been treated in the Bulgarian standards and regulations [1], nor is it sufficiently clarified in the technical literature, the research of the breakwater construction and the degree of protection of the harbor area should be carried out using the deviations given in Table 19.

For reference, the average multiannual sea level elevation according to the Baltic system is as follows:

Northern part of Bourgas Bay	(-31.7 cm);
Southern part of Bourgas Bay	(-27.9 cm);
Sozopol	(-27.7 cm);
Varna	(-27.3 cm);

3.3 Wave properties in deep water for E and SE

The wave properties in deep water for both directions with most intensive wave motion are obtained by statistical data processing and are shown in Table 20 and Table 21.

Table 20 Wave properties in deep water – E; Source: [18]

Return period [years]	Wave height [m]			Period [s]
	(H _{av})	H _{1%}	H _{5%}	T _{av}
1	2.8	6.75	5.45	7.3
5	3.8	9.2	7.4	8.4
25	4.5	10.9	8.75	9.1
50	4.9	11.85	9.55	9.2

Table 21 Wave properties in deep water - SE; Source: [18]

Return period [years]	Wave height [m]			Period [s]
	(H _{av})	H _{1%}	H _{5%}	T _{av}
1	2	4.85	3.4	6.4
5	3.4	5.75	4.7	6.8
25	2.7	6.55	5.25	7.1
50	2.9	7	5.65	7.4

As stated in section 3.2, the design probability of exceedance in the system for wave height should be adopted 1% for vertical and sloped coastal structures and 5% when assessing the degree of protection of the harbor area. The values with recurrence period of 1, 5 and 25 years are valid for sediment flow analysis and the sedimentation coefficient in the area at issue in order to maintain the specified design depth at the harbor entrance and in the harbor area [8].

3.4 Transformation of the wave properties with directions E and SE from deep water to depth 35m and 12m using wave modeling software WAM and SWAN [1]

For the assessment of the wave transformation from deep water to depth 35m and 12m, the wave modeling software products WAM and SWAN are used. For the given wave parameters in deep water (wave height, wave vector direction and wave period) in a water environment with a certain depth, the model calculates the change in the wave vector direction and in the wave height.

The refraction pattern (change in the wave vector direction) is calculated by numerical solution of the wave vector conservation equation. On the other hand the wave height transformation is calculated by solving the wave energy conservation equation, according to which the wave energy flow change is proportional to the rate of its dissipation.

The modeling is carried out in 2 stages: first the refraction is simulated, then the wave height transformation.

The refraction is calculated by numerical solution of the wave vector conservation equation. In a rectangular Cartesian coordinate system in which the axis OX is directed eastward, and the axis OY – northward, the components of the wave vector \vec{k} along the axes OX and OY are defined accordingly as k_x and k_y . The angle θ is defined as the angle that \vec{k} forms with the positive direction of the OX axis.

$$\nabla \times \vec{k} = \begin{vmatrix} \frac{\partial}{\partial x} & \frac{\partial}{\partial y} \\ k_x & k_y \end{vmatrix} = \frac{\partial k_y}{\partial x} - \frac{\partial k_x}{\partial y} = 0, \quad (3.2)$$

where the components of the wave vector \vec{k} are defined as follows:

$$k_x = \frac{\omega}{c} \cos \theta, \quad k_y = \frac{\omega}{c} \sin \theta \quad (3.3)$$

Since $\omega = const$, $\nabla \times \vec{k} = \begin{vmatrix} \frac{\partial}{\partial x} & \frac{\partial}{\partial y} \\ k_x & k_y \end{vmatrix} = \frac{\partial k_y}{\partial x} - \frac{\partial k_x}{\partial y} = 0$, (3.2) takes the form:

$$\frac{\partial}{\partial x} \frac{\sin \theta}{c} - \frac{\partial}{\partial y} \frac{\cos \theta}{c} = 0. \quad (3.4)$$

The solution of the equation (3.4) with known wave period in deep water and depth field, will give the wave approach propagation angle field θ in the shallow water region of the researched area. Equation (3.4) is solved numerically with regard to θ , complying with the following boundary conditions. Depending on the wave depth, the outer limit of the computational area is divided into several zones. In deep water ($h > h_{tr}$) at the boundary, θ is assumed to be equal to θ_{deep} . In the transformation zone it is accepted, that the gradient of θ in the direction perpendicular to the boundary, is equal to zero.

The transformation of wave height is determined by the wave energy balance equation:

$$\frac{\partial}{\partial x} (Ec_g \cos \theta) + \frac{\partial}{\partial y} (Ec_g \sin \theta) = -D \quad (3.5)$$

where D – wave energy dissipation velocity.

The breaking of the waves is limited by the significance of the limiting wave height H_m . To determine the dissipation rate D of the irregular waves transformation, it is necessary to know the portion of the broken waves Q_h at a certain depth. The height of the breaking wave H_m is defined by the Misch criterion which includes an empirical parameter $\bar{\gamma}$:

$$H_m = \frac{0.88}{k} \tan h \left(\frac{\bar{\gamma}kh}{0.88} \right), \quad \bar{\gamma} = 0.5 + 0.4 \tan h \left(\frac{33H_{rms\ deep}}{L_{deep}} \right), \quad (3.6)$$

where the index “deep” relates to deep water. L is the wave length with respect to T_p , and h is the water depth.

In Table 22 and Table 23 are presented the wave properties with directions E and SE at depth 35m – at the entrance of the Bourgas Bay [18][1].

Table 22 Wave properties with direction E at depth 35m; Source: [18]

Recurrence once every ... years	Wave height [m]			Period T [s]
	H _{av}	H _{1%}	H _{5%}	T _{av}
1	2.75	6.70	5.40	7.3
5	3.05	7.60	6.25	8.4
25	3.65	8.25	6.90	9.1
50	4.05	9.10	7.65	9.2

Table 23 Wave properties with direction SE at depth 35m; Source: [18]

Recurrence once every ... years	Wave height [m]			Period T [s]
	H _{av}	H _{1%}	H _{5%}	T _{av}
1	1.90	4.30	3.40	6.4
5	2.25	4.60	3.90	6.8
25	2.40	4.85	4.15	7.1
50	2.50	5.00	4.55	7.4

The wave properties at depth 12m for directions E and SE are given in Table 24 and Table 25 [1].

Table 24 Wave properties with direction E at depth 12m; Source: [1]

Recurrence period	Wave height [m]			Period [s]	Wave length [m]
	H _{av}	H _{1%}	H _{5%}	T _{av}	L _{av}
Once a year	2.2	5	4.1	7.3	67
Once every 5 years	2.85	6.35	5.25	8.4	85
Once every 25 years	3.4	7.5	6.2	9.1	89
Once every 50 years	3.65	8	6.65	9.2	90

Table 25 Wave properties with direction SE at depth 12m; Source: [1]

Recurrence period	Wave height [m]			Period [s]	Wave length [m]
	H _{av}	H _{1%}	H _{5%}	T _{av}	L _{av}
Once a year	1.6	3.7	3	6.4	56
Once every 5 years	1.85	4.25	3.45	6.8	61
Once every 25 years	2.05	4.65	3.85	7.1	64
Once every 50 years	2.15	4.9	4	7.4	68

3.5 Determining of the wave properties – direction S

3.5.1 Wave properties in deep water:

The wave properties height, length and period in deep water ($\bar{\lambda}_d$, \bar{h}_d and \bar{T}) are determined from the predefined wave generating factors wind velocity, maximum wind duration and length of fetch (V_w , t_w and L_w) for the given direction of the design wind [16]. For coastal structures I and II class the design storm is with probability of recurrence once every 50 years [2].



Figure 30: Wind fetch – direction S; Source: Google Maps 4/10/2013

The required wind properties for the 8 main directions are presented in Table 14. The maximum wind action duration from S is 8.83h while the maximum wind velocity with probability of exceedance in the system 2% is 29 m/s. The fetch length is measured from Google Maps – 14 km (Figure 30).

The average wave height in deep water \bar{h}_d in metres and the average period \bar{T} in seconds are read from the graph in Figure 31, as for the dimensionless variables gt_w/V_w and gL_w/V_w^2 , and the corresponding envelope curve gd/V_w^2 , the ratios $g\bar{h}_d/V_w^2$ and $g\bar{T}/V_w$ are read. For the calculations is chosen the ratio that results in smaller wave height and period. The values gt_w/V_w and gL_w/V_w^2 are entered in a logarithmic scale on the x-axis on Figure 31, bearing in mind that the fetch length L_w is in meters and the wind duration t_w is in seconds ([2] art. 16. /1/).

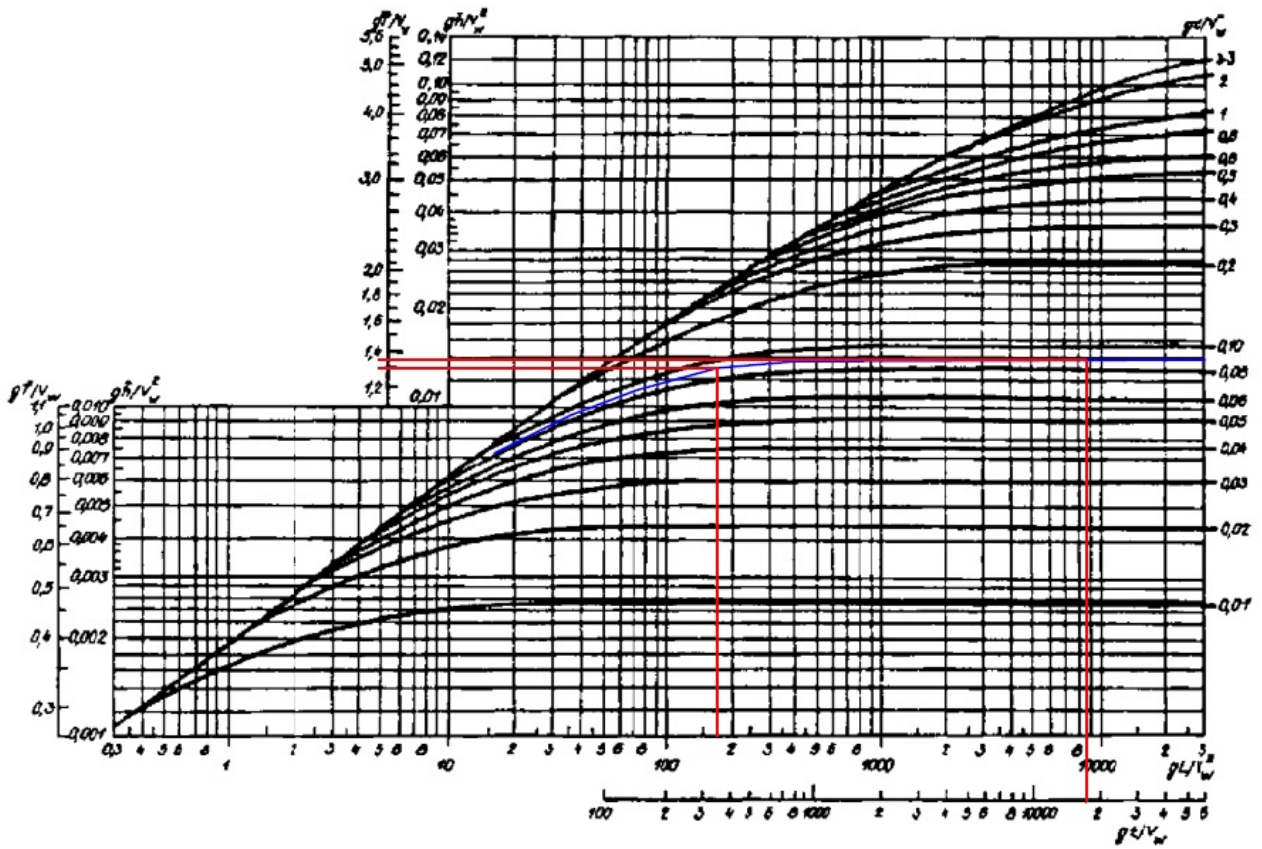


Figure 31: Graph for determining wave parameters period and wave height from the wind properties velocity, fetch and duration; Source: [3]

$$\frac{gt_w}{V_w} = \frac{9.81m/s^2 \cdot 31788s}{29m/s} = 10753 \quad (3.7)$$

$$\frac{gL_w}{V_w^2} = \frac{9.81m/s^2 \cdot 14000m}{(29m/s)^2} = 163 \quad (3.8)$$

$$\frac{gd}{V_w^2} = \frac{9.81m/s^2 \cdot 8m}{(29m/s)^2} = 0.09 \quad (3.9)$$

where d is the average water depth in the bay.

The values read from $\frac{gt_w}{V_w} = \frac{9.81m/s^2 \cdot 31788s}{29m/s} = 10753$ (3.7) are:

$$g\bar{h}_d/V_w^2 = 0.015 \quad (3.10)$$

$$g\bar{T}/V_w = 1.35 \quad (3.11)$$

The values read from $\frac{gL_w}{V_w^2} = \frac{9.81m/s^2 \cdot 14000m}{(29m/s)^2} = 163$ (3.8) are:

$$g\bar{h}_d/V_w^2 = 0.012 \quad (3.12)$$

$$g\bar{T}/V_w = 1.29 \quad (3.13)$$

The smaller and thus authoritative ratios are read from $\frac{gL_w}{V_w^2} = \frac{9.81m/s^2 \cdot 14000m}{(29m/s)^2} = 163$ (3.8).

The average period \bar{T} and the average wave height \bar{h} in deep water are calculated as follows:

$$\bar{T} = \frac{1.29.29m/s}{9.81m/s^2} = 3.81s \quad (3.14)$$

$$\bar{h} = \frac{0.012.(29m/s)^2}{9.81m/s^2} = 1.03m \quad (3.15)$$

The average wave length in deep water is defined by the formula:

$$\bar{\lambda}_d = \frac{g.\bar{T}^2}{2.\pi} = \frac{9.81m/s.3.81s^2}{2.\pi} = 22.7m \quad (3.16)$$

The wave height with 1% probability of exceedance in the system $h_{1\%}$ in meters is estimated by the formula:

$$h_{1\%} = k_{1\%} \cdot \bar{h}, \quad (3.17)$$

where $k_{1\%}$ is a coefficient read from the graph on Figure 32 for the dimensionless variable $\frac{gL_w}{V_w^2} = \frac{9.81m/s^2.14000m}{(29m/s)^2} = 163(3.8)$ ([2] art. 21. /1/).

$$\frac{gL_w}{V_w^2} = 163 \quad \rightarrow \quad k_{1\%} = 2.2$$

$$h_{1\%} = k_{1\%} \cdot \bar{h} = 2.2 \cdot 1.03m = 2.26m$$

According to [2] art. 7 /3/2., the calculative wave height probability of exceedance when determining the degree of protection of the harbor area is to be adopted 5%. In this case the 5% wave height ($h_{5\%}$) is valid for the diffraction analysis in the harbor. The coefficient $k_{5\%}$ is read from the curve $i=5\%$ on Figure 32.

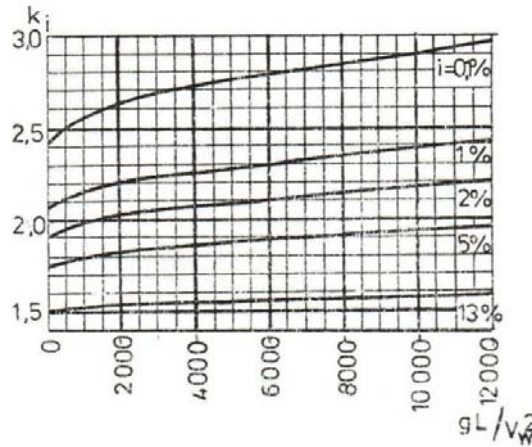


Figure 32: Graph for determining the coefficient k_i ; Source: [3]

$$\frac{gL}{V_w^2} = 163 \quad \rightarrow \quad k_{5\%} = 1.83$$

$$h_{5\%} = k_{5\%} \cdot \bar{h} = 1.83 \cdot 1.03m = 1.88m$$

3.5.2 Wave properties in shallow water

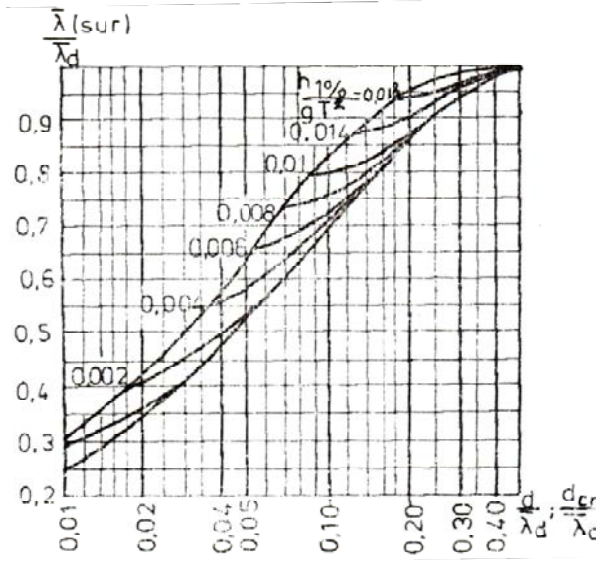


Figure 33: Graph for determining the value of $\bar{\lambda}$ in shallow water and $\bar{\lambda}_{sur}$ in the surf zone; Source: [3]

The length of the waves moving from deep to shallow water is determined by the graph on Figure 33 for the dimensionless quantities $d/\bar{\lambda}_d$ and $h_{1\%}/gT^2$. Moreover the wave period is assumed equal to the one in deep water. ([2] Art. 23. /3/).

$$\frac{d}{\bar{\lambda}_d} = \frac{8m}{22.7m} = 0.35 \quad (3.18)$$

$$\frac{h_{1\%}}{gT^2} = \frac{2.26m}{9.81m/s^2 \cdot (3.81s)^2} = 0.02 \quad (3.19)$$

The value for the ratio $\bar{\lambda}/\bar{\lambda}_d$ read from Figure 33 is equal to $\bar{\lambda}/\bar{\lambda}_d = 0.99$

The average wave length $\bar{\lambda}$ in shallow water is calculated as follows:

$$\bar{\lambda} = 0.99 \cdot \bar{\lambda}_d = 0.99 \cdot 22.7m = 22.5m \quad (3.20)$$

4 Numerical modeling of wave transformation and refraction from E, SE and S from 35m depth to the surf zone

The wave distribution in shallow water regions with highly indented coastline, complex bathymetry and the presence of islands or man-made moles and will include not only shoaling, refraction, but also energy dissipation and the diffraction phenomenon. In such cases, the use of models failing to analyze diffraction may lead to significant discrepancies such as intersection of wave rays and unrealistic values of obtained wave heights.

The numerical modeling of wave refraction and transformation in shallow water and in the harbor area is conducted using the software COPLA-RD, granted for use to the University of Architecture, Civil Engineering and Geodesy – Sofia by E.T.S. de Ingenieros de Caminos, Avda de los Castros, Santander, Espana.

4.1 Theoretical basis of the software COPLA-RD

The software COPLA-RD is a nonlinear model of the diffraction, based on the presentation of waves after the Stokes theory, as the wave height is known as far as the members of the second order, and includes a third order correction of the wave phase velocity. The theoretical basis of the model is presented by Kirby (1983).

For the creation of the model, the following assumptions have been made:

1. The sea bottom is gradually sloping. By comparing experimental data with calculations from the software, it has been established that for a bottom slope of less than 1:3, the obtained results are satisfactory.
2. Weak nonlinearity. Since the model is based on Stokes the wave theory, it is valid for Ursell parameter values of $UR < 40$.

$$U_R = \frac{HL^2}{d^3}, \quad (4.1)$$

where H – wave height,

L – wave length,

d – water depth.

In order to expand the scope of the model for shallow water ($UR > 40$), the dispersion equation derived by Hedges 1976 was introduced:

$$\sigma^2 = gk \tanh \left(kd \left(1 + \frac{|A|}{d} \right) \right),$$

where σ - angular frequency of the wave,

A – wave amplitude,

$$k = \frac{2\pi}{L} \text{ - wave number,}$$

g – acceleration due to gravity.

For the given depth (shallow water) this equation resembles the one for a solitary wave, while at greater depth it approximates the linear theory equation – $\sigma^2 = gk \tanh(kd)$.

3. The change in wave direction can be considered in the sector $\pm 60^\circ$ relative to the initial direction, i.e. outside this range results must be regarded as incorrect.

The model includes the ability to detect the energy losses depending on the modeled situation, as the following possibilities are foreseen:

- laminar surface and bottom boundary layers;
- laminar surface boundary layer and turbulent bottom boundary layer;
- permeable bottom;
- wave breaking.

For this purpose, the following equation is used:

$$\frac{\partial A}{\partial x} = \frac{i}{2k} \frac{\partial^2 A}{\partial y^2} - \frac{\omega}{2} A,$$

where ω - factor accounting for the energy dissipation,

i – imaginary number.

In the given case ω is defined by the expression:

$$\omega = \frac{2\sigma k f |A| (1-i)}{3\pi \sin(d) 2kh \sinh(kd)},$$

where f –resistance coefficient, adopted $f=0.01$.

The energy dissipation in the surf zone due to wave breaking is taken into account through the factor ω . This makes it possible to calculate the wave height not only until, but also after the first wave breaking.

The so called “thin water film” technique enables the modeling of waves in the presence of capes, islands and breakwaters. This technique allows these shapes to be replaced with shoals with a very small water depth ($d=1\text{cm}$). Thus through the criterion for wave breaking and energy dissipation in the surf zone, the obtained wave height there is less than half a centimeter, possessing an insignificant amount of energy and has no further impact behind the facility. This approach does not provide the option to consider the reflection coefficient k_{Ref} , e.g. the obtained results correspond to $k_{\text{Ref}}=0$.

The results of the conducted calculations with the software COPLA-RD for all computational cases are listed in section 4.3.

4.2 Wave properties in shallow water

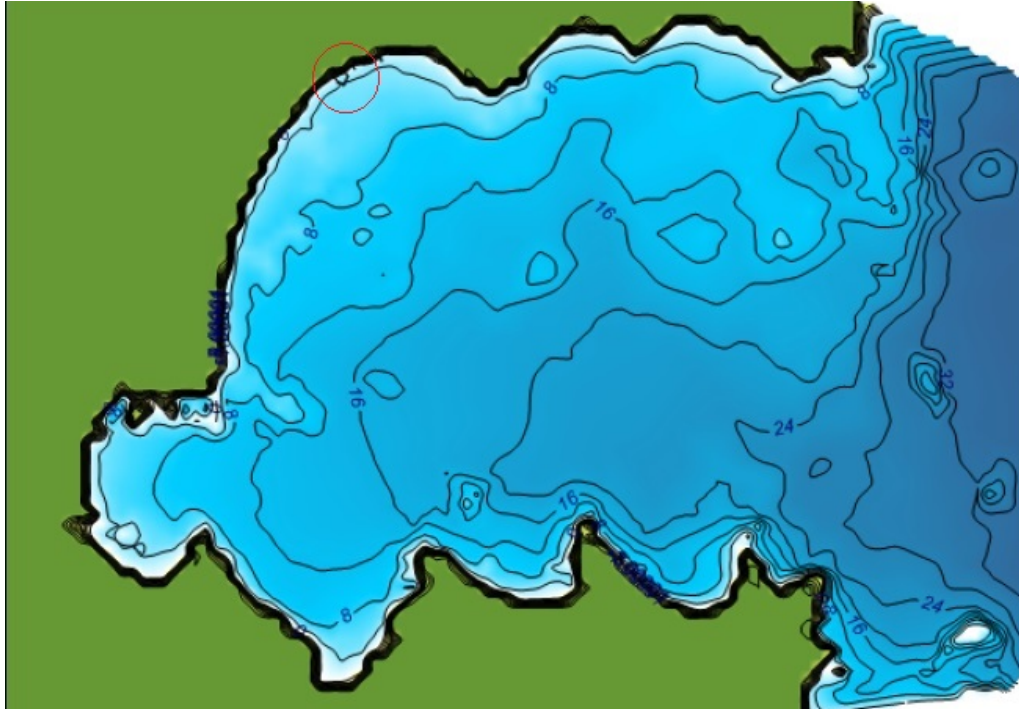


Figure 34: Bathymetric map of Bourgas Bay

Figure 34 presents a bathymetric map of the studied region. Figure 35 shows the layout of the harbor.

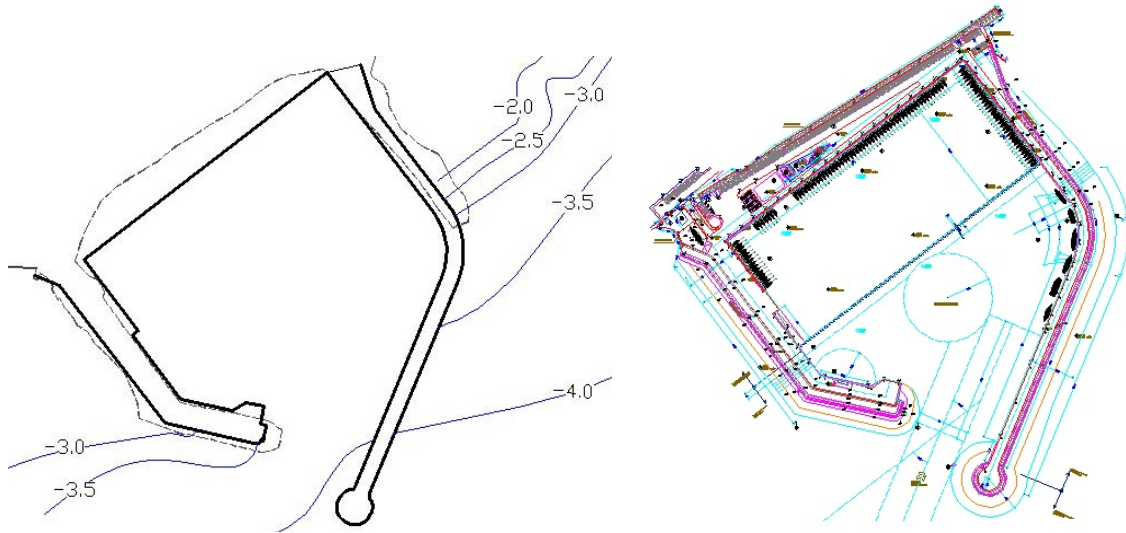


Figure 35: Harbor layout

The input data for the software COPLA-RD regarding wave properties from the three main directions for a recurrence period of 50 years is listed in Table 26, Table 27 and Table 28.

Table 26 Wave properties at depth 35m – direction E; Source: Table 22

Recurrence	Wave height [m]			Period [s]
	H _{av}	H _{1%}	H _{5%}	T _{av}
Once every 50 years	4.05	9.10	7.65	9.2

Table 27 Wave properties at depth 35m – direction SE; Source: Table 23

Recurrence	Wave height [m]			Period [s]
	H _{av}	H _{1%}	H _{5%}	T _{av}
Once every 50 years	2.50	5.00	4.55	7.4

Table 28 Wave properties at depth 35m – direction S; Source: Chapter 3.5

Recurrence	Wave height [m]			Period [s]
	H _{av}	H _{1%}	H _{5%}	T _{av}
Once every 50 years	1.03	2.26	1.88	3.81

4.3 Results of the numerical wave modeling

The results of the numerical wave modeling from E, SE and S in graphic form are presented on the following pages.

4.3.1 Waves from East (E)

Computation grid scheme – direction E

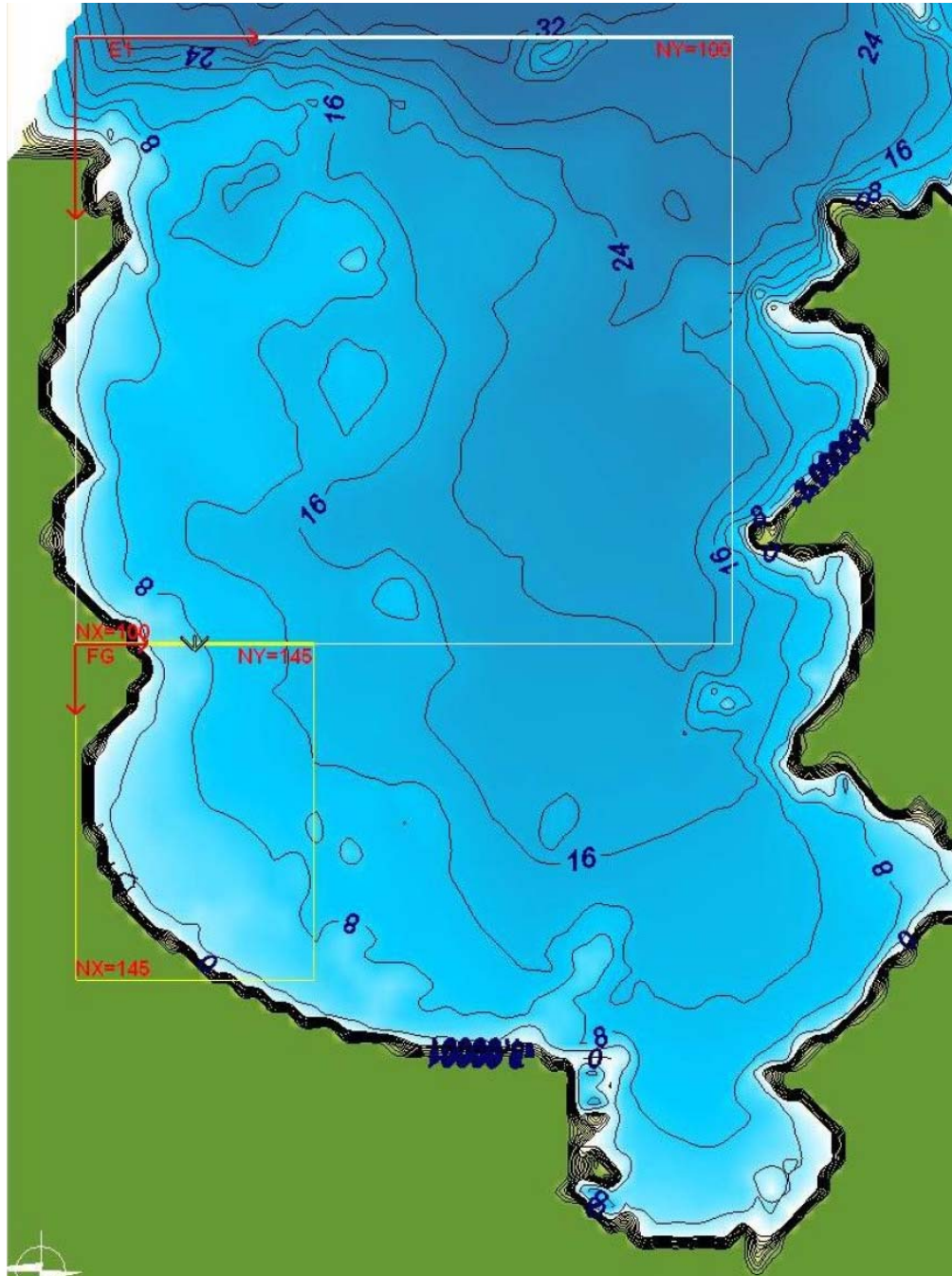


Figure 36: Computational grid – direction E

Numerical modeling of wave transformation and refraction

Wave height

Case study: E01

Direction: E

01: Storm with recurrence period once every 50 years, $H_{1\%}$

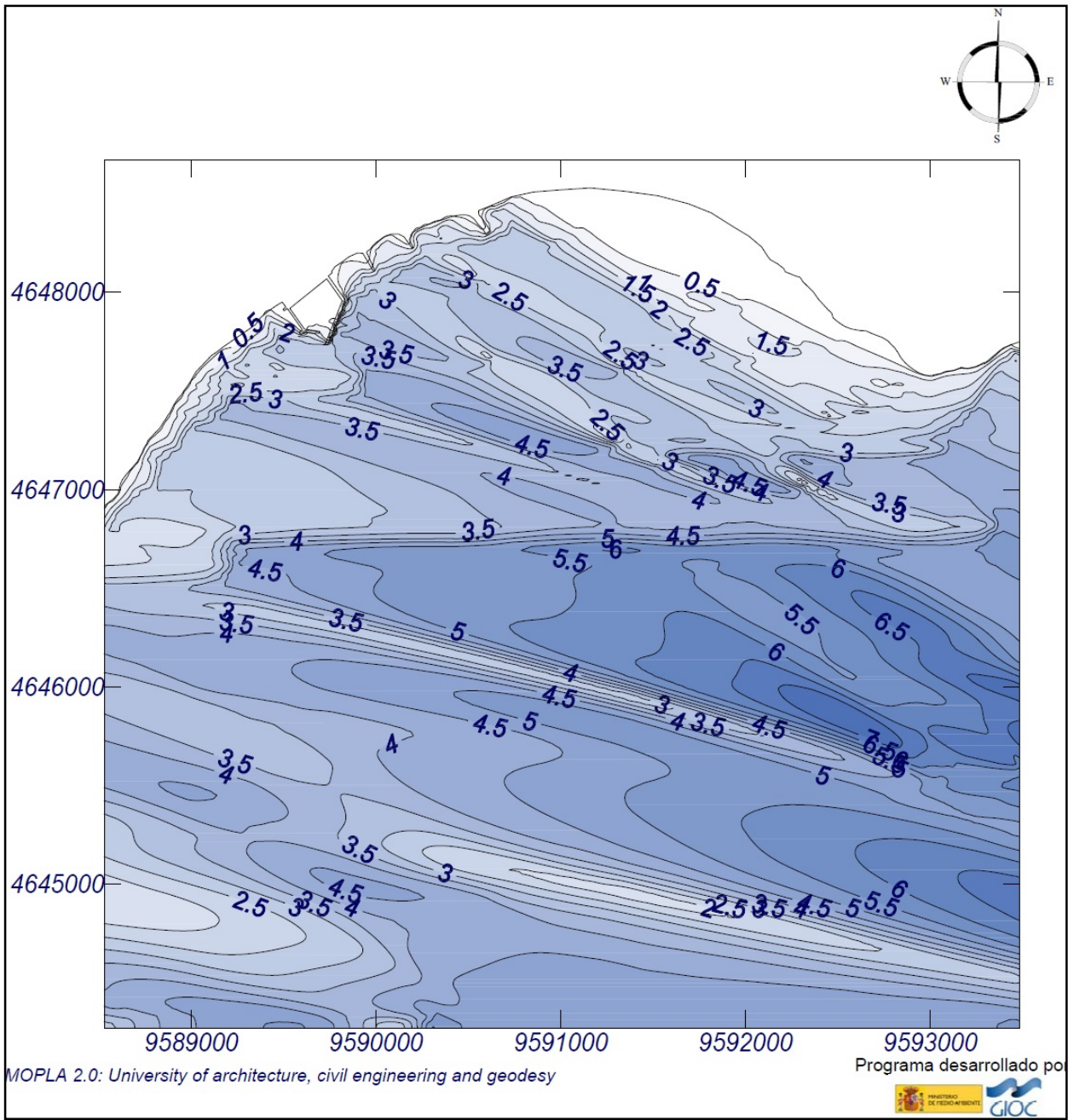
Simulation properties:

Period: 9.2 s

Input wave height: 9.1 m

Direction: 0° (E)

Maximum water level rise: 0.65 m



Numerical modeling of wave transformation and refraction

Wave height

Case study: E01

Direction: E

01: Storm with recurrence period once every 50 years, $H_{1\%}$

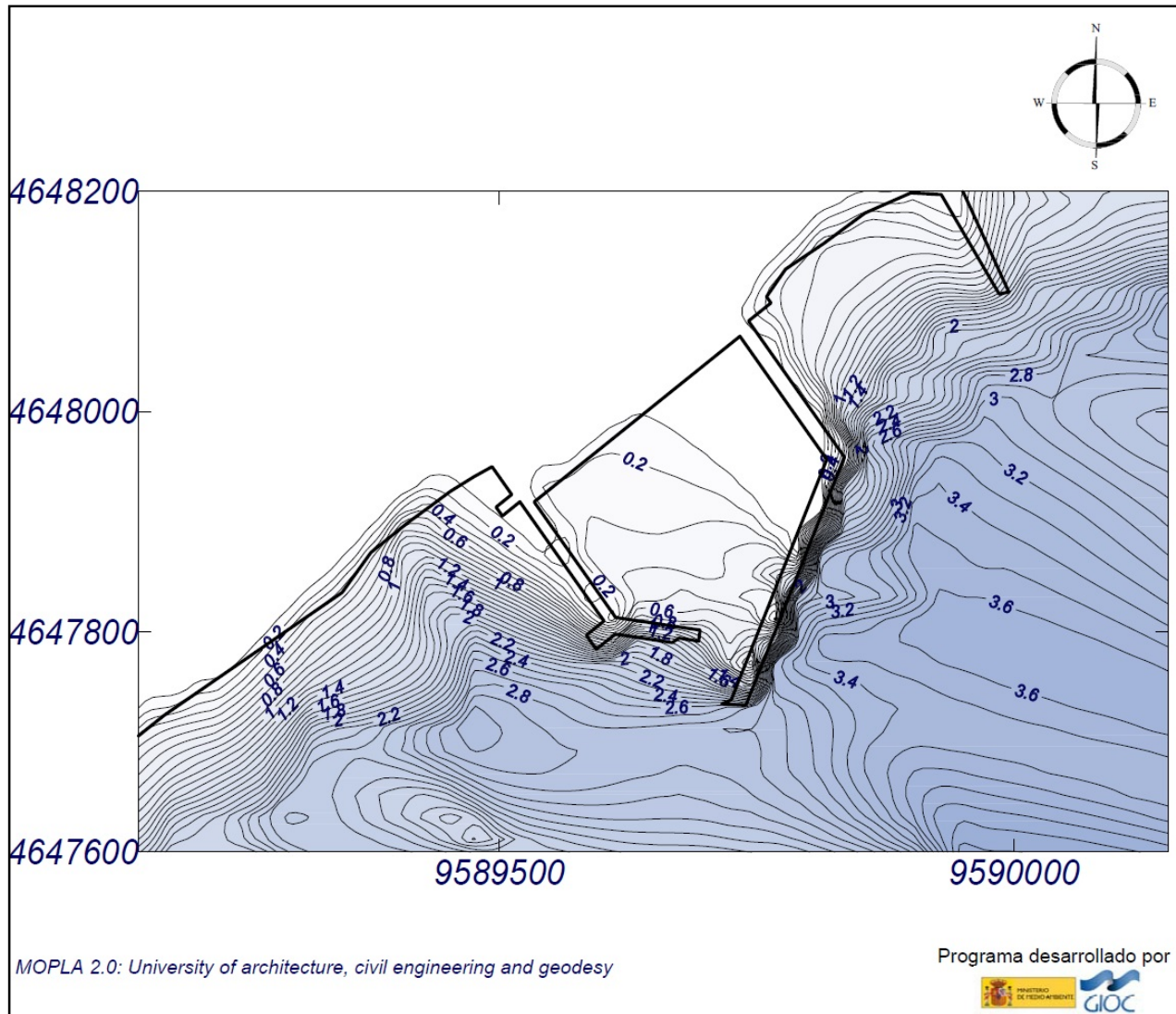
Simulation properties:

Period: 9.2 s

Input wave height: 9.1 m

Direction: 0° (E)

Maximum water level rise: 0.65 m



Numerical modeling of wave transformation and refraction

Wave currents and bathymetry

Case study: E01

Direction: E

01: Storm with recurrence period once every 50 years, $H_{1\%}$

Simulation properties:

Period: 9.2 s

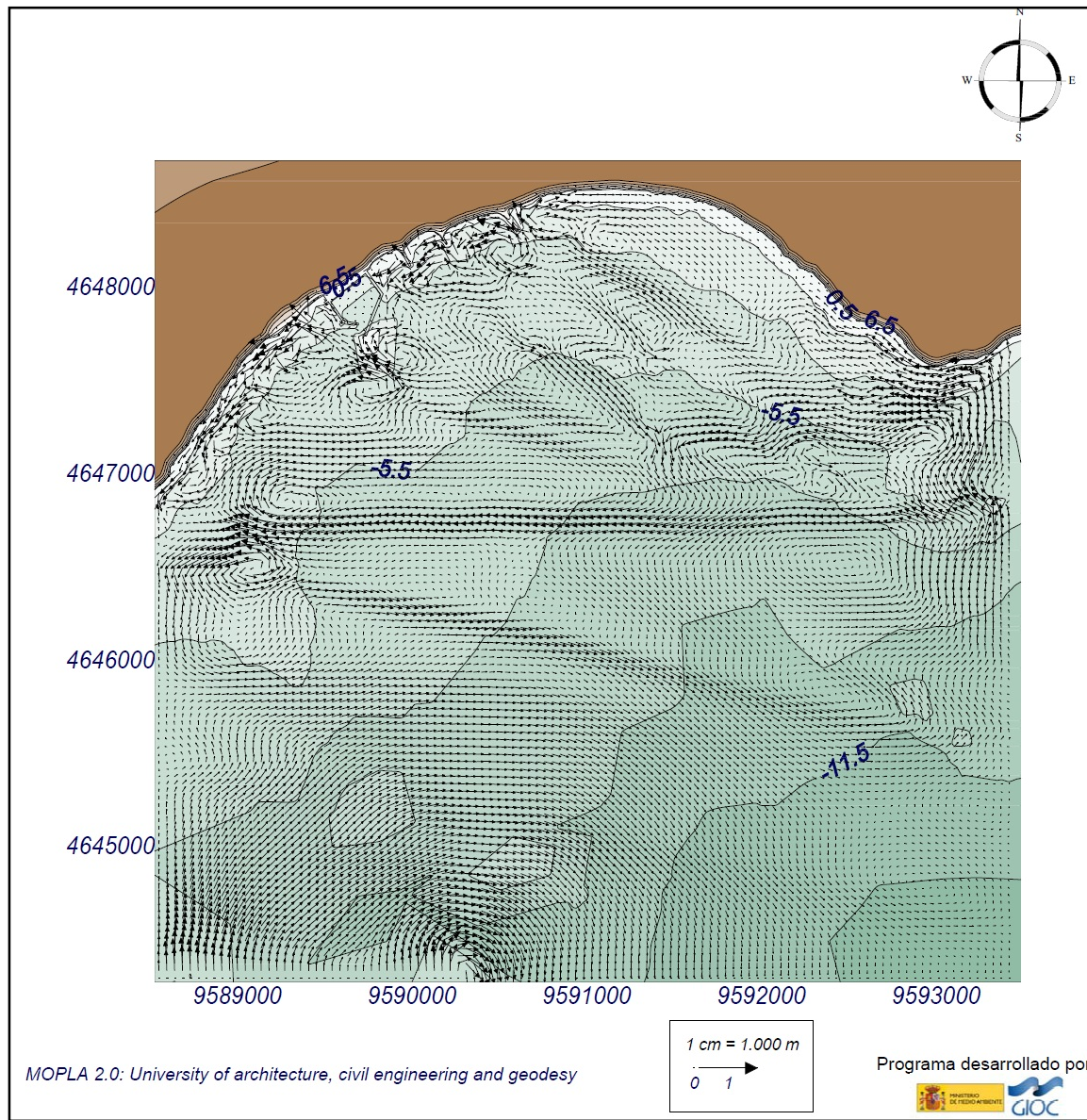
Chezy coefficient C: $10\text{m}^{1/2}/\text{s}$

Input wave height: 9.1 m

Vortex viscosity ε : $10\text{ m}^2/\text{s}$

Direction: 0° (E)

Maximum water level rise: 0.65 m



Numerical modeling of wave transformation and refraction

Direction of wave rays in computational grid points

Case study: E01

Direction: E

01: Storm with recurrence period once every 50 years, $H_{1\%}$

Simulation properties:

Period: 9.2 s

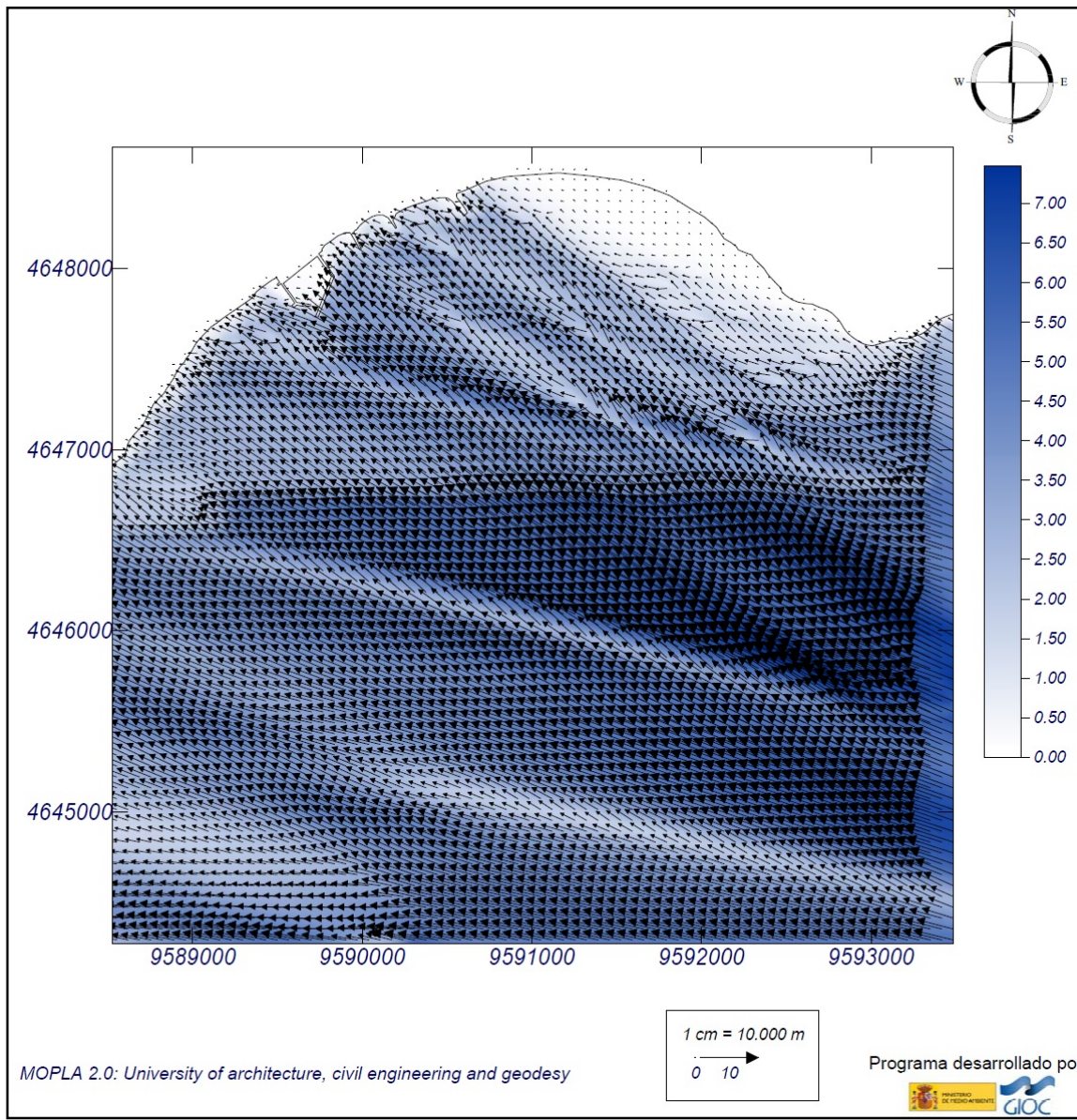
Chezy coefficient C : $10\text{m}^{1/2}/\text{s}$

Input wave height: 9.1 m

Vortex viscosity ε : $10\text{m}^2/\text{s}$

Direction: 0° (E)

Maximum water level rise: 0.65 m



Numerical modeling of wave transformation and refraction

Wave height

Case study: E02

Direction: E

02: Storm with recurrence period once every 50 years, $H_{5\%}$

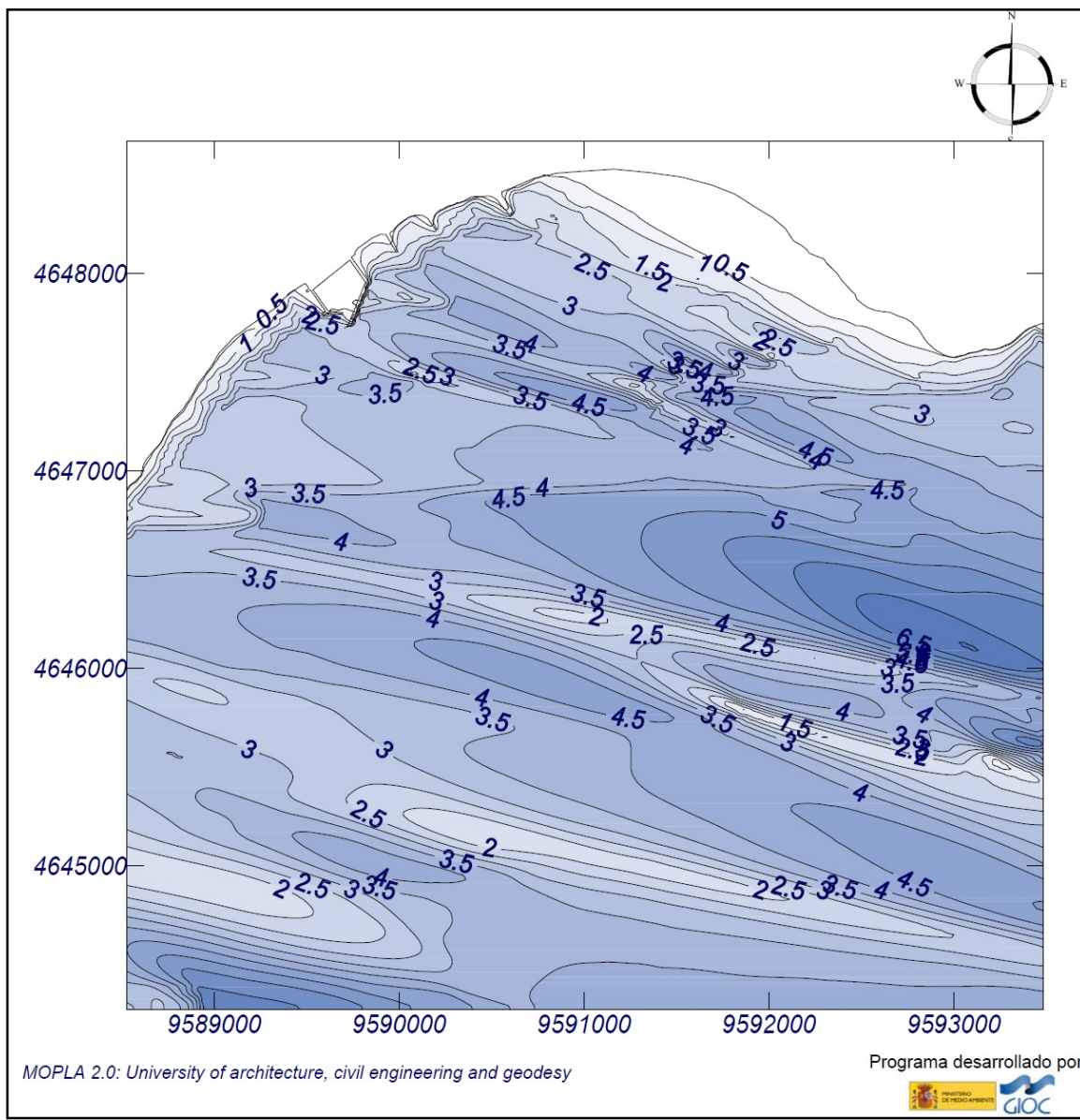
Simulation properties:

Period: 9.2 s

Input wave height: 7.65 m

Direction: 0° (E)

Maximum water level rise: 0.65 m



Numerical modeling of wave transformation and refraction

Wave height

Case study: E02

Direction: E

02: Storm with recurrence period once every 50 years, $H_{5\%}$

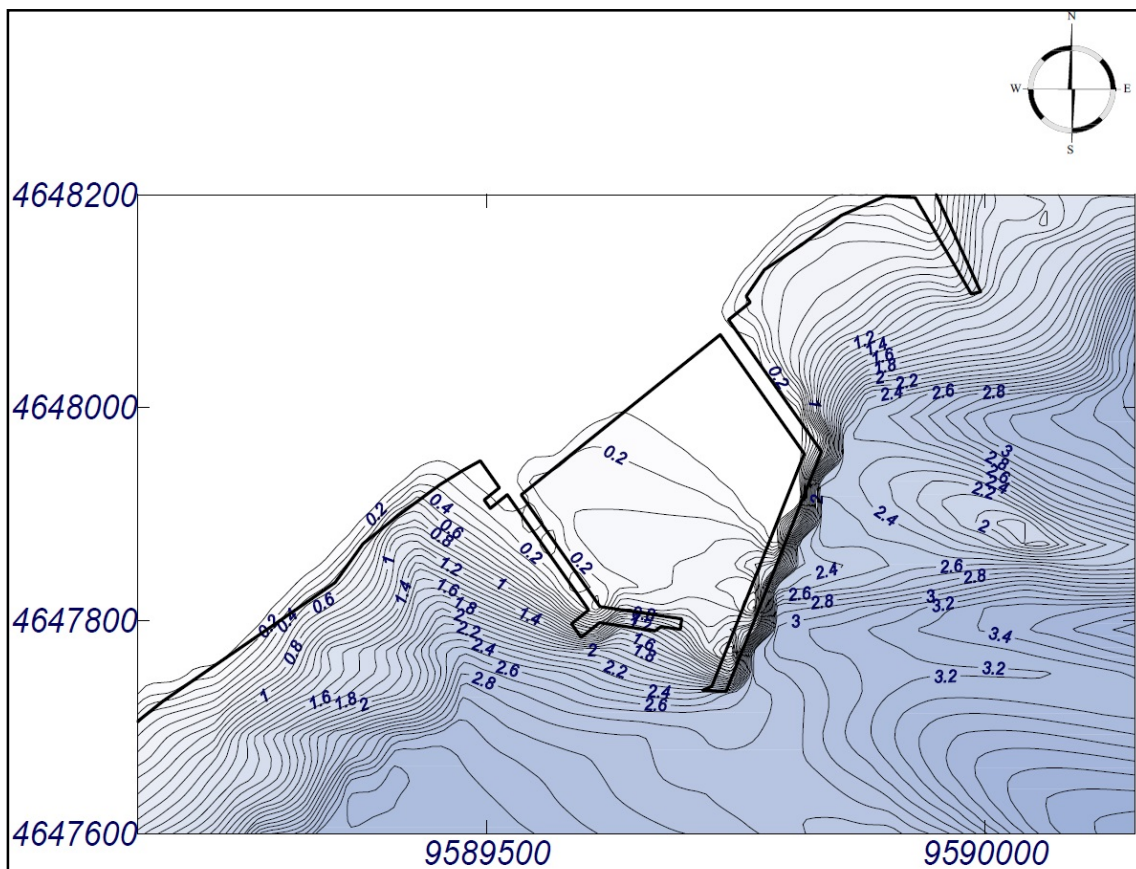
Simulation properties:

Period: 9.2 s

Input wave height: 7.65 m

Direction: 0° (E)

Maximum water level rise: 0.65 m



MOPLA 2.0: University of architecture, civil engineering and geodesy

Programa desarrollado por



Numerical modeling of wave transformation and refraction

Wave currents and bathymetry

Case study: E02

Direction: E

02: Storm with recurrence period once every 50 years, $H_{5\%}$

Simulation properties:

Period: 9.2 s

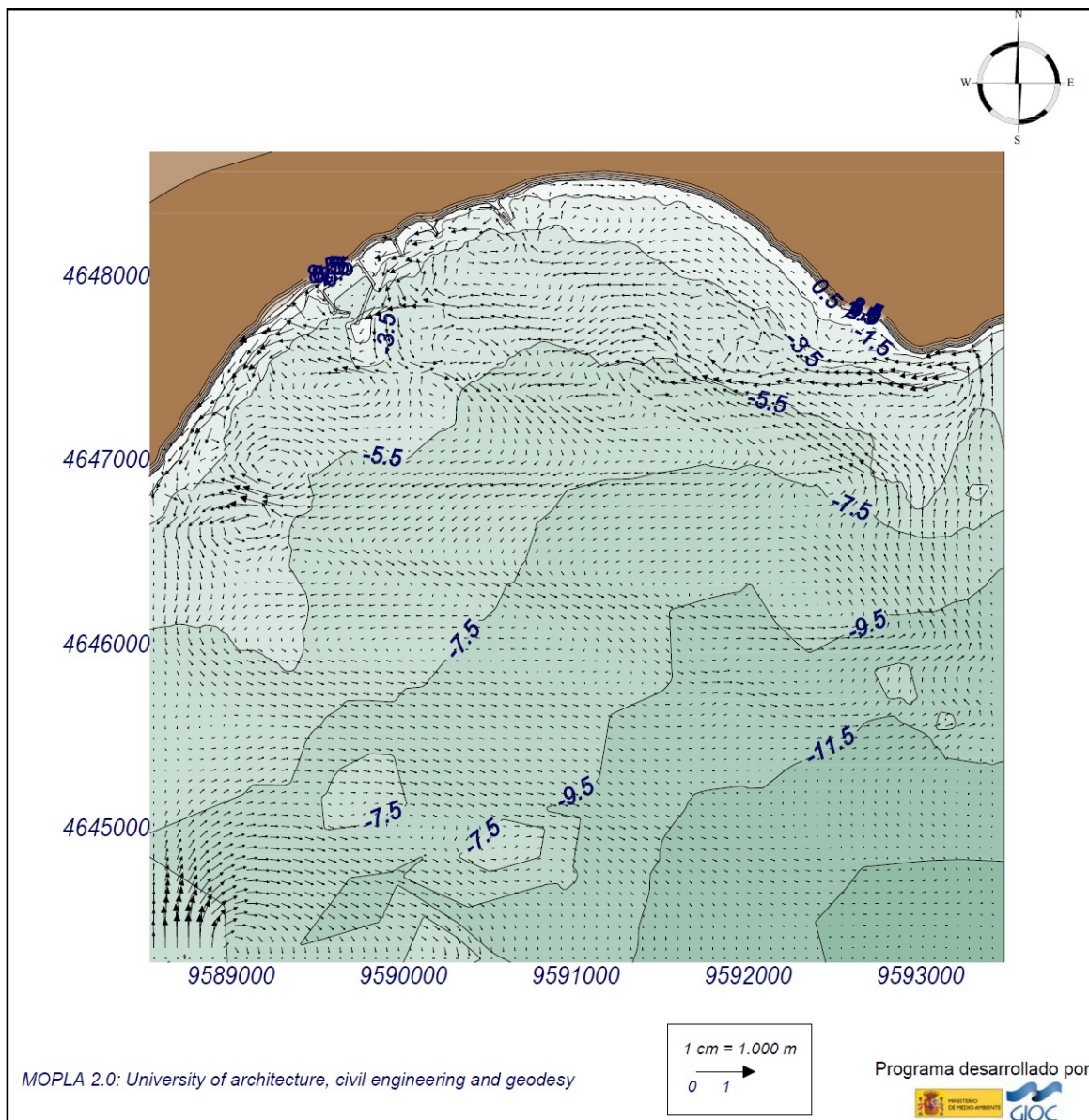
Chezy coefficient C: $10\text{m}^{1/2}/\text{s}$

Input wave height: 7.65 m

Vortex viscosity ε : $10\text{ m}^2/\text{s}$

Direction: 0° (E)

Maximum water level rise: 0.65 m



Numerical modeling of wave transformation and refraction

Direction of wave rays in computational grid points

Case study: E02

Direction: E

02: Storm with recurrence period once every 50 years, $H_{5\%}$

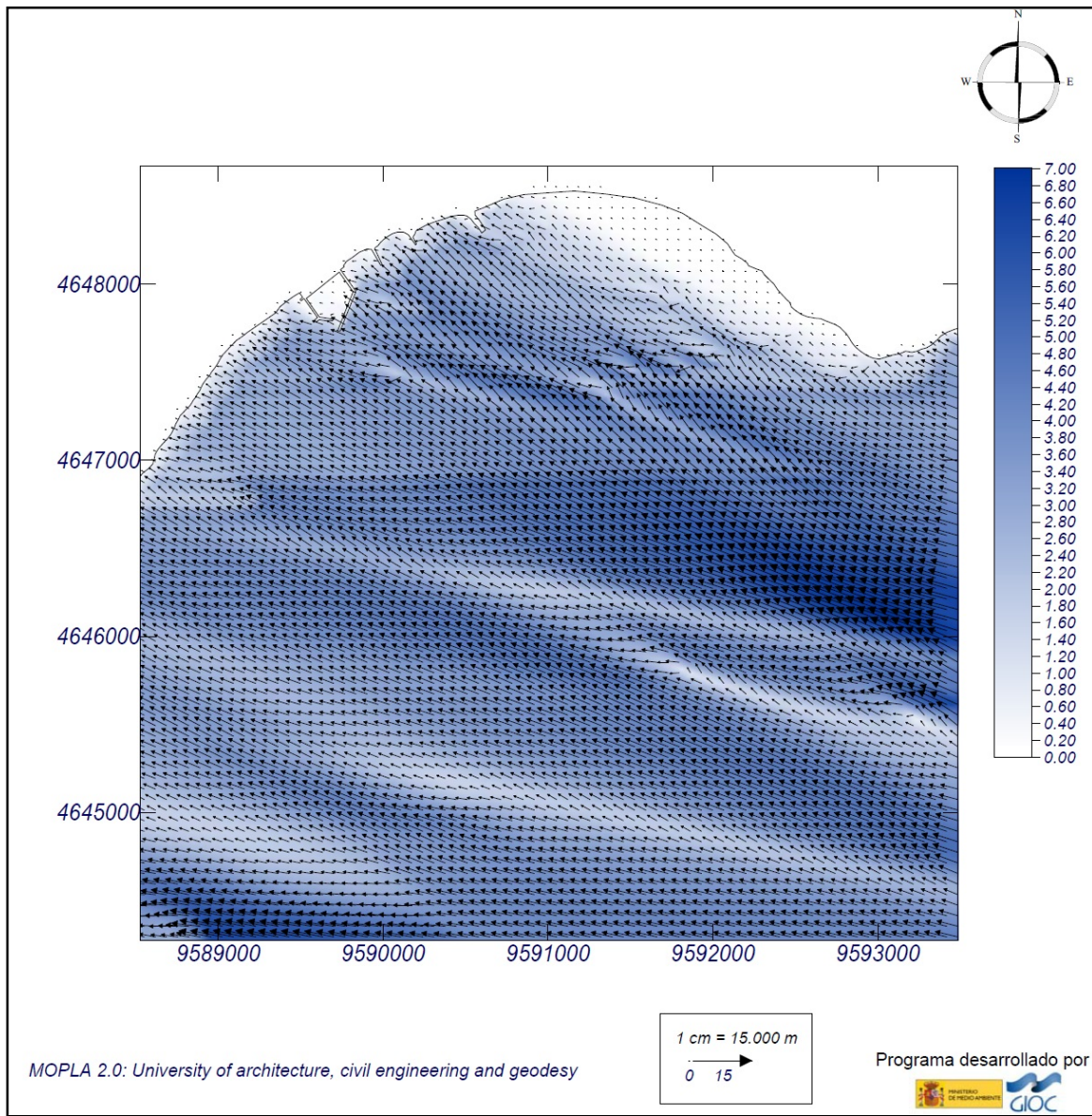
Simulation properties:

Period: 9.2 s

Input wave height: 7.65 m

Direction: 0° (E)

Maximum water level rise: 0.65 m



4.3.2 Waves from Southeast (SE)

Computation grid scheme – direction SE

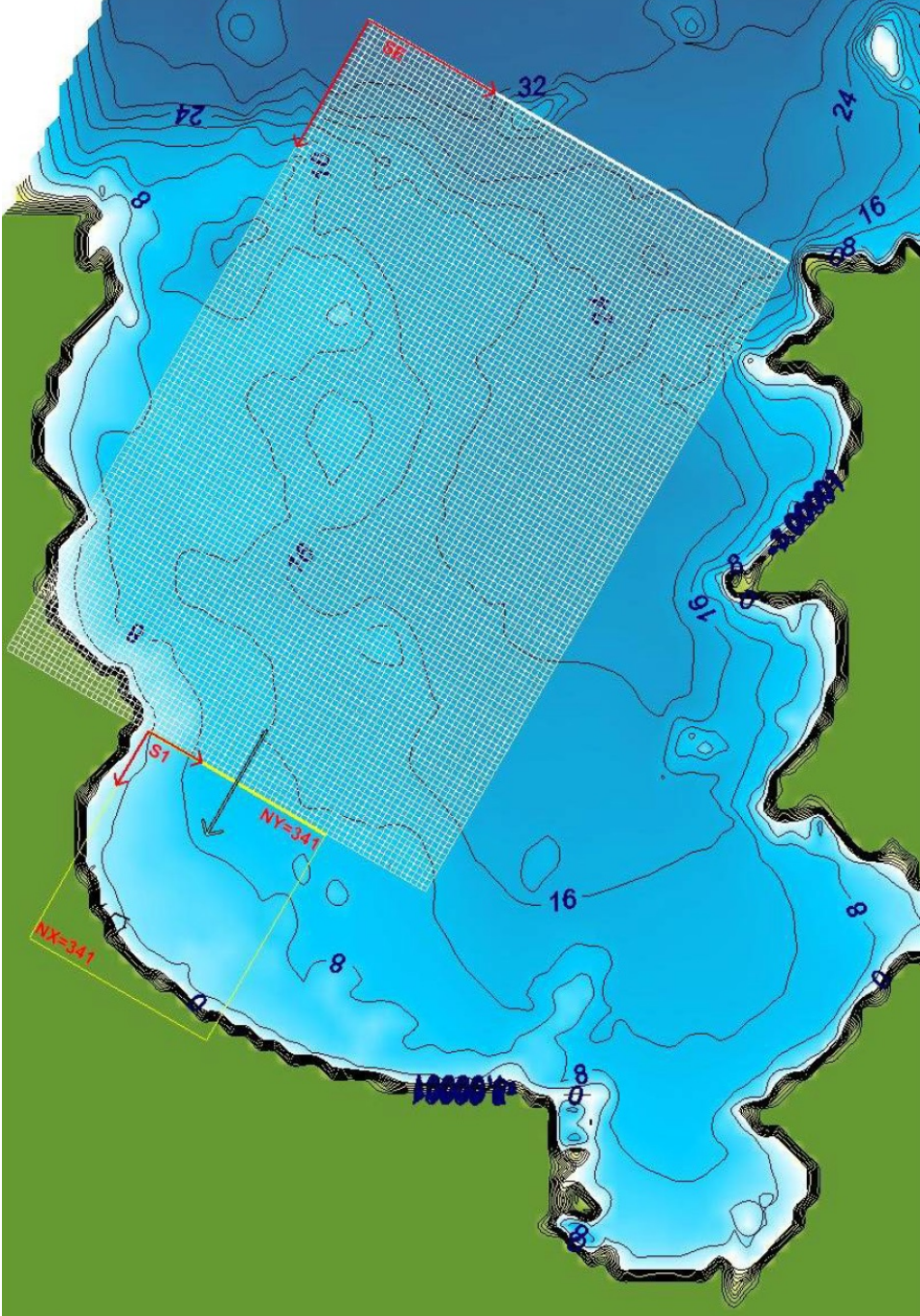


Figure 37: Computational grid – direction SE

Numerical modeling of wave transformation and refraction

Wave height

Case study: SE01

Direction: SE

01: Storm with recurrence period once every 50 years, $H_{1\%}$

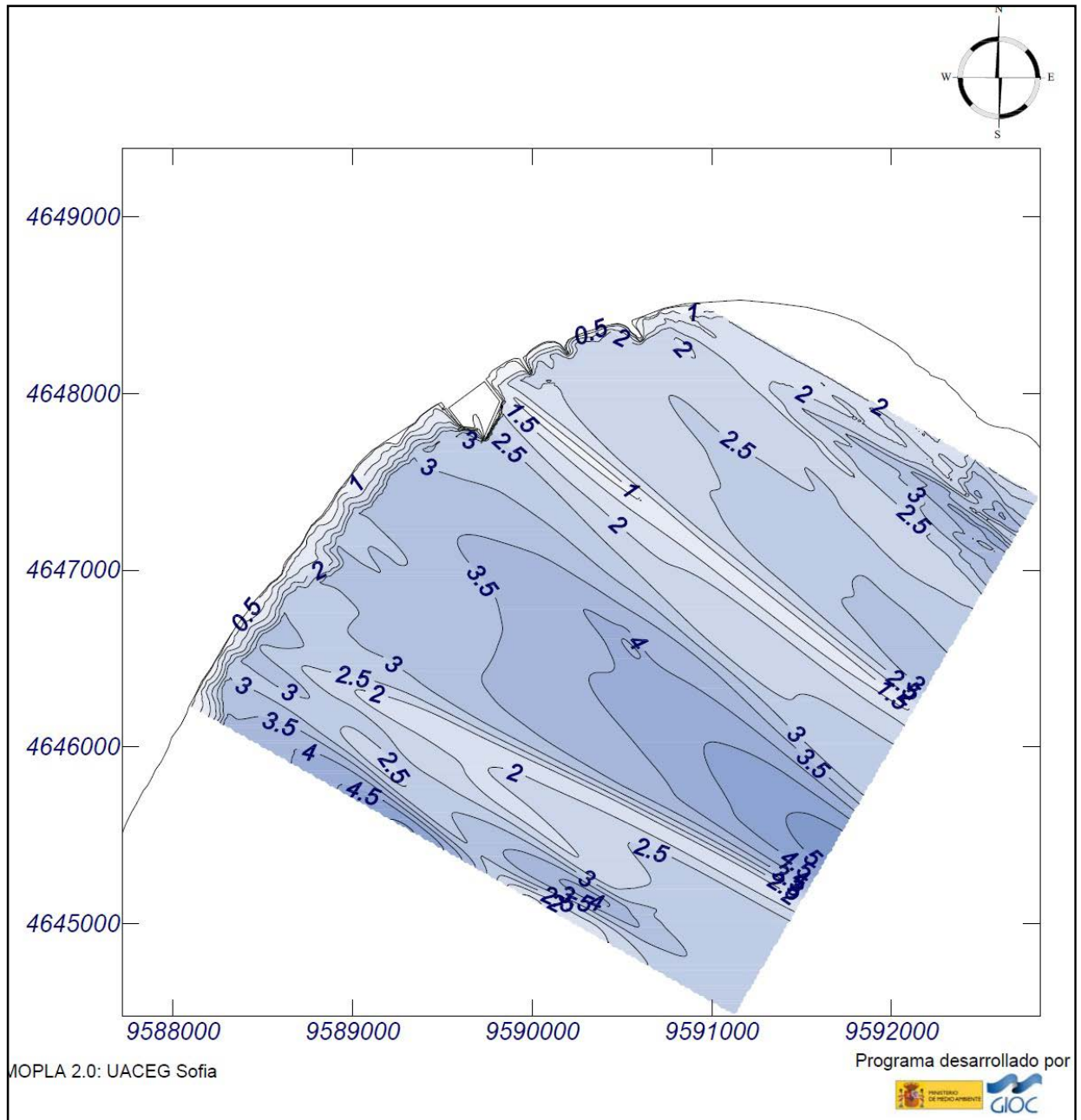
Simulation properties:

Period: 7.4 s

Input wave height: 5.0 m

Direction: 0° (S60.0E)

Maximum water level rise: 0.65 m



Numerical modeling of wave transformation and refraction

Wave height

Case study: SE01

Direction: SE

01: Storm with recurrence period once every 50 years, $H_{1\%}$

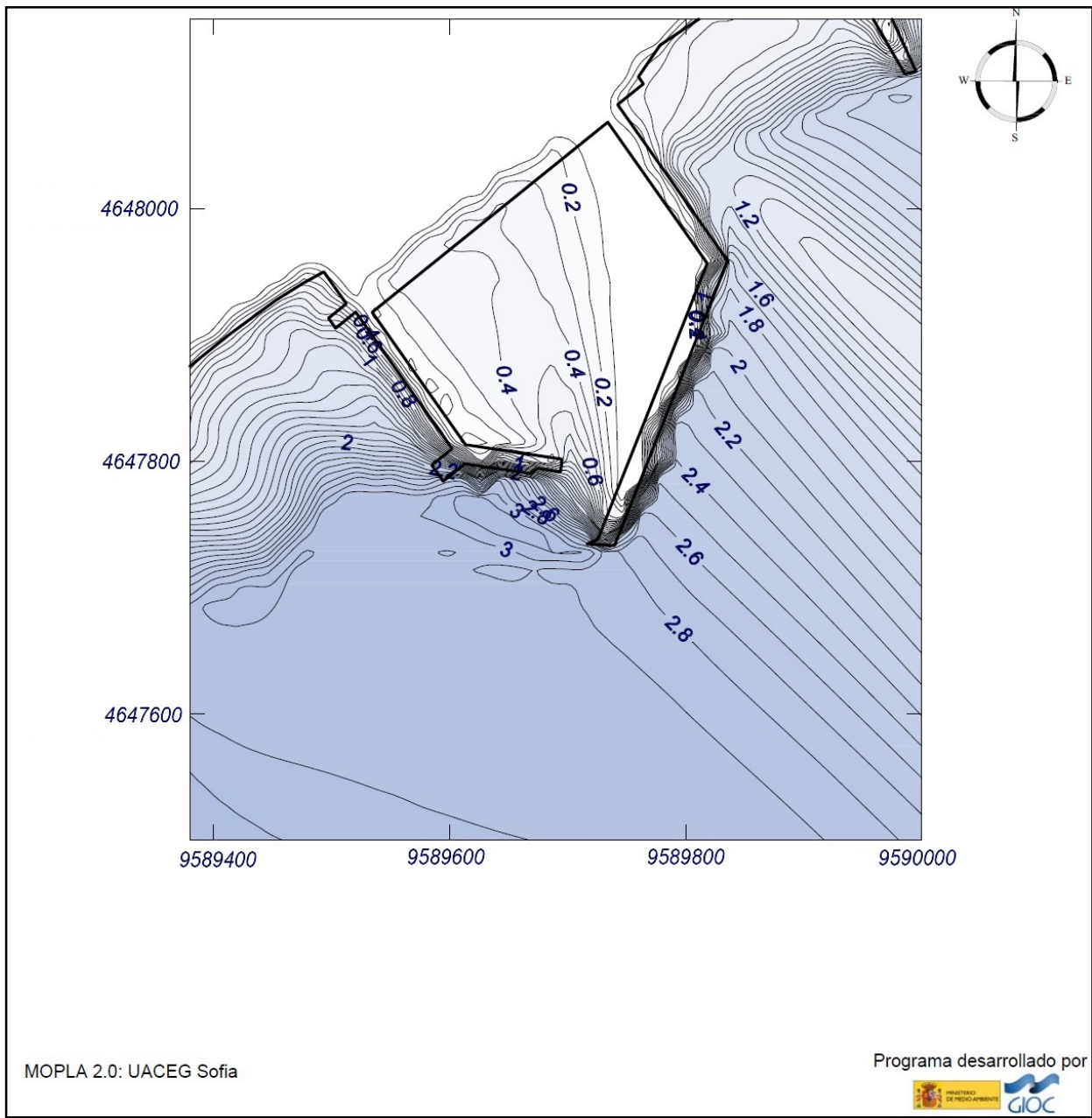
Simulation properties:

Period: 7.4 s

Input wave height: 5.0 m

Direction: 0° (S60.0E)

Maximum water level rise: 0.65 m



Numerical modeling of wave transformation and refraction

Wave currents and bathymetry

Case study: SE01

Direction: SE

01: Storm with recurrence period once every 50 years, $H_{1\%}$

Simulation properties:

Period: 7.4 s

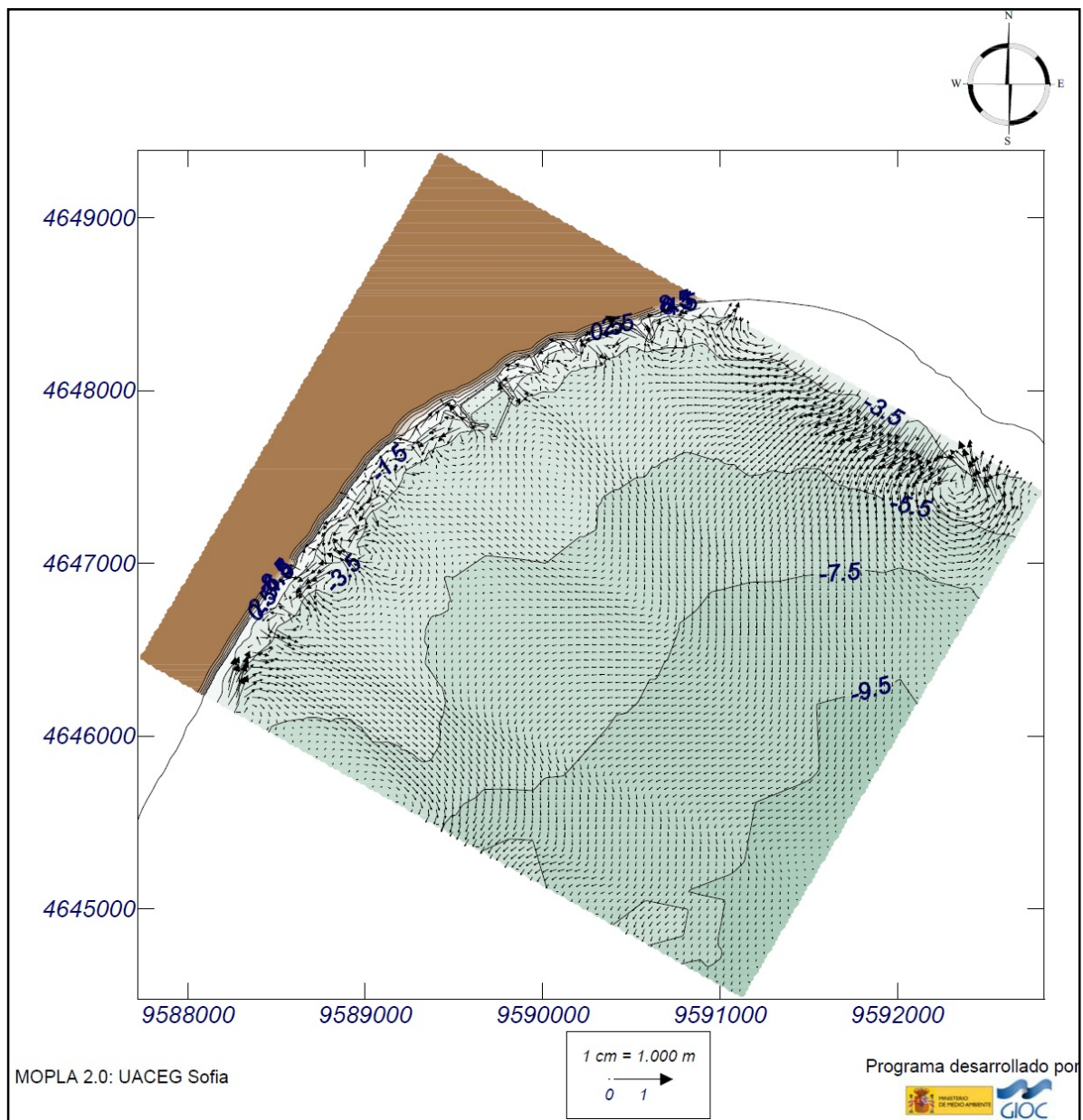
Chezy coefficient C: $10\text{m}^{1/2}/\text{s}$

Input wave height: 5.0 m

Vortex viscosity ϵ : $5\text{ m}^2/\text{s}$

Direction: 0° (S60.0E)

Maximum water level rise: 0.65 m



Numerical modeling of wave transformation and refraction

Direction of wave rays in computational grid points

Case study: SE01

Direction: SE

01: Storm with recurrence period once every 50 years, $H_{1\%}$

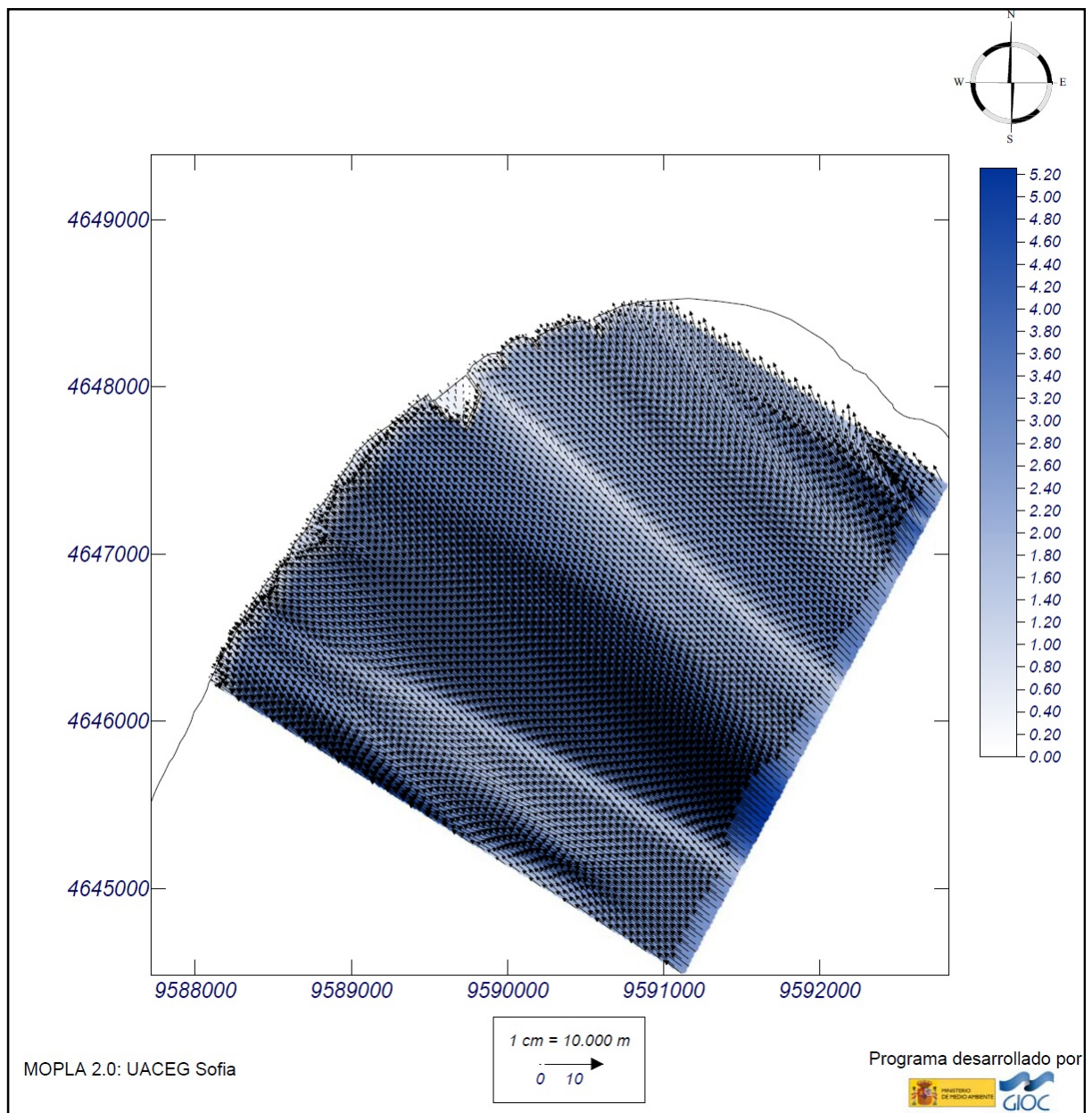
Simulation properties:

Period: 7.4s

Input wave height: 5.0 m

Direction: 0° (S60.0E)

Maximum water level rise: 0.65 m



Numerical modeling of wave transformation and refraction

Wave height

Case study: SE02

Direction: SE

02: Storm with recurrence period once every 50 years, $H_{5\%}$

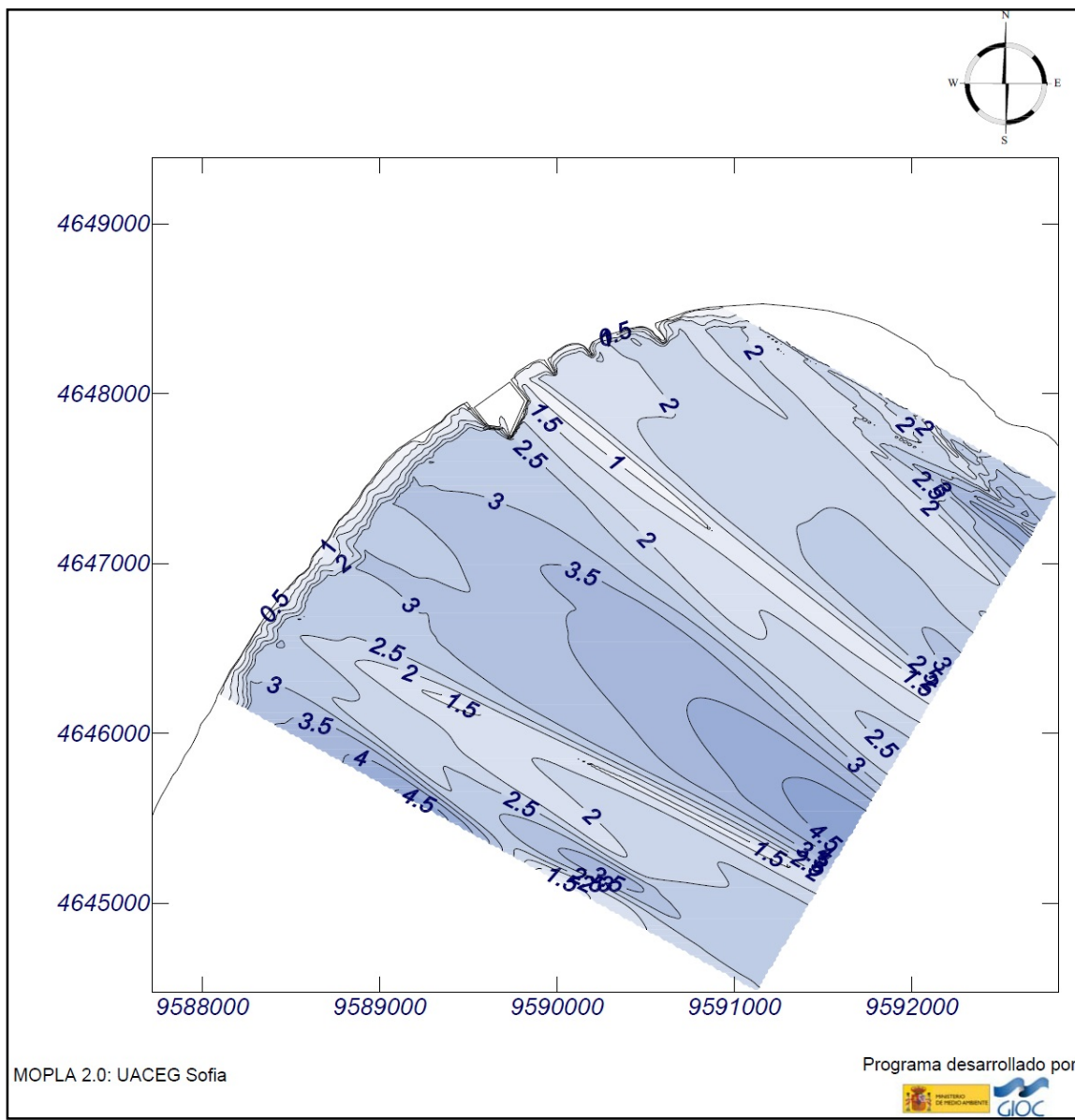
Simulation properties:

Period: 7.4 s

Input wave height: 4.55 m

Direction: 0° (S60.0E)

Maximum water level rise: 0.65 m



Numerical modeling of wave transformation and refraction

Wave height

Case study: SE02

Direction: SE

02: Storm with recurrence period once every 50 years, $H_{5\%}$

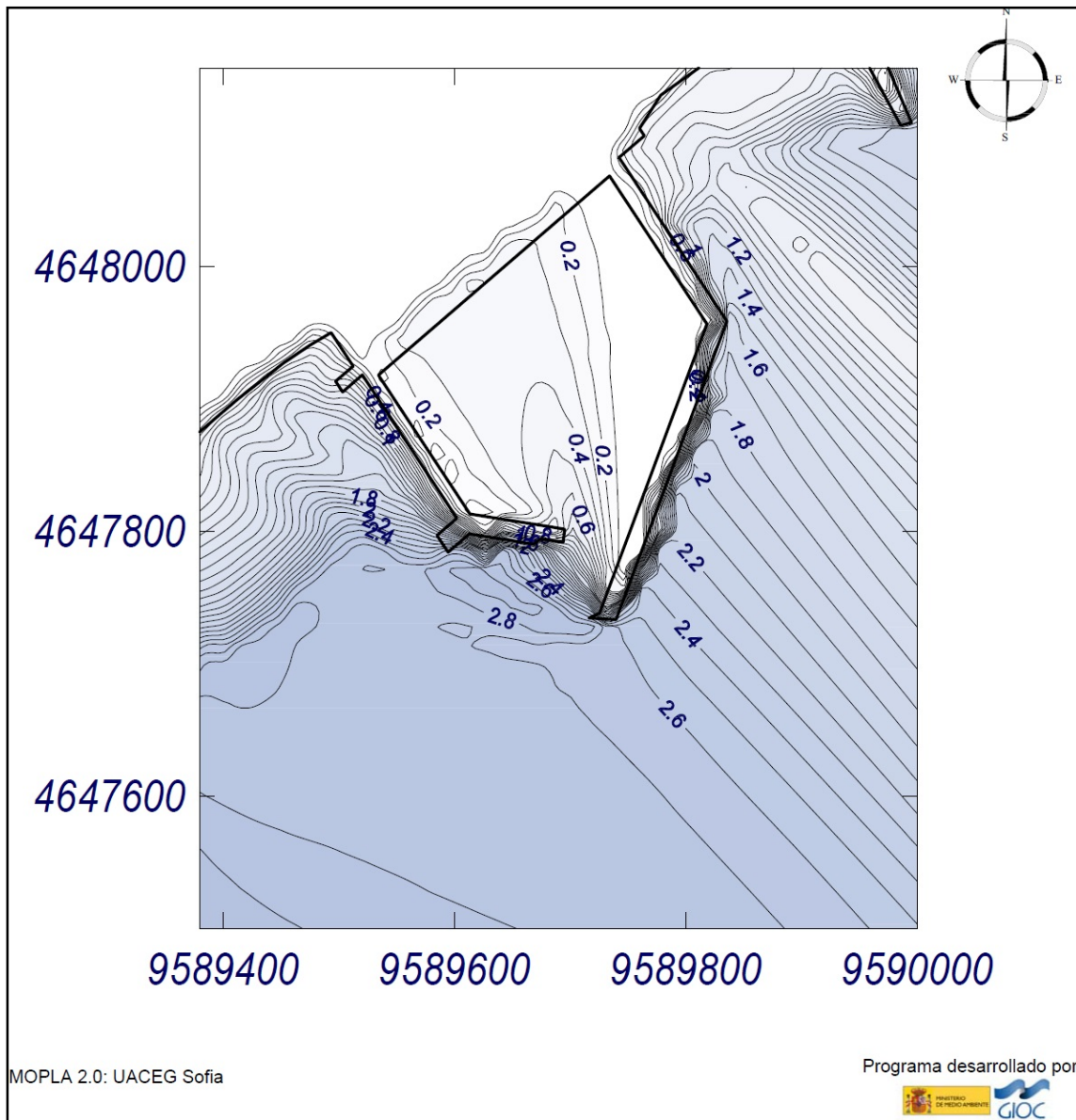
Simulation properties:

Period: 7.4 s

Input wave height: 4.55 m

Direction: 0° (S60.0E)

Maximum water level rise: 0.65 m



Numerical modeling of wave transformation and refraction

Wave currents and bathymetry

Case study: SE02

Direction: SE

02: Storm with recurrence period once every 50 years, $H_{5\%}$

Simulation properties:

Period: 7.4 s

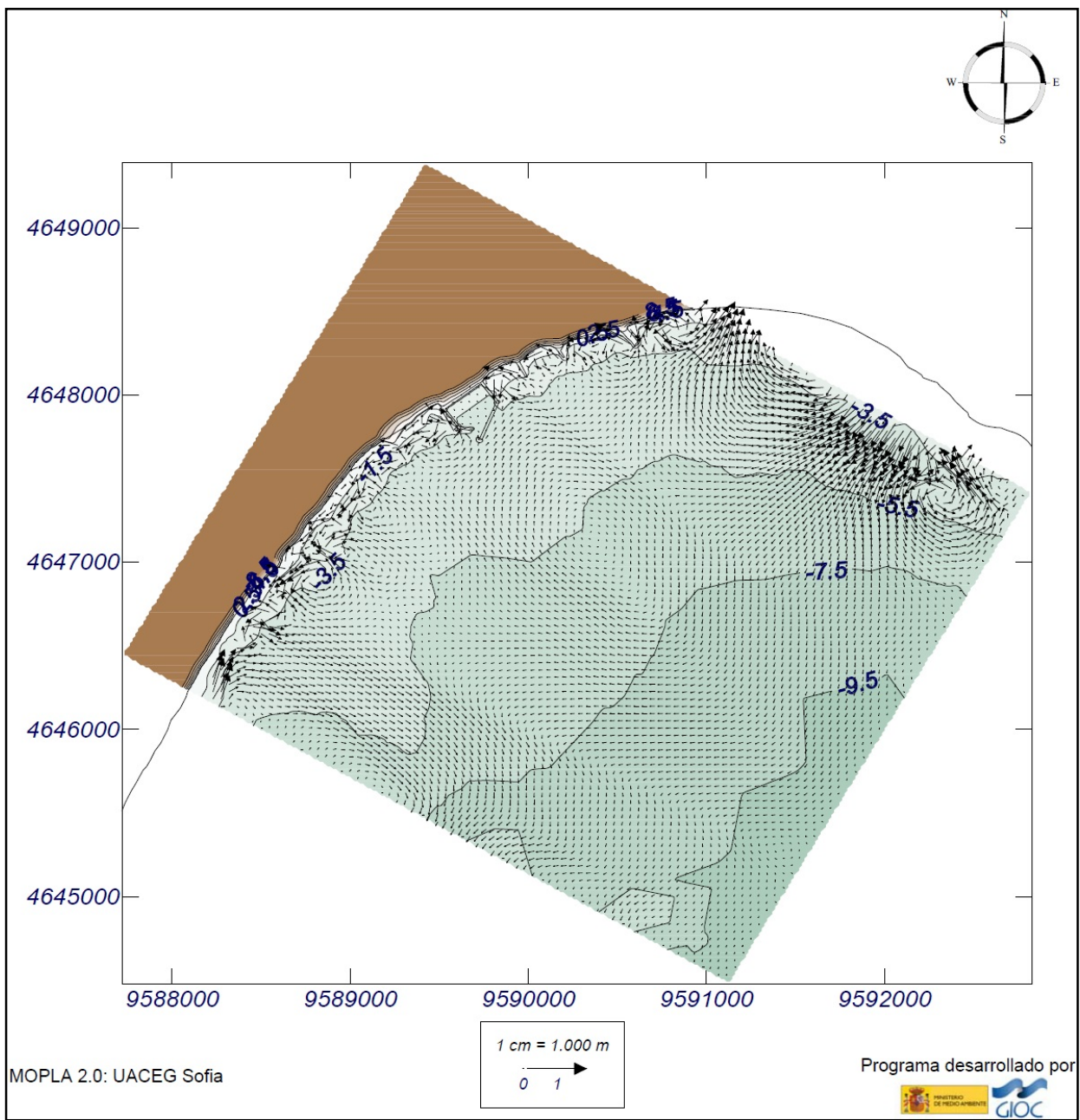
Chezy coefficient C: $10\text{m}^{1/2}/\text{s}$

Input wave height: 4.55 m

Vortex viscosity ϵ : $5\text{ m}^2/\text{s}$

Direction: 0° (S60.0E)

Maximum water level rise: 0.65 m



Numerical modeling of wave transformation and refraction

Direction of wave rays in computational grid points

Case study: SE02

Direction: SE

02: Storm with recurrence period once every 50 years, $H_{5\%}$

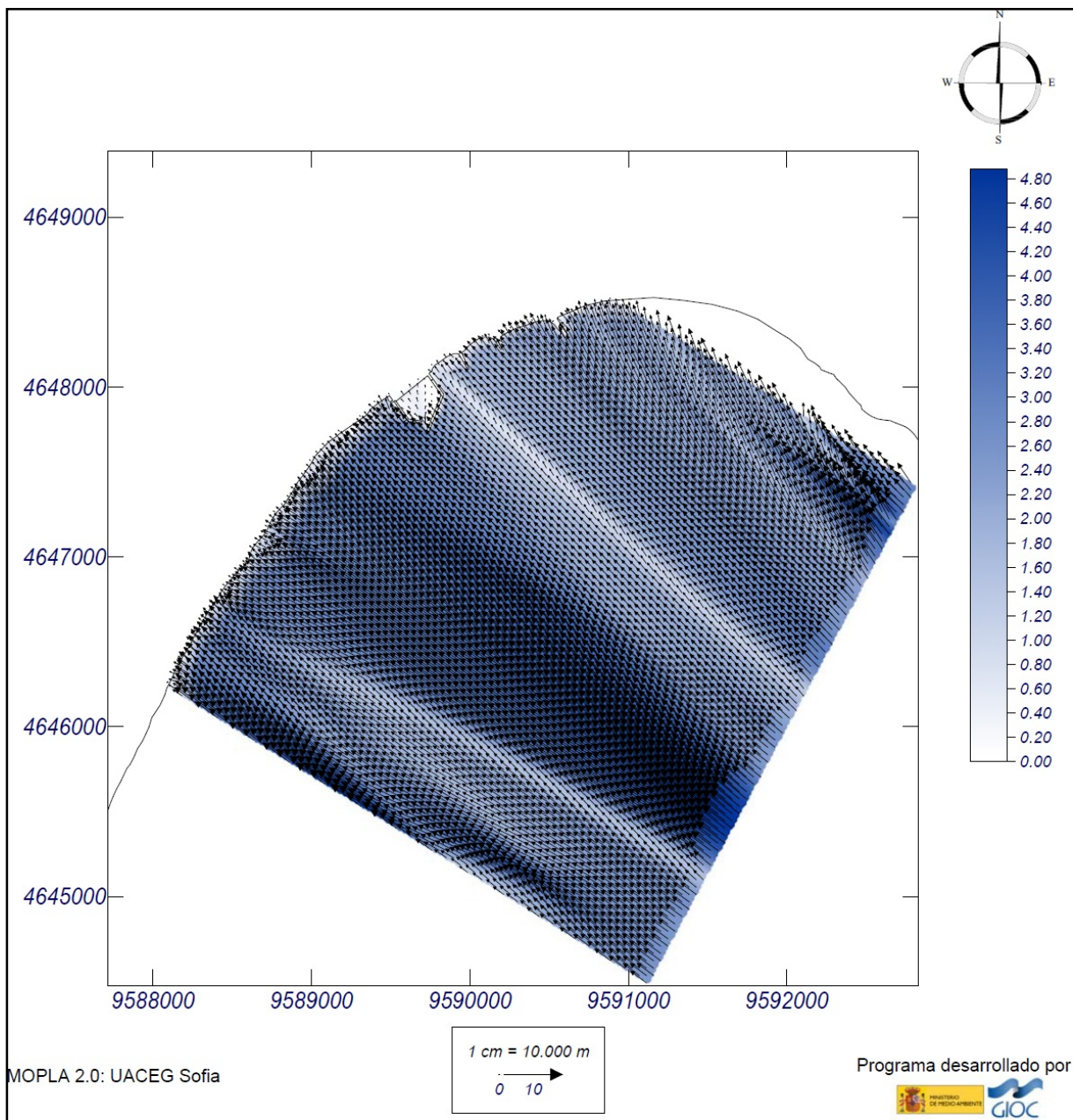
Simulation properties:

Period: 7.4 s

Input wave height: 4.55 m

Direction: 0° (S60.0E)

Maximum water level rise: 0.65 m



4.3.3 Waves from South (S)

Computation grid scheme – direction S



Figure 38: Computational grid – direction S

Numerical modeling of wave transformation and refraction

Wave height

Case study: S01

Direction: S

01: Storm with recurrence period once every 50 years, $H_{1\%}$

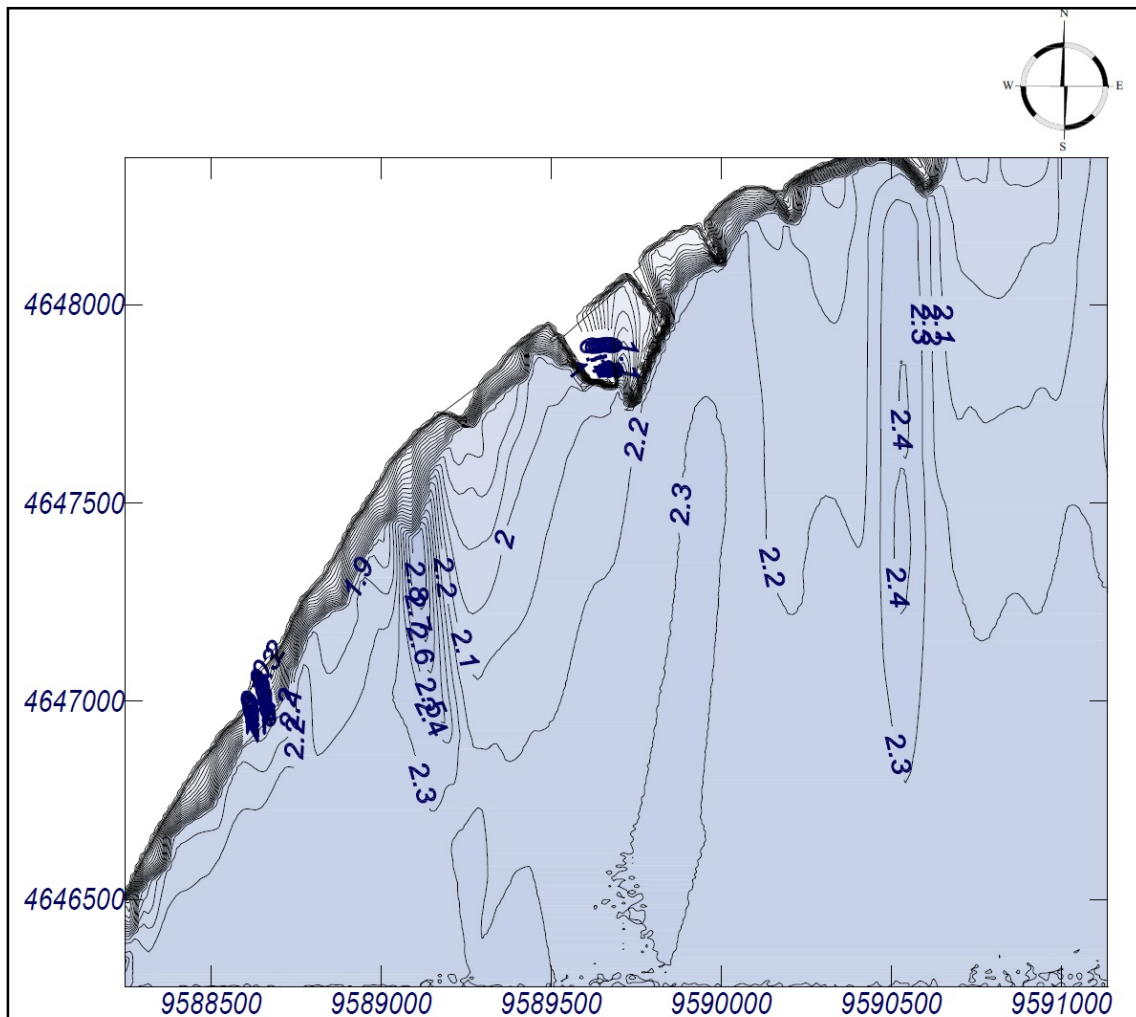
Simulation properties:

Period: 3.6 s

Input wave height: 2.3 m

Direction: 0° (S)

Maximum water level rise: 0.65 m



MOPLA 2.0: University of architecture, civil engineering and geodesy

Programa desarrollado por



Numerical modeling of wave transformation and refraction

Wave height

Case study: S01

Direction: S

01: Storm with recurrence period once every 50 years, $H_{1\%}$

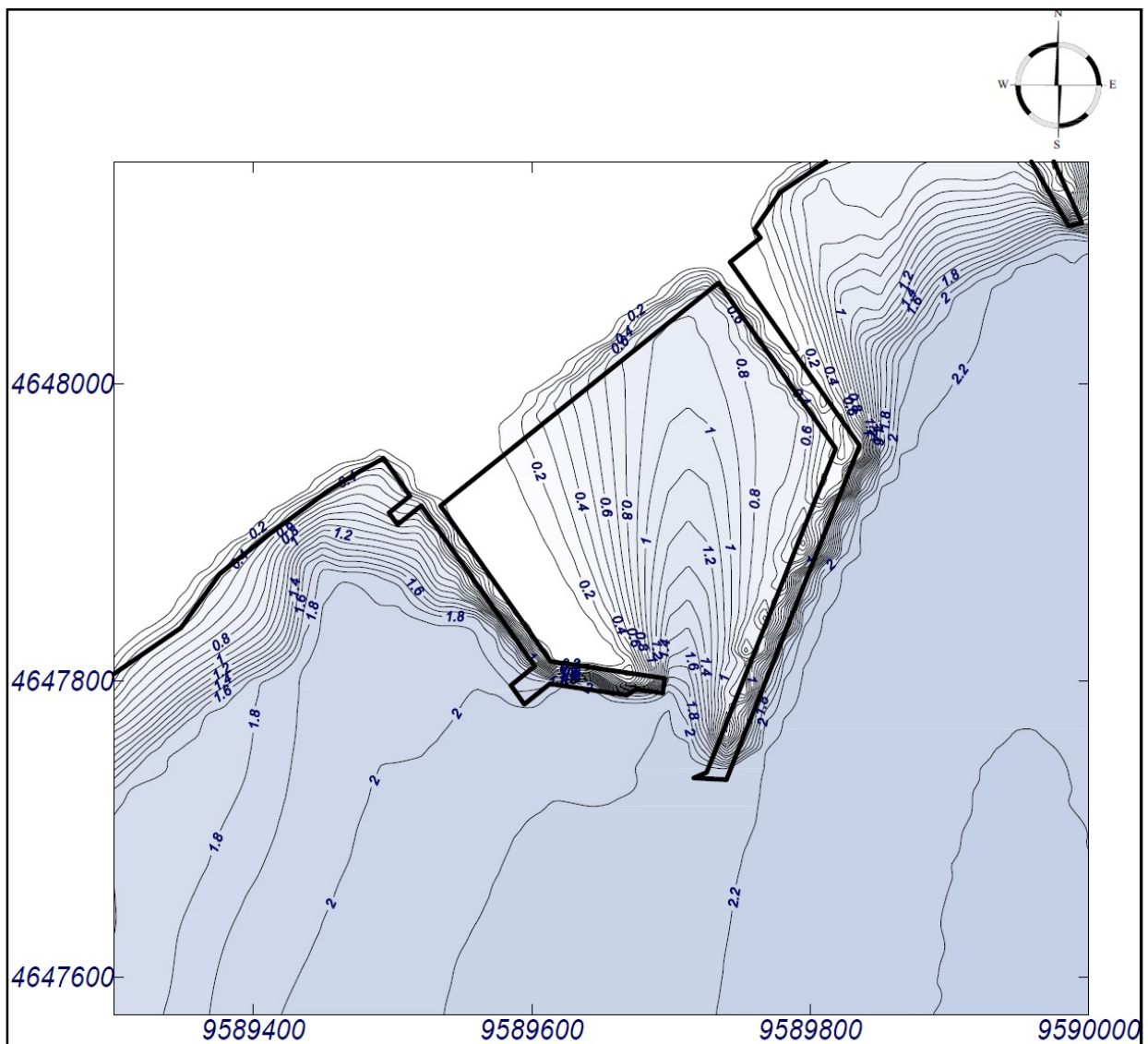
Simulation properties:

Period: 3.6 s

Input wave height: 2.3 m

Direction: 0° (S)

Maximum water level rise: 0.65 m



MOPLA 2.0: University of architecture, civil engineering and geodesy

Programa desarrollado por



Numerical modeling of wave transformation and refraction

Direction of wave rays in computational grid points

Case study: S01

Direction: S

01: Storm with recurrence period once every 50 years, $H_{1\%}$

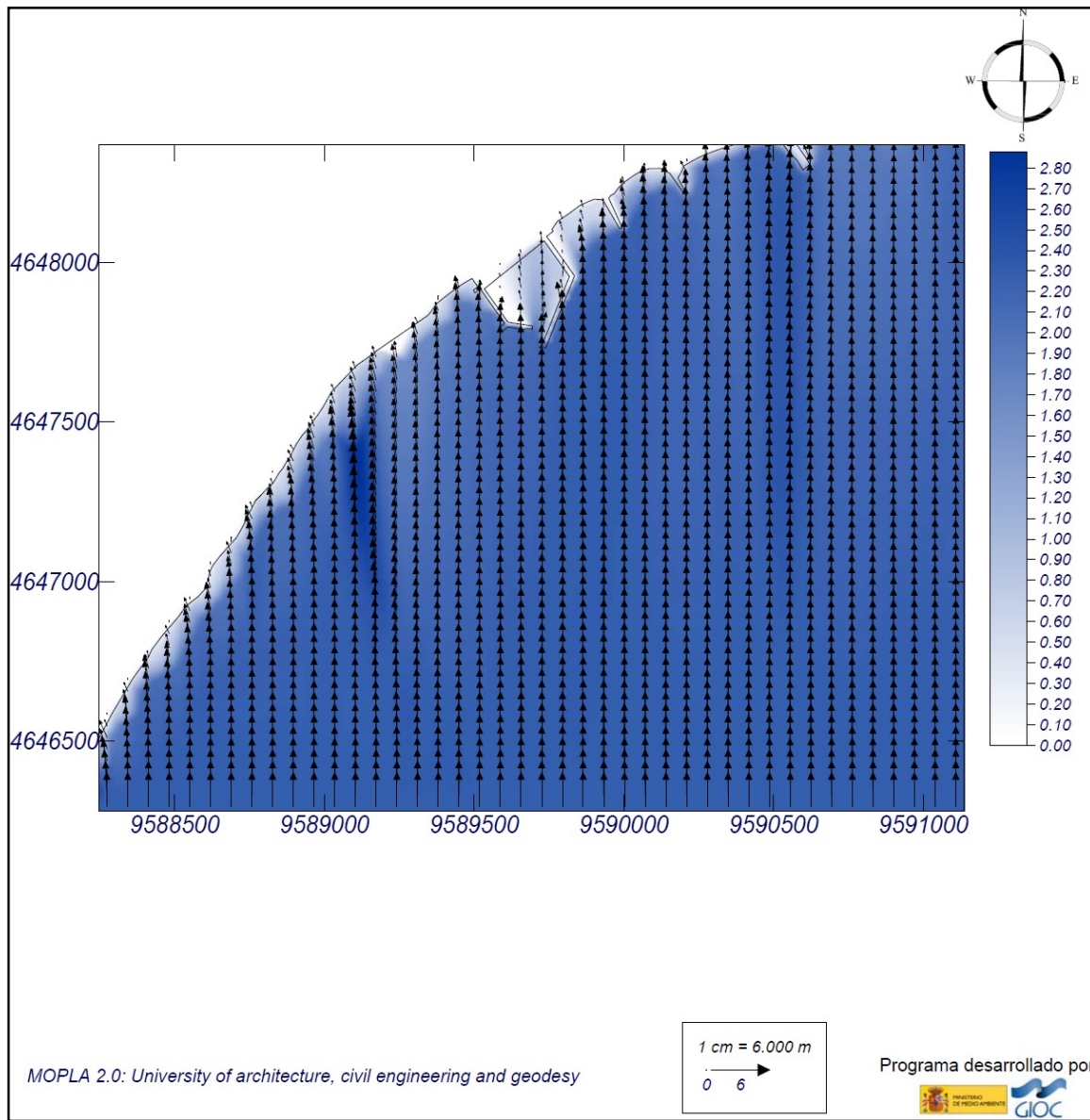
Simulation properties:

Period: 3.6 s

Input wave height: 2.3 m

Direction: 0° (S)

Maximum water level rise: 0.65 m



Numerical modeling of wave transformation and refraction

Wave height

Case study S02

Direction: S

02: Storm with recurrence period once every 50 years, $H_{5\%}$

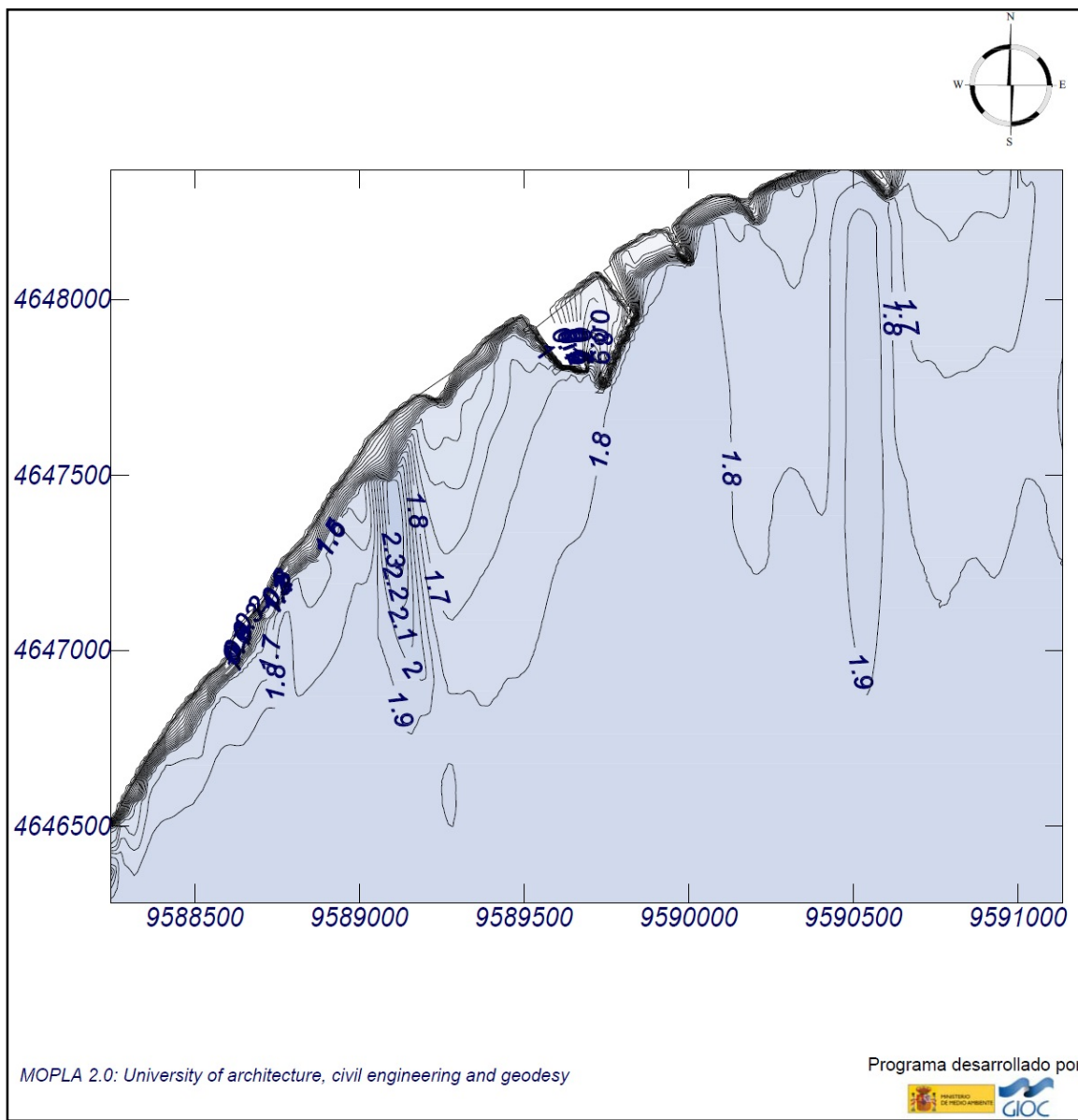
Simulation properties:

Period: 3.6 s

Input wave height: 1.88 m

Direction: 0° (S)

Maximum water level rise: 0.65 m



Numerical modeling of wave transformation and refraction

Wave height

Case study S02

Direction: S

02: Storm with recurrence period once every 50 years, $H_{5\%}$

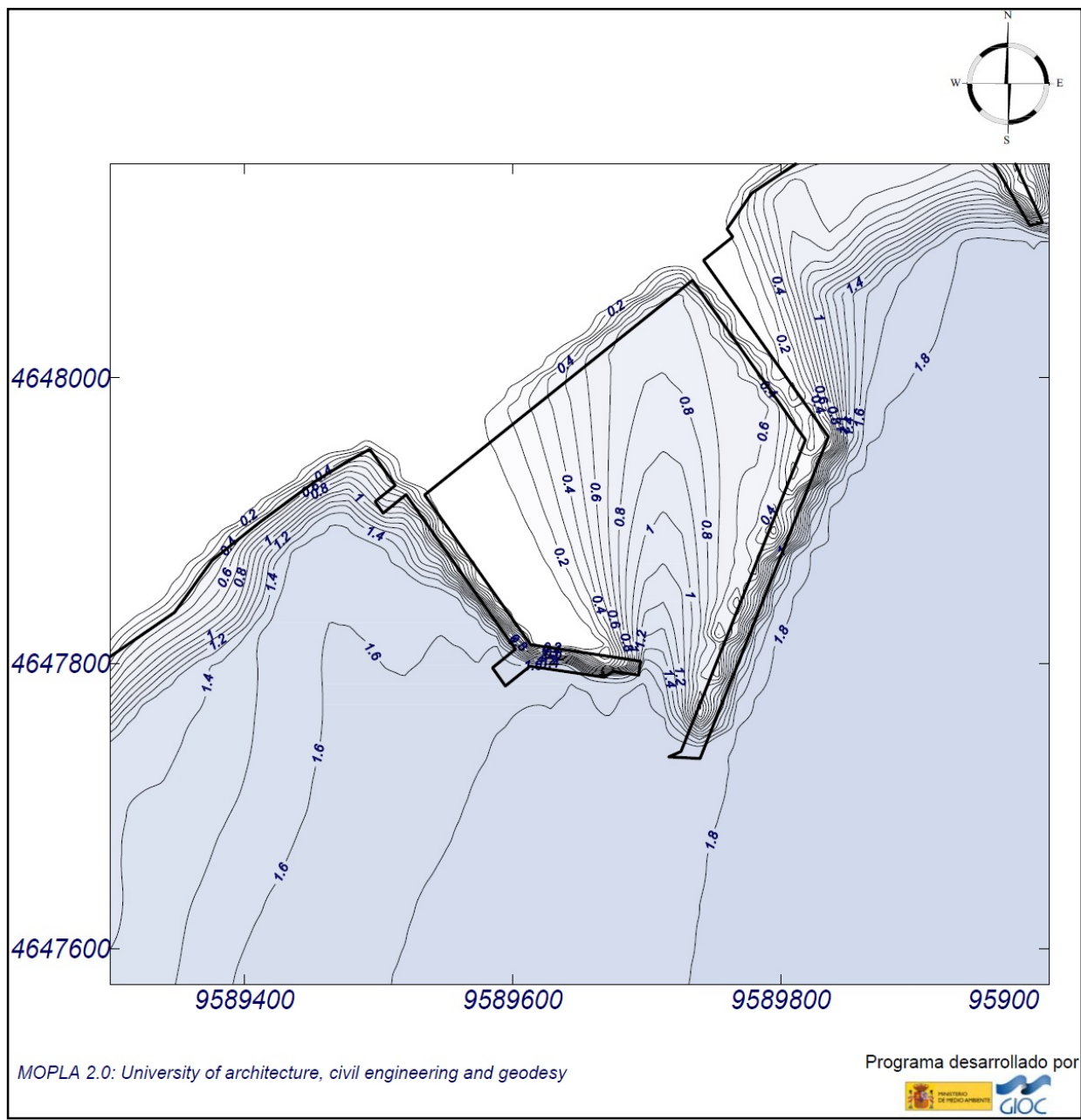
Simulation properties:

Period: 3.6 s

Input wave height: 1.88 m

Direction: 0° (S)

Maximum water level rise: 0.65 m



Numerical modeling of wave transformation and refraction

Direction of wave rays in computational grid points

Case study S02

Direction: S

02: Storm with recurrence period once every 50 years, $H_{5\%}$

Simulation properties:

Period: 3.6 s

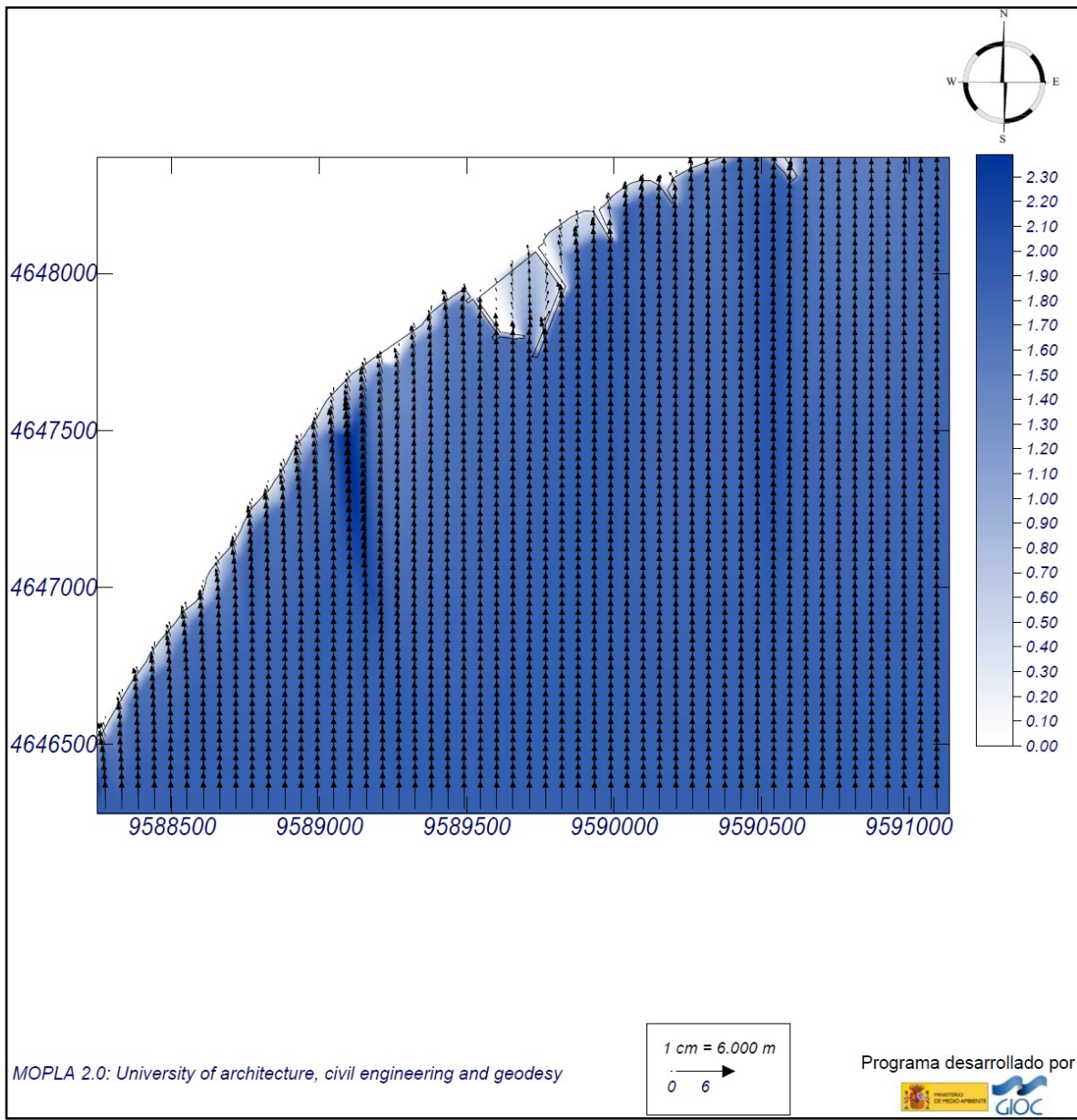
Chezy coefficient C: $10\text{m}^{1/2}/\text{s}$

Input wave height: 1.88 m

Vortex viscosity ϵ : $5\text{ m}^2/\text{s}$

Direction: 0° (S)

Maximum water level rise: 0.65 m



4.4 Analysis of the results obtained through numerical modeling

The wave heights in characteristic points A-J along the breakwater toe and at the harbor entrance determined by means of numerical modeling are presented in Table 29.

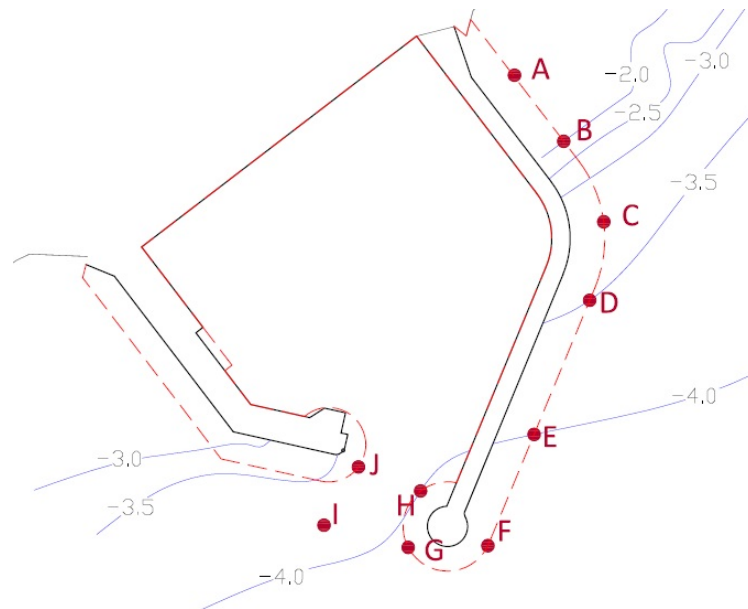


Figure 39: Scheme of characteristic points for computation analysis

Table 29: Computed wave heights (from chapter 4.3)

Point	A	B	C	D	E	F	G	H	I	J
Water depth [m]	1	2	3.2	3.5	4	4.5	4.2	3.5	3.5	3
E01: Period 9.2s, Input wave height 9.1m										
Wave height $H_{1\%}$ [m]	0.4	1	2.6	3.2	3.4	3.5	2.8	1.6	2.4	2
E02: Period 9.2s, Input wave height 7.65m										
Wave height $H_{5\%}$ [m]	0.3	1	2.2	2.4	2.6	3	2.6	2.2	1.8	1.6
SE01: Period 7.4s, Input wave height 5.0m										
Wave height $H_{1\%}$ [m]	0.6	0.8	1.6	1.8	2.4	2.8	3	2.4	3.2	2
SE02: Period 7.4s, Input wave height 4.55m										
Wave height $H_{5\%}$ [m]	0.4	0.7	1.5	1.7	2.2	2.4	2.8	2.2	2.9	1.7
S01: Period 3.2s, Input wave height 1.43m										
Wave height $H_{1\%}$ [m]	0	0.1	1.2	1.3	1.3	1.3	1.4	1.2	1.3	1.2
S02: Period 9.2s, Input wave height 1.17m										
Wave height $H_{5\%}$ [m]	0	0	1	1.1	1.1	1.2	1.2	1	1.2	1

The most adverse storms for the three source directions are with recurrence time of 50 years. A brief description of each of the three wave directions follows:

Waves with direction E

As stated above, this direction includes the input wave motion in deep water in the whole sector from N to E. Because of the particular configuration of the coastline and the bathymetry of the Bourgas Bay the waves from the three input directions N, NE and E enter the bay as input swell where the N and NE waves undergo significant refraction when passing around Cape Emine and then around Cape Pomorie and finally enter the Bourgas Bay from E. This gives grounds for the E direction to be investigated as the least favorable from this sector.

The results for “direction of wave rays in the computational grid points” in graphic form (section 4.3.1) show that the wave rays with initial direction E in deep water reach the zone of fishing harbor Sarafovo with direction SE – ESE.

Due to the varying depth along the Northern quay-mole, the latter is attacked by waves of different height and therefore it is useful to divide the facility into three zones when determining the wave load, the weight of the armour units and the height of the wave turning wall (see Figure 40). The assumed design wave properties for the dimensioning of the facility in the three zones, as well as the average water depth for each zone are shown in Table 35. The maximum diffracted wave height entering the harbor is ca. 0.70m. The wave conditions in the region are presented in section 4.3.1.

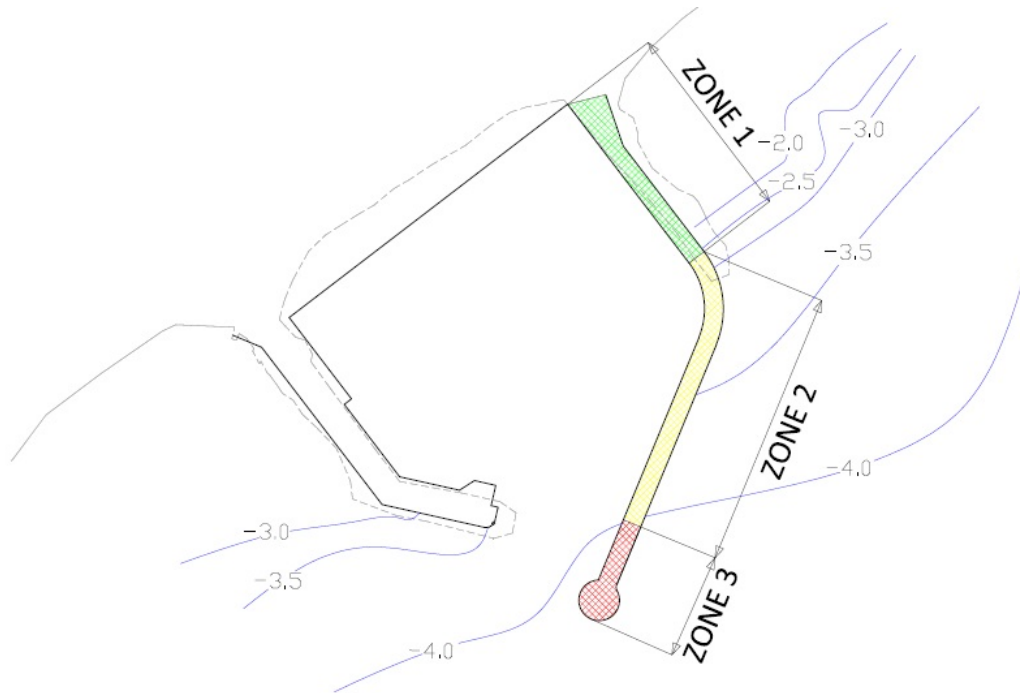


Figure 40: Wave load zones along the Northern breakwater

Waves with direction SE

The graphic results from the modeling (section 4.3.2) show that the SE waves do not undergo transformation in terms of their direction.

Similarly to the waves from E, due to varying depth along the facility, it will be attacked by waves of different height between 3.0 m. and 1.6 m. The maximum diffracted wave height entering the harbor basin is ca. 0.60 m.

Waves with direction S

Results indicate that the southern waves, generated in the bay of Burgas, also reach the harbor without any change in their direction in the computational grid points for recurrence period 50 years (section 4.3.3).

The maximum wave height for a storm with recurrence time 50 years and probability of exceedance in the system 1% is estimated to be ca. 2.0m. The maximum diffracted wave height in the harbor basin in this case exceeds 1.20m.

The layout arrangement studied enable reliable wave protection for virtually all days in an average year and ca. 330-340 days in a year with probability of recurrence with respect to storm conditions once every 50 years

Conditions for resonance phenomena in the harbor area are extremely unlikely to occur. Such conditions would be created through a massive earthquake or an explosion in the Black Sea [19].

5 Calculation of wave transformation and refraction from 12m depth to the protective structure according to the "Standards for loads and impacts of hydraulic structures by waves, ice and vessels" [2], valid presently in Bulgaria

5.1 Wave properties at 12m depth

The wave properties at depth 12m are calculated by means of the wave models WAM and SWAN as a preliminary research for the project (article 3.4) The input data for the calculation of the wave properties is presented in Table 24 and Table 25. Adopted as design wave parameters are the ones with probability of exceedance 1% and probability of recurrence once every 50 years - $H_{1\%}=8.0m$ with a period of $T_{av}=9.2s$ for waves from E and $H_{1\%}=4.9m$ with a period of $T_{av}=7.4s$ for waves from SE. It is assumed that the wave period from deep water to the breakwater remains unchanged.

The mean wave length in deep water $\bar{\lambda}_d$ is calculated by using the formula $\lambda d = \frac{g \cdot \bar{T}^2}{2\pi} \approx 1.562 \cdot \bar{T}^2$ (5.1):

$$\bar{\lambda}_d = \frac{g \cdot \bar{T}^2}{2\pi} \approx 1.562 \cdot \bar{T}^2 \quad (5.1)$$

$$\bar{\lambda}_{d,E} = \frac{9.81 \cdot 9.2^2}{2\pi} = 132m \text{ – for waves from E}$$

$$\bar{\lambda}_{d,SE} = \frac{9.81 \cdot 7.4^2}{2\pi} = 85m \text{ – for waves from SE.}$$

5.2 Plan of refraction

The plan of refraction is drawn according to the "Standards for loads and impacts of hydraulic structures by waves, ice and vessels", Section 1, Art. 24/2 [2], as follows:

Towards the initial isobath H_0 (-12m) two rays are drawn in the according wave direction at distance $a_d = (1 \div 2) \cdot \bar{\lambda}_d$ from one another 200m for waves from the East and 150m for waves from the Southeast (drawing 2). Even isobaths are considered principal while the odd ones are medial (intermediate). The latter are averaged with a smoothing curve. The rays change their direction namely there.

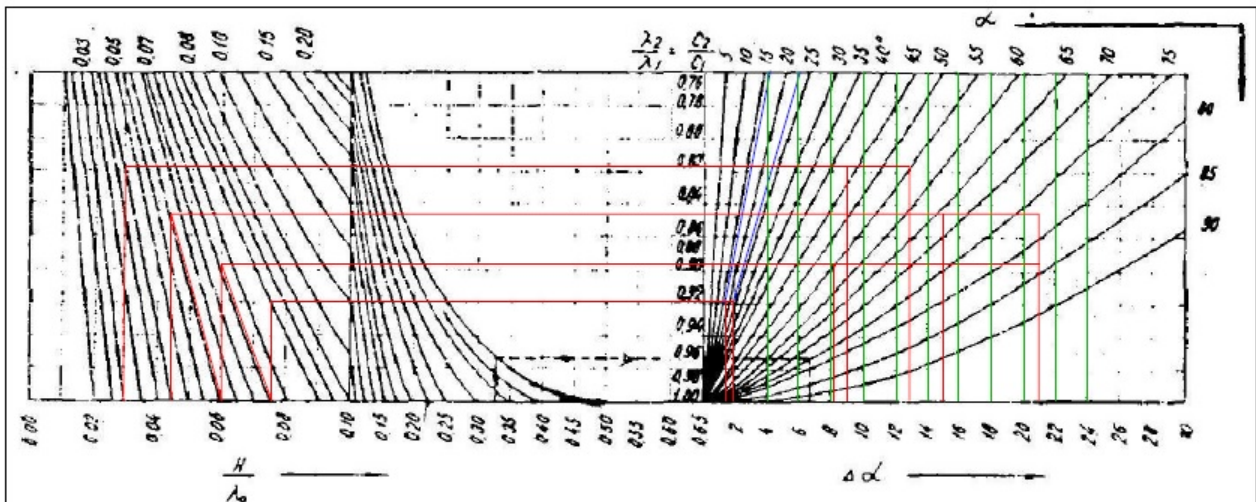


Figure 41: Nomogram for determining refraction in shallow water; Source: [3]

Figure 41 is a nomogram that determines the refraction of waves in shallow water. It is used in the following manner: From the point corresponding to the ratio $\frac{d_1}{\lambda_d}$ at the base of the scale on the left a vertical line is drawn upwards until it crosses the curve $\frac{d_0}{\lambda_d}$. From this point a horizontal line is drawn from left to right until it intersects with the curve α_0 (the angle between the wave ray at the initial depth and the normal to the medial isobath between H_0 and H_1). The vertical line from this point to the base of the nomogram reads $\Delta\alpha_0$. This angle indicates the degree of deviation of the wave ray towards the side of the lesser depth [19].

Similarly the wave refraction is followed until the wave rays reach the protective facilities.

The refraction coefficient at the harbor entrance is calculated as the square root of the ratio between the wave rays distance at the initial depth (a_d) and the distance between them at the place in question (a_i).

The refraction coefficient for eastern waves $K_{r,E}$ is calculated and presented in Table 30, whereas $K_{r,SE}$ for southeastern waves - in

Table 31.

Table 30 Plan of wave refraction for direction E

d_i [m]	$d_i/\overline{\lambda_{d,E}}$	Point number	Ray 1		Point number	Ray 2		$a_{i,E}$ [m]	$K_{r,E}$
			$\alpha_{i,E}$ [°]	$\Delta\alpha_{i,E}$ [°]		$\alpha_{i,E}$ [°]	$\Delta\alpha_{i,E}$ [°]		
12	0.091							200	1
		1	16.5	1.44	6	22.9	1.96		
10	0.076							197.8	1.01
		2	54.61	8.25	7	60.8	10.06		
8	0.061							211	0.97
		3	77.11	20.94	8	66.14	15.08		
6	0.045							390.4	0.72
		4	54.75	12.85	9	43.37	9.02		
4	0.030							574.2	0.59
		5	-	-	10	-	-		
2	0.015							580.1	0.59

$$K_{r,E} = \sqrt{\frac{a_{d,E}}{a_{i,E}}} = \sqrt{\frac{200}{580}} = 0.59 \quad (5.2)$$

Table 31 Plan of wave refraction for direction SE

d_i [m]	$d_i/\overline{\lambda_{d,SE}}$	Point number	Ray 1		Point number	Ray 2		$a_{i,SE}$ [m]	$K_{r,SE}$
			$\alpha_{i,SE}$ [°]	$\Delta\alpha_{i,SE}$ [°]		$\alpha_{i,SE}$ [°]	$\Delta\alpha_{i,SE}$ [°]		
12	0.141							150	1
		1	23	2.15	6	23.3	2.18		
10	0.118							152.7	0.99
		2	20.06	1.43	7	21.5	1.49		
8	0.094							155	0.98
		3	16.4	2.05	8	18.6	2.31		
6	0.071							162	0.96
		4	17.4	3.2	9	21	3.88		
4	0.047							173.2	0.93
		5	-	-	10	-	-		
2	0.024							176.4	0.92

$$K_{r,SE} = \sqrt{\frac{a_{d,SE}}{a_{i,SE}}} = \sqrt{\frac{150}{176}} = 0.92 \quad (5.3)$$

5.3 Wave properties in the surf zone – determining the critical breaker depth d_{cr}

The boundary between shallow water and surf zone is defined by the critical depth d_{cr} at which the first breaking of the wave is observed. The surf zone is limited between the first and the last wave breaking.

5.3.1 Sequence for calculating the basic wave parameters in the surf zone [2]

The depth at which the first wave breaking occurs is determined through successive approximations using lines 2, 3 and 4 for the according bottom slope on Figure 42.

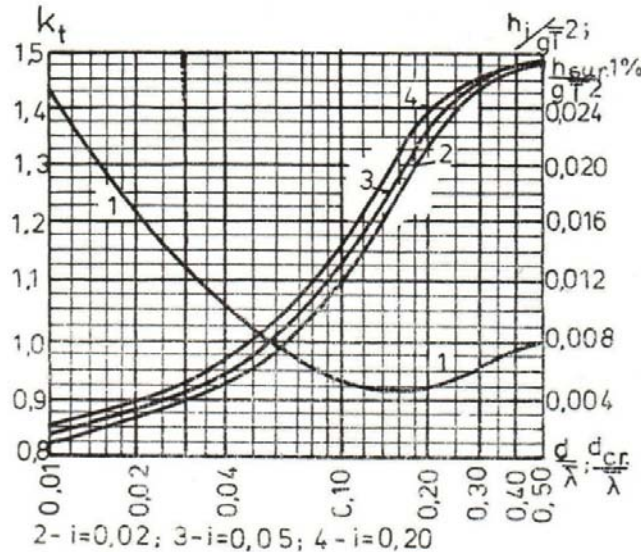


Figure 42: Graph for determining k_t ; Source: [3]

From the ratio $\frac{h_{d=12m}^{1\%}}{gT^2}$ and the curve corresponding to the mean bottom slope, the ratio $\frac{d_{cr}^I}{\lambda_d}$ is estimated.

For the obtained first order approximation critical depth d_{cr}^I $h_{d=d_{cr}^I}^{1\%}$ is calculated using the formula:

$$h_{d=d_{cr}^I}^{1\%} = k_t \cdot k_l \cdot k_r \cdot h_{deep}^{1\%}, \text{ where:} \quad (5.1)$$

k_t – transformation coefficient defined by graph 1 from Figure 42 for the respective value of $\frac{d_{cr}^I}{\lambda_d}$;

k_l – summarized coefficient for wave energy losses. It is read from Figure 43 for the line that corresponds to the mean bottom slope;

k_r – refraction coefficient for the respective wave direction;

$h_{deep}^{1\%}$ - deepwater wave height with probability of exceedance 1%.

Afterwards the process is repeated and for $\frac{h_{d=d_{cr}^I}^{1\%}}{gT^2}$ d_{cr}^{II} is obtained – second order approximation critical depth. The procedure is repeated until $|d_{cr}^n - d_{cr}^{n-1}| < 0.10m$. Therefore d_{cr}^n is the depth at which every hundredth wave in the system breaks. The height of this wave is:

$$h_{d=d_{cr}^n}^{1\%} = k_t \cdot k_l \cdot k_r \cdot h_{deep}^{1\%}.$$

The remaining smaller waves with higher probability of exceedance will break in shallower water.

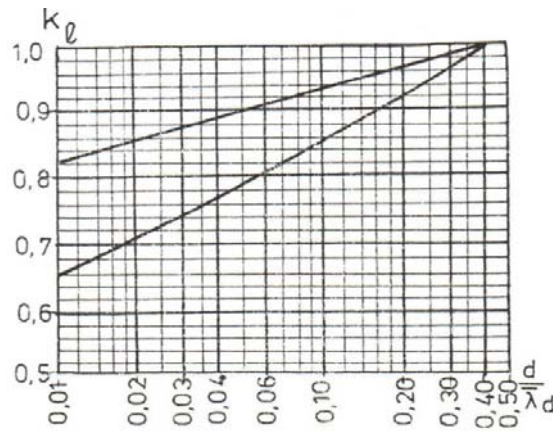


Figure 43: Graph for determining k_l ; Source: [3]

$$d_{cr,u} = k_u^{n-1} \cdot d_{cr}, \text{ where} \quad (5.2)$$

$d_{cr,u}$ - the depth at which the ultimate destruction of the wave profile occurs and the nature of water particles movement changes – from movement by open elliptical orbits to reciprocating forward motion as a water flow

k_u - coefficient depending on the mean bottom slope in the surf zone (i_{sur}). It is determined by using Figure 44.

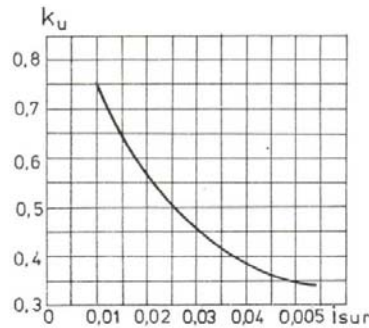


Figure 44: Graph for determining k_u ; Source: [3]

n - number of wave breakings ($n=2,3,4$ and more), as both of the following inequalities have to be fulfilled:

$$k_u^{n-2} \geq 0.43 \quad (5.3)$$

$$k_u^{n-1} < 0.43 \quad (5.4)$$

The wave height in the surf zone h_{sur} is estimated by using Figure 45 for $d_{cr} > d > d_{cr,u}$ and the ratio d/d_{cr} for the respective bottom slope (0.05 – 0.015), $h/h_{d=d_{cr}}^{1\%}$ is defined.

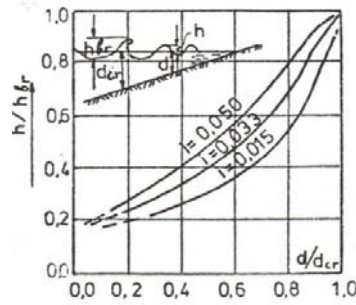


Figure 45: Graph for the estimation of h_{sur} ; Source: [3]

The wave length in the surf zone $\bar{\lambda}_{sur}$ is estimated according to Figure 46 from the ratio $d/\bar{\lambda}_d$ and the top envelope curve.

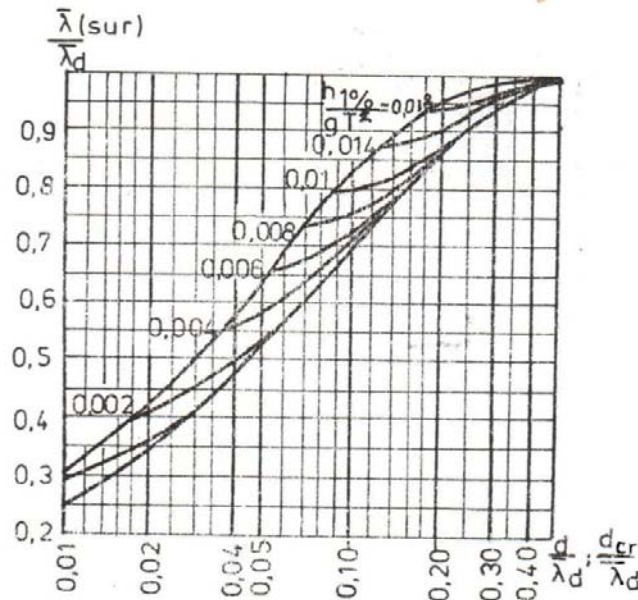


Figure 46: Graph for determining $\bar{\lambda}_{sur}$; Source: [3]

5.3.2 Performed calculations for the particular project – subject of the Master’s thesis:

Waves from E

$$\frac{h_{d=12m}^{1\%}}{gT^2} = \frac{8}{9.81 \cdot 9.2^2} = 0.01 ; i_{sur} = 0.015$$

Using Figure 42, curve 2, it is read: $\frac{d_{cr}^l}{\lambda_d} = 0.083$

$$d_{cr}^l = 0.083 \cdot 132 = 10.95m$$

1) At depth 10.95m:

k_t and k_l are read from Figure 42 and Figure 43 for the ratio $\frac{d_{cr}^l}{\lambda_d} = 0.083$;

$$k_r^{10.95m} = 1.0$$

$$h_{d=10.95m}^{1\%} = k_t \cdot k_l \cdot k_r \cdot h_{deep}^{1\%} = 0.95 \cdot 0.84 \cdot 1.0 \cdot 11.85$$

$$h_{d=10.95m}^{1\%} = 9.46m$$

$$\frac{h_{d=10.95m}^{1\%}}{gT^2} = \frac{9.46}{9.81 \cdot 9.2^2} = 0.0114 \rightarrow \frac{d_{cr}^{II}}{\lambda_d} = 0.094$$

$$d_{cr}^{II} = 0.094 \cdot 132 = 12.41m$$

2) At depth 12.41m:

k_t and k_l are read from Figure 42 and Figure 43 for the ratio $\frac{d_{cr}^{II}}{\lambda_d} = 0.094$;

$$k_r^{12.41m} = 1.0$$

$$h_{d=12.41m}^{1\%} = k_t \cdot k_l \cdot k_r \cdot h_{deep}^{1\%} = 0.94 \cdot 0.86 \cdot 1.0 \cdot 11.85$$

$$h_{d=12.41m}^{1\%} = 9.58m$$

$$\frac{h_{d=12.41m}^{1\%}}{gT^2} = \frac{9.58}{9.81 \cdot 9.2^2} = 0.0115 \rightarrow \frac{d_{cr}^{III}}{\lambda_d} = 0.095$$

$$d_{cr}^{III} = 0.095 \cdot 132 = 12.54m$$

3) At depth 12.54m:

k_t and k_l are read from Figure 42 and Figure 43 for the ratio $\frac{d_{cr}^{III}}{\lambda_d} = 0.095$;

$$k_r^{12.54m} = 1.0$$

$$h_{d=12.54m}^{1\%} = k_t \cdot k_l \cdot k_r \cdot h_{deep}^{1\%} = 0.94 \cdot 0.86 \cdot 1.0 \cdot 11.85$$

$$h_{d=12.54m}^{1\%} = 9.58m$$

$$\frac{h_{d=12.54m}^{1\%}}{gT^2} = \frac{9.58}{9.81 \cdot 9.2^2} = 0.0115 \rightarrow \frac{d_{cr}^{IV}}{\lambda_d} = 0.095$$

$$d_{cr}^{IV} = 0.095 \cdot 132 = 12.54m$$

$$\mathbf{d_{cr}^{IV} = d_{cr}^{III} = d_{cr,E} = 12.54m}$$

$d_{cr,E}$ – critical depth for the breaking of waves from E

$$k_u = 0.75$$

$n = 3 \rightarrow 0.75^1 = 0.75 \geq 0.43$; $0.75^2 = 0.56 > 0.43$ – the first condition is satisfied, but the second one is not;

$n = 4 \rightarrow 0.75^2 = 0.56 \geq 0.43$; $0.75^3 = 0.42 < 0.43$ – both conditions are satisfied

$$d_{cr,u,E} = k_u^{n-1} \cdot d_{cr} = 0.75^3 \cdot 12.54$$

$$\mathbf{d_{cr,u,E} = 5.30m}$$

4) At depth 5.5 m ($12.54 > 5.5 > 5.3m$):

$$\frac{d}{d_{cr}} = \frac{5.5}{12.54} = 0.44.$$

From Figure 45 for bottom slope 0.015 it is read $\frac{h_{sur}}{h_{cr}} = 0.28$.

$$h_{sur} = 0.28 \times 9.58 = 2.68m$$

$\frac{d}{\lambda_d} = \frac{5.5}{132} = 0.026$. From the top envelope curve on Figure 46 the ratio $\frac{\lambda_{sur}}{\lambda_d} = 0.47$ is obtained.

$$\rightarrow \lambda_{sur} = 0.47 \times 132 = 62m$$

Waves from SE

$$\frac{h_{d=12m}^{1\%}}{gT^2} = \frac{4.9}{9.81 \cdot 7.4^2} = 0.009 \rightarrow \frac{d_{cr}^I}{\lambda_d} = 0.073$$

$$d_{cr}^I = 0.073 \cdot 85 = 6.20m$$

1) At depth 6.20m:

k_t and k_l are read from Figure 42 and Figure 43 for the ratio $\frac{d_{cr}^I}{\lambda_d} = 0.073$;

$$k_r^{6.20m} = \sqrt{\frac{150}{162}} = 0.96$$

$$h_{d=6.20m}^{1\%} = k_t \cdot k_l \cdot k_r \cdot h_{deep}^{1\%} = 0.97 \cdot 0.82 \cdot 0.96 \cdot 7.0$$

$$h_{d=6.20m}^{1\%} = 5.40m$$

$$\frac{h_{d=6.20m}^{1\%}}{gT^2} = \frac{5.40}{9.81 \cdot 7.4^2} = 0.01 \rightarrow \frac{d_{cr}^{II}}{\lambda_d} = 0.087$$

$$d_{cr}^{II} = 0.087 \cdot 85 = 7.4m$$

2) At depth 7.4m:

k_t and k_l are read from Figure 42 and Figure 43 for the ratio $\frac{d_{cr}^{II}}{\lambda_d} = 0.087$;

$$k_r^{7.4m} = \sqrt{\frac{150}{158}} = 0.97$$

$$h_{d=7.4m}^{1\%} = k_t \cdot k_l \cdot k_r \cdot h_{deep}^{1\%} = 0.94 \times 0.85 \times 0.97 \times 7.0$$

$$h_{d=7.4m}^{1\%} = 5.48m$$

$$\frac{h_{d=7.4m}^{1\%}}{gT^2} = \frac{5.48}{9.81 \cdot 7.4^2} = 0.01 \rightarrow \frac{d_{cr}^{III}}{\lambda_d} = 0.087$$

$$d_{cr}^{III} = 0.087 \cdot 85 = 7.4m$$

$$d_{cr}^{III} = d_{cr}^{II} = d_{cr,SE} = 7.4m$$

$d_{cr,SE}$ – critical depth for Southeastern waves

$$k_u = 0.75$$

$n = 3 \rightarrow 0.75^1 = 0.75 \geq 0.43$; $0.75^2 = 0.56 > 0.43$ – the first condition is satisfied, but the second one is not;

$n = 4 \rightarrow 0.75^2 = 0.56 \geq 0.43$; $0.75^3 = 0.42 < 0.43$ - both conditions are satisfied

$$d_{cr,u,SE} = k_u^{n-1} \cdot d_{cr} = 0.75^3 \cdot 7.4$$

$$d_{cr,u,SE} = 3.12m$$

3) At depth 5.5 m ($7.4 > 5.5 > 3.12m$):

$$\frac{d}{d_{cr}} = \frac{5.5}{7.4} = 0.74.$$

From Figure 45 for bottom slope 0.015 it is read $\frac{h_{sur}}{h_{cr}} = 0.45$.

$$\rightarrow h_{sur} = 0.45 \times 5.48 = 2.5m$$

$\frac{d}{\lambda_d} = \frac{5.5}{85} = 0.065$. From the top envelope curve on Figure 46 the ratio $\frac{\overline{\lambda_{sur}}}{\lambda_d} = 0.7$ is obtained.

$$\rightarrow \overline{\lambda_{sur}} = 0.7 \times 85 = 59.5m$$

5.3.3 Results

The results for the wave properties at depth 5.5m for waves from E and SE are summarized in Table 32:

Table 32 Wave properties at depth 5.5m for waves from E and SE

	$\overline{\lambda_d}$ [m]	$h_{1\%}$ [m] (d=12m)	T [s]	d_{cr} [m]	$d_{cr, u}$ [m]	h_{sur} [m] (d=5.5m)	$\overline{\lambda_{sur}}$ [m]
E	132	8	9.2	12.54	5.3	2.7	62
SE	85	4.9	7.4	7.4	3.1	2.5	59.5

6 Diffracted wave height evaluation in the shadow region

6.1 Wave diffraction – directions E and SE

The results for the diffracted wave height from E and SE with probability of exceedance 5% (obtained in article 4.3) are given in Figure 47 and Figure 48.

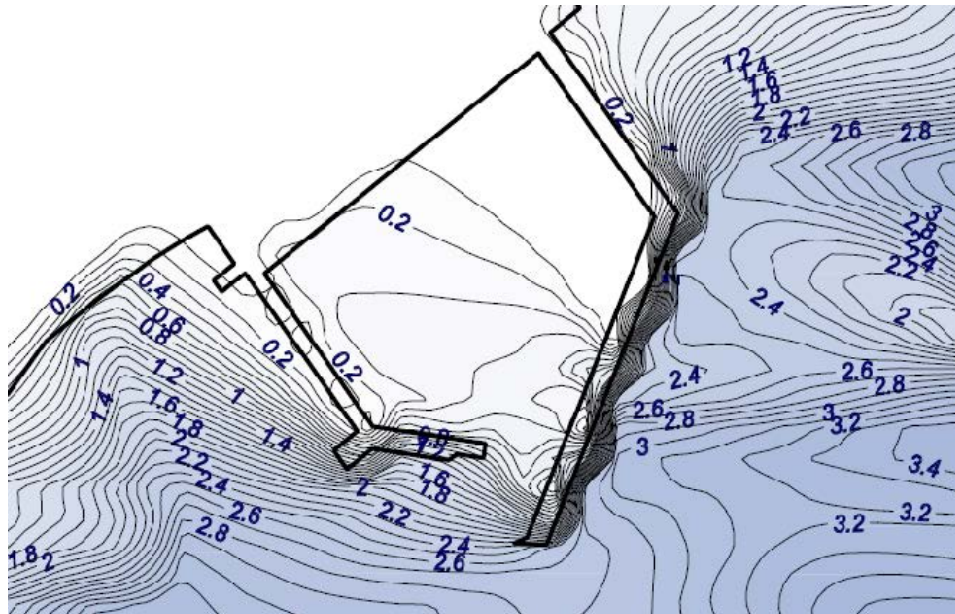


Figure 47: Wave height from E (case E02)

The wave fronts reach the northern breakwater almost perpendicularly with a height of ca. 3.0 m. In front of the harbor entrance the eastern waves have already undergone diffraction around the breakwater head and their height is slightly above 2.0 m, while those next to the southern breakwater are ca. 1.5 m high. After passing through the entrance, the diffracted wave height is 0.6 meters – three times smaller – and when reaching the inner side of the southern mole-quay and the rear quay wall, its height is rapidly reduced to 0.2 m.

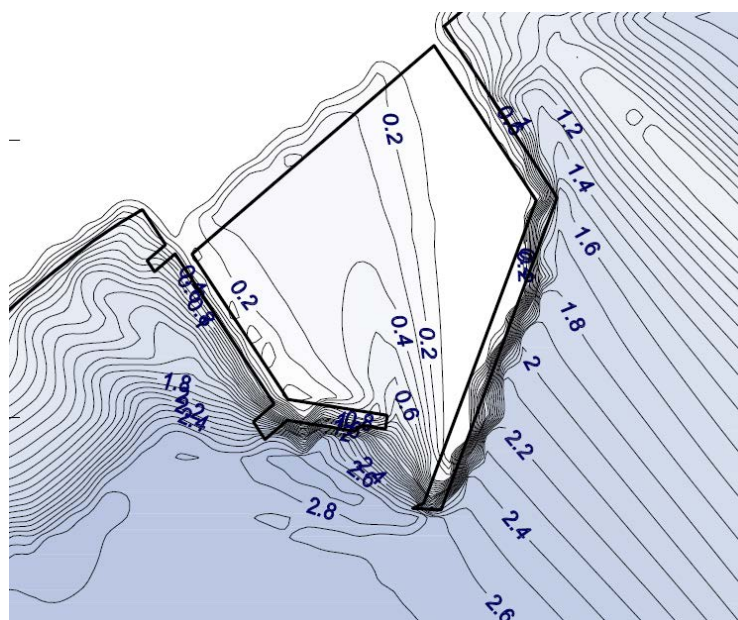


Figure 48: Wave height from SE (case SE02)

The SE waves immediately at the harbor entrance have a height of 2.8m. They undergo diffraction around the northern mole-quay head and their height rapidly decreases to 0.6 m in front of the southern breakwater head, while near the rear quay wall they are merely 0.3m high.

6.2 Wave diffraction – direction S

6.2.1 Numerical modeling using Copla-RD

The wave height from S is significantly smaller than the one from E and SE, but the layout of the Northern breakwater provides sufficient protection against wave impact from the latter two directions. From S, however, the entrance of the harbor is open for wave invasion and so the waves with this direction enter deep into the harbor area with the least loss of height and energy due to diffraction.

On Figure 49 it is visible that the S wave with a height of 1.8 meters enters deep into the harbor, reaching the rear quay wall with a height of 0.7m.

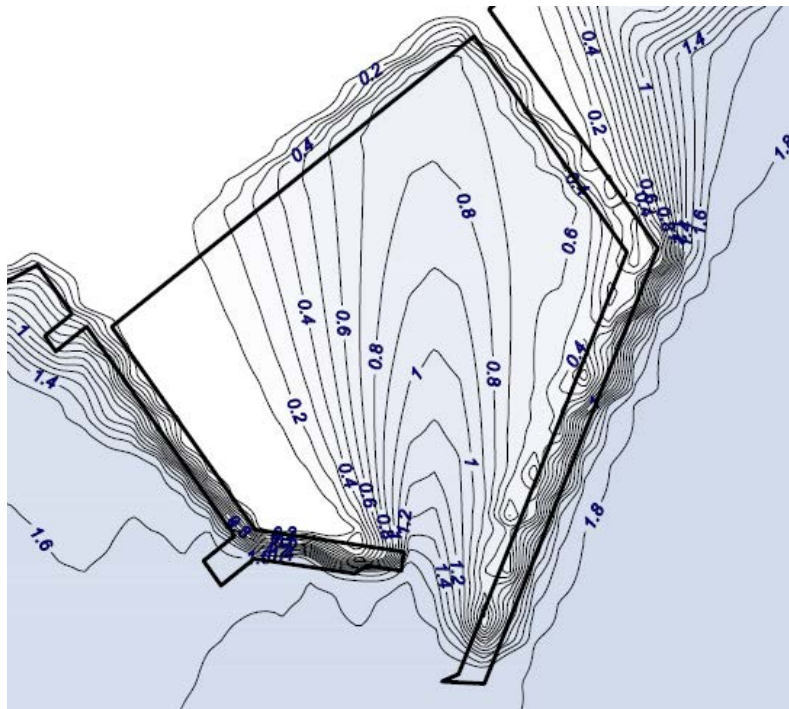


Figure 49: Wave height from S (case S02)

6.2.2 Graphical calculation using a method given in [6]

The diffracted wave height inside the harbor is determined using diagram 2-42 on page 2-93 of the Shore Protection Manual (1984) [6] for the opening with a width equal to 2 times the wavelength. The length of the wave from S that reaches the harbor entrance is calculated in section 3.5.2 - $\bar{\lambda} = 22.5m$. Figure 50 presents the same diagram, placed in the middle of the harbor entrance. The isolines in the graph represent the diffraction coefficient k_d .

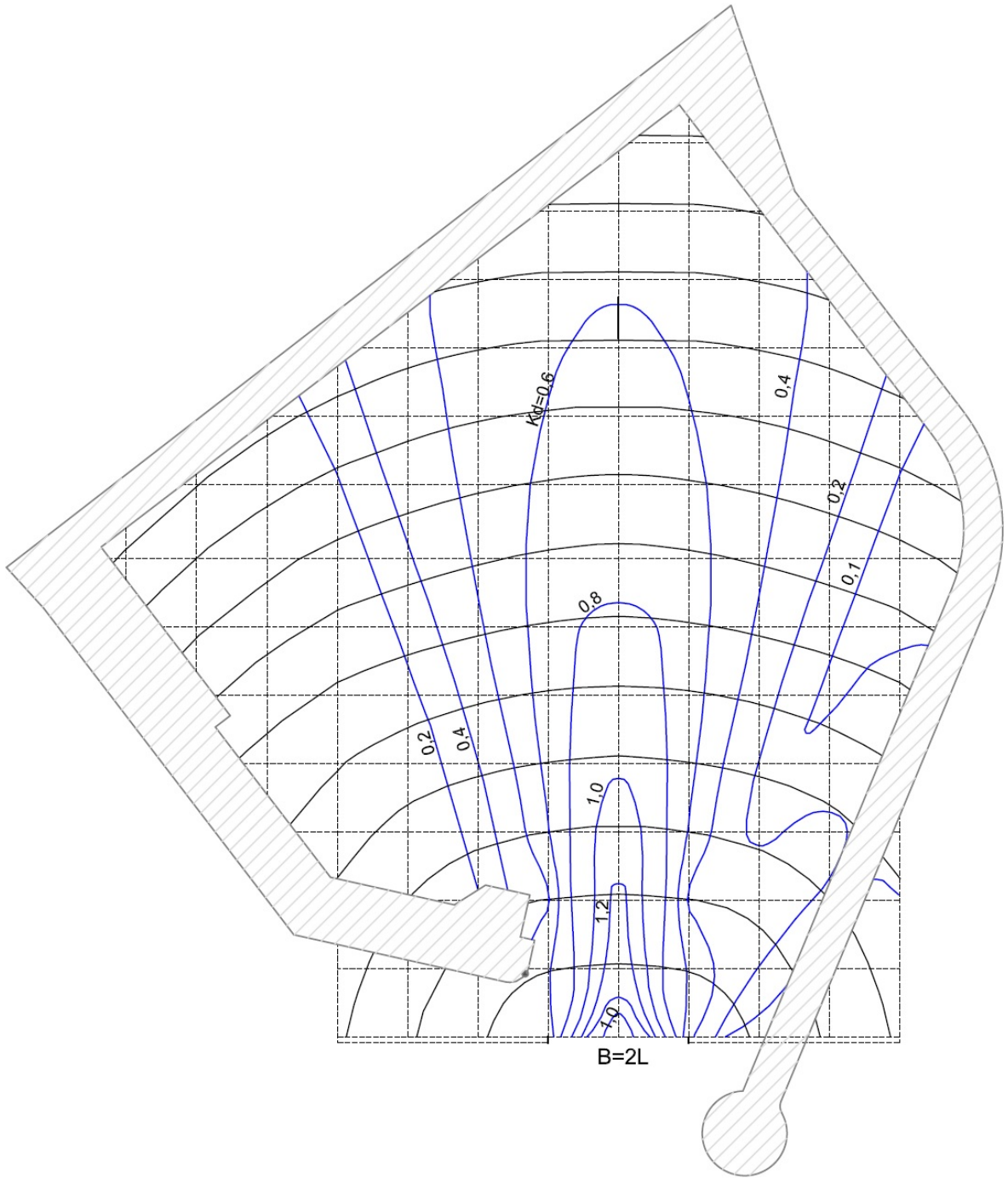


Figure 50: Diffraction coefficient in the shadow region

Figure 51 shows the wave height in the harbor after diffraction around the breakwaters.

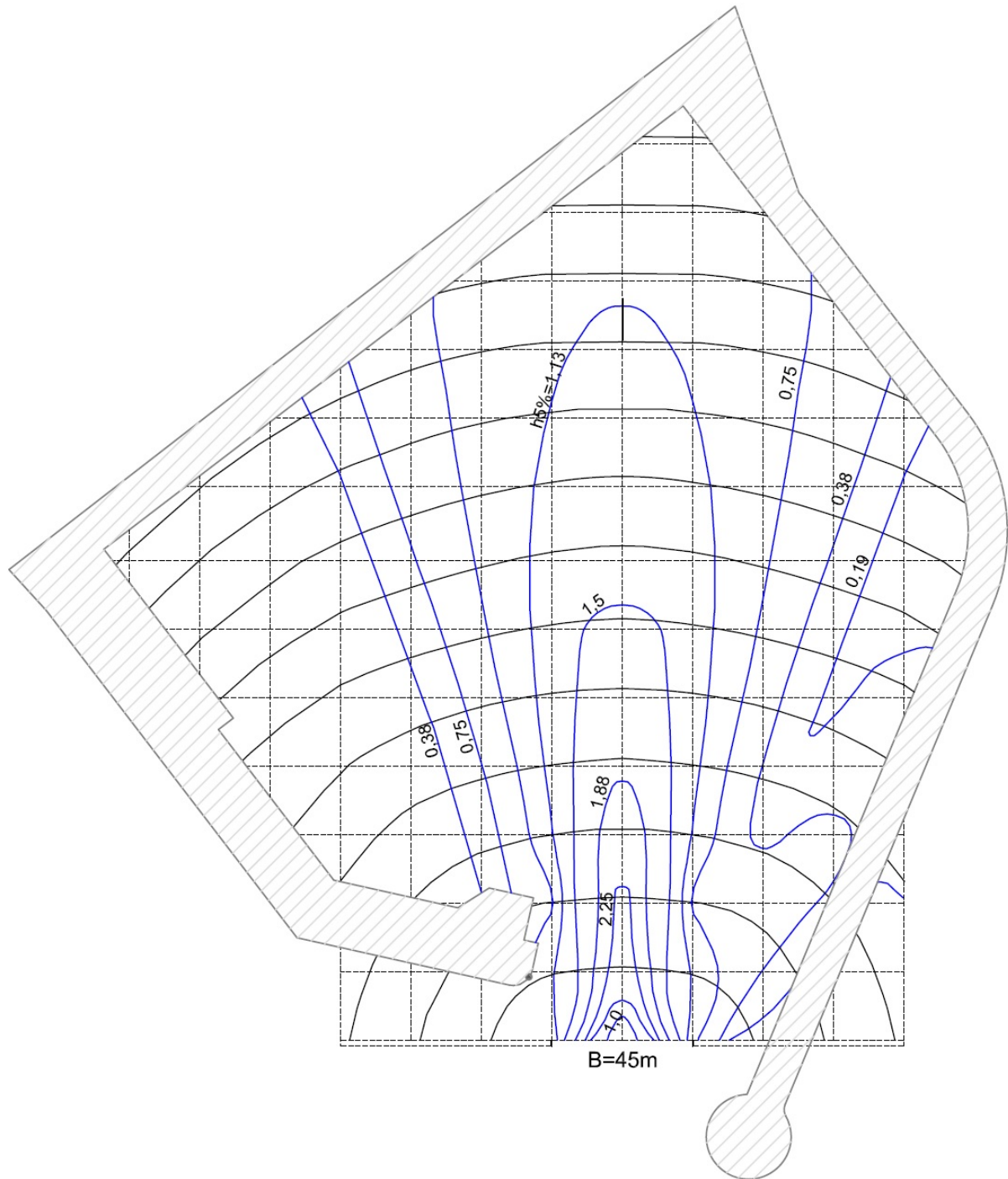


Figure 51: Diffracted wave height in the shadow region (direction S)

The admissible wave height in fishing harbors is not specified in the regulatory framework of Bulgaria. In [28] as such is stated $h_s = 0.4\text{ m}$ which means that the admissible value of $h_{5\%} = 0.5\text{m}$.

7 Comparison of the wave properties obtained by applying different methods of calculation

In this section are compared the wave heights calculated using the following methods:

- Numerical modeling of the wave transformation and refraction from a depth of 35 meters to the fishing harbor range (directions E, SE and S)
- Numerical modeling of wave diffraction inside the harbor area (direction S)
- Manual calculation of wave transformation and refraction from a depth of 12 meters to the fishing harbor range according to [2] (directions E and SE)
- Wave properties calculations according to [2] (direction S)
- Wave diffraction calculation inside the harbor using a diagram from SPM [6] (direction S)

The comparisons are performed for educational purposes. They serve the juxtaposition of different calculation methods used in the engineering practice. In this case the two methods of calculation are: numerical modeling of the wave parameters from the three main directions using MOPLA and calculation of wave parameters in shallow water according to [2] valid in Bulgaria.

7.1 Wave height immediately in front of the harbor

Directions E and SE

The values in the following tables are obtained in sections 4.3.1, 4.3.2 and 5.3.2.

Table 33 Wave height comparison at the harbor entrance – directions E and SE

Calculation method	Wave height $h_{1\%}$ [m]	
	E	SE
MOPLA	3.40	2.80
“Standards...” [2]	2.68	2.50
Difference[%]	16	11

Table 34 Wave height comparison at harbor entrance – direction S

Calculation method	Wave height with direction S	
	$h_{1\%}$ [m]	$h_{5\%}$ [m]
MOPLA	2.20	1.88
“Standards...” [2]	2.26	1.80
Difference[%]	3	4

The differences between the wave heights could be considered insignificant. They are mainly due to the difference in accuracy and detailedness between both methods. The sophisticated numerical model embeds an accurate bathymetrical map, while for the analytical one the isobaths are smoothed in order

to reduce the error in assessing the change in wave rays direction. Therefore, a maximum difference of 16% is acceptable and expected.

The results obtained from the numerical modeling are higher in all considered cases and therefore will be used as input data for the breakwater design and further calculations.

7.2 Wave height inside the harbor after diffraction

The results from the numerical modeling of the diffraction around the breakwaters are presented in Figure 49 in graphic format, and in Figure 51 – those from manually assessed diffraction pattern using a graph published in SPM [6]. The input data for the two studies is presented in section 0.

According to Figure 49 the wave height entering deep into the harbor area and reaching the rear quay wall is 0.9m. The wave height according to the SPM graph (Figure 51) is between 0.8 and 1.0 m, i.e. the difference between the two is negligible.

8 Construction of the northern breakwater-quay by reconstructing groyne 7

In order to ensure the necessary stability and strength and the long-term smooth operation of the wave protective harbor facilities, a number of factors has to be incorporated in their design, the most important of which are the topographic, hydrodynamic and the geologic conditions.

8.1 Input data for the reconstruction

8.1.1 Topographic conditions

As input data for the design a digital geodetic survey was provided. It is presented in Appendix 1 to the Master's assignment.

Figure 52 shows the existing groyne 7 before the reconstruction. Its length is 160m and its width varies from 17 to 25m. The cross-section is at its narrowest in the middle part of the groyne from the Eastern side. This narrowing is caused mainly by wave action on the facility.



Figure 52: Aerial view of groyne 7. Source: Google Earth

According to the project, the groyne is to be reconstructed and prolonged with change in direction in order to protect the harbor against wave action, as well as secure approach to the harbor.

8.1.2 Hydrodynamic conditions

The hydrodynamic conditions as input data for the design of the wave protective structure are presented in section 7. An excerpt containing the basic design wave parameters is enclosed below.

The wave properties in shallow water with the corresponding probability of exceedance are assessed while taking into consideration the processes of transformation, refraction and the overall wave energy losses connected with wave propagation in shallow water.

The graphical relationship between the wave height, the wave breaking depth and the bottom slope are shown in Figure 53. The obtained results for each zone are presented in Table 35 as advisory. The bottom slope $\tan\beta$ is equal to 0.02.

Zone 1	$h_b/gT^2=2.0m/(9.81m/s^2 \cdot (9.2s)^2)=0.0024$	$h_b/d_b=0.89$	$h_b=0.89 \cdot 2.50$	$h_b=2.2m$
Zone 2	$h_b/gT^2=3.4m/(9.81m/s^2 \cdot (9.2s)^2)=0.0041$	$h_b/d_b=0.87$	$h_b=0.87 \cdot 3.90$	$h_b=3.5m$
Zone 3	$h_b/gT^2=3.6m/(9.81m/s^2 \cdot (9.2s)^2)=0.0043$	$h_b/d_b=0.87$	$h_b=0.87 \cdot 4.90$	$h_b=4.3m$

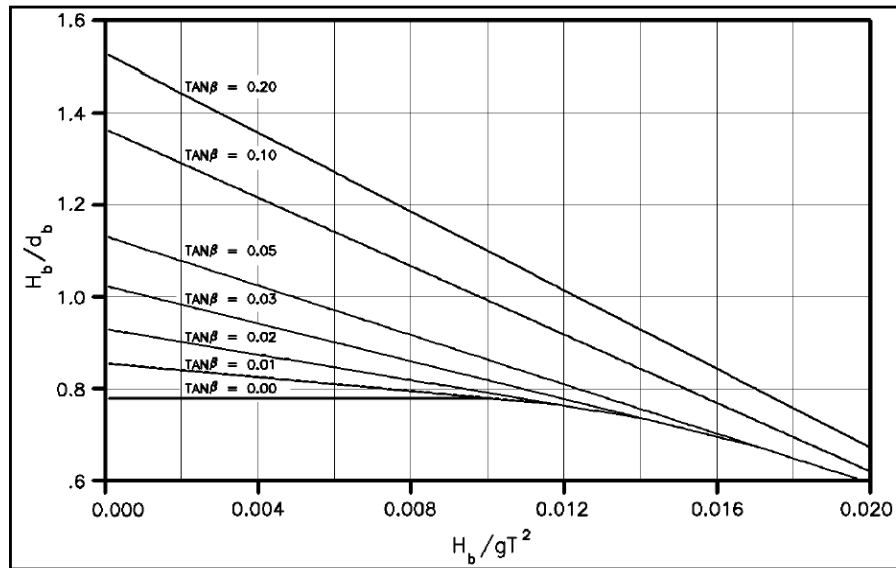


Figure 53: Graph for determining the maximum possible wave height, Wiegel 1972; Source: [6]

Table 35 Wave properties and water depth in the three wave impact zones along the mole-quay

Zone №	$h_{1\%}$, once every 50 years[m]		T_{av} [s]	L_{av} [m]	d [m]
	Calculated	Advisory			
1	2.00	2.20	9.2	42.7	2.50
2	3.40	3.50	9.2	56.6	3.90
3	3.60	4.30	9.2	63.2	4.90

8.1.3 Geologic conditions

Geomorphological characteristics

The region of fishing harbor Sarafovo is part of the Burgas depression. In front of it the beach is composed of coarse and medium sized sand with carbonate content 15% [12].

The coast in the harbor region is an abrasion landslide with height 4-5m. Directly in front of the water line the bottom is composed of clay covered with fine sand ($D=0.15mm$) which reaches the 5m isobath. The thickness of the sand deposits varies from 5cm to 1.5m and during extreme storms (under waves from E and SE) baring of the rock bottom has been observed. The average underwater bottom slope is 0.015.

In proximity to the harbor is located landslide Sarafovo (Figure 54) which is approximately 3000 m long, 280 m wide and covers an area of $0.84 km^2$. It is cirque shaped with three stepped bands separated

by declines. The sliding surface is at depth 15m and is situated in paleogenic clays , above which clayey, limestone and sandstone strata are sliding [14].

The landslide has a total volume of ca. 3 600 000 m³. It has intensified in 1936, 1940, 1979 and 1997, and has destroyed a considerable area of agricultural land. Until constructing the protective seawall along the coast, the slip velocity in the area reached 0.5-2.5 m/year.

Currently, after the measures performed for the strengthening of landslide Sarafovo, the latter is stabilized and the geological processes in the area do not present any danger for the construction and operation of Fishing Harbor Sarafovo[14].

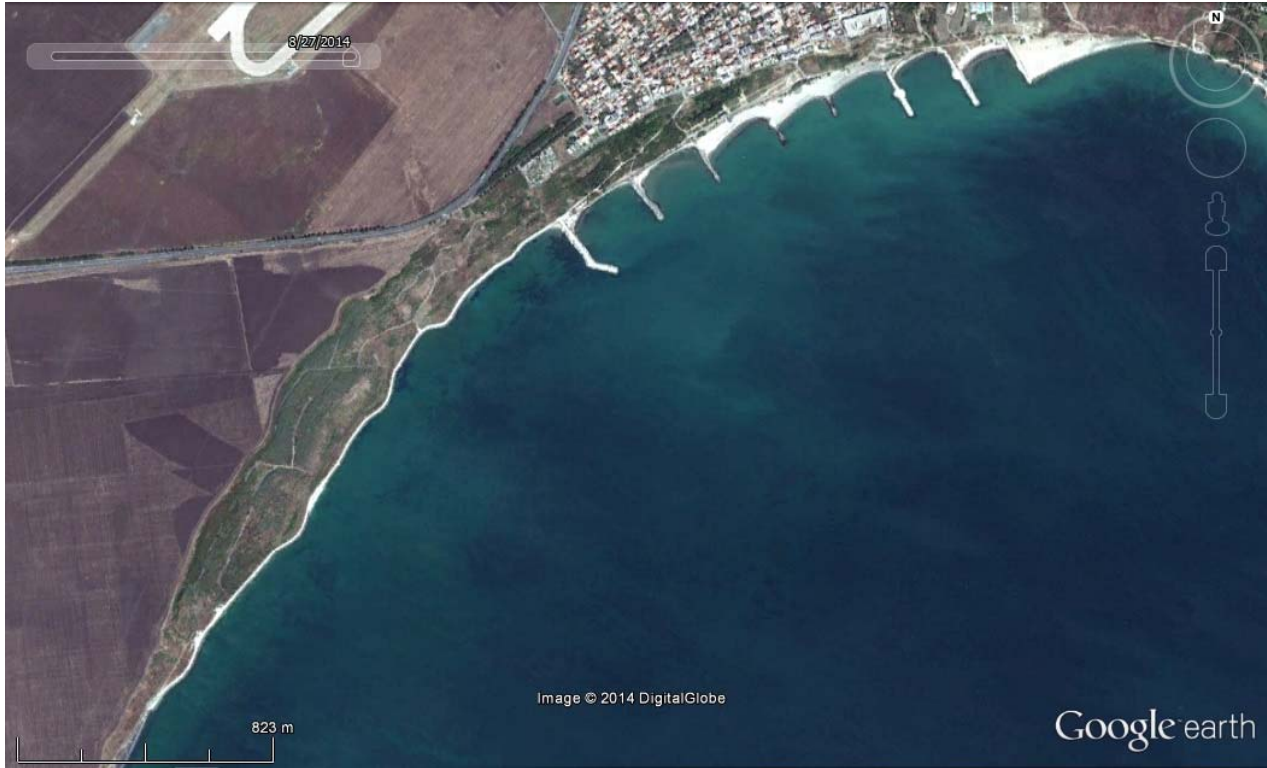


Figure 54: Aerial photo of Landslide Sarafovo; Source: Google Earth 19/9/2013

Geological and lithological structure

To elucidate the geological and lithological structure of the region, a site survey was conducted in November 2011. The survey includes:

- 4 motor drillings with a total length of 58m - 25 undisturbed and 2 disturbed soil samples have been taken.
- 4 dynamic penetrations
- 9 vertical electric drillings

The locations of the provided samples is disclosed in the geo-engineering investigation for the project [32].

From the provided soil samples, 8 undisturbed and 1 disturbed sample have been examined in the testing laboratory at “Geotechnics” chair at UACEG.

In [32] The geological profiles are presented.

Through the performed research, the following geological strata have been identified:

Geological stratum № 1 – fine uniform sand

Geological stratum № 2– Silty clay

The values of the mechanical properties of the earth base are shown in the following Table 36.

Table 36 Mechanical properties of the geological strata; Source: [1]

Geological stratum	fine uniform sand	silty clay
bulk density ρ_n [g/cm ³]	1.65	1.88
dry density ρ_s [g/cm ³]	2.65	2.77
av. density of solid constituents ρ_d [g/cm ³]	1.36	1.46
pore volume n	0.487	0.486
void ratio e	0.95	0.945
natural water content w_n [%]	21	29.2
maximum water content w_r [%]	35.8	33.3
saturation degree S_r	0.58 - 1	0.88
liquid limit w_L [%]	-	56.7
plastic limit w_p [%]	-	24.1
plasticity index I_p [%]	-	32.6
consistency index I_c	-	0.762
angle of internal friction ϕ (calculative)[°]	29	21
cohesion c_n [kPa]	0	32
undrained shear strength S_u [kPa]	-	50
Elasticity modulus E_0 [MPa]	18	12
design load R_0 [MPa]	0.20	0.23

Figure 55 depicts a typical cross section of the Northern quay-mole. The elements of the construction are numbered as follows:

- 1 – still water level in the harbor basin
- 2 - rock pad 100 – 500 kg
- 3 – steel sheet pile wall Larssen type with a concrete cap
- 4 – tie rod of horizontal anchor
- 5 – quarry stone backfill
- 6 – road construction
- 7 – wave turning wall from pre-cast concrete sections with dimensions 358/315/600
- 8 – rubble concrete foundation and anchor
- 9 – rockfill 500 – 1500 kg
- 10 – quarry stone core
- 11 – armor layer of tetrapods
- 12 – seabed (silty clay)

Figure 56 shows the outline (1) of the existing rubble mound groyne 7, as well as the preserved rockfill (2).

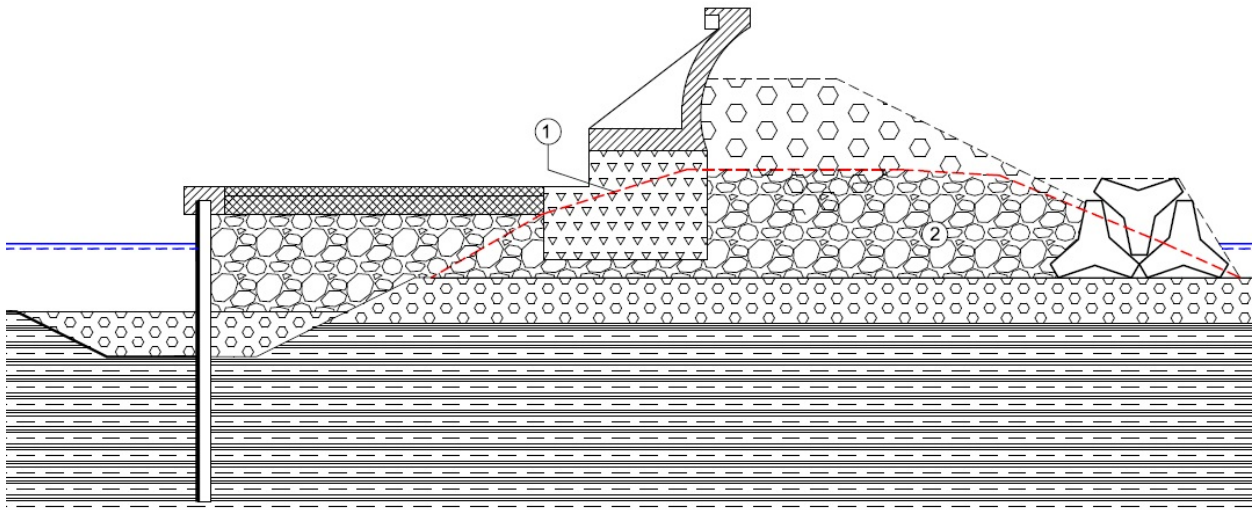


Figure 56: Cross section of the Northern quay-mole showing the existing groyne contour

The northern quay-mole of Fishing Harbor Sarafovo is a protective structure with combined functions. It is composed of an attached rubble-mound breakwater and a steel sheet pile quay wall. The existing groyne, built originally for landslide protection, is to be reshaped and complemented to form the rockfill core for the new breakwater facility. The core is protected on the sea side by a layer of large rock pieces (500 – 1500 kg). An armor layer of tetrapods in two rows weighing 4t in zones 1 and 2 and 8t in zone 3 (around the breakwater head) is used for wave energy dissipation. An opening with dimensions 2x8m is embedded in the body of the quay-mole to ensure the water circulation inside the harbor (drawing 6). It consists of precast reinforced concrete cassettes placed on a rockfill padding. A pre-cast wave turning wall made of reinforced concrete placed on a rubble concrete foundation forms the crest of the facility. On the lee side a quay for fishing vessels is constructed out of steel sheet piles. In shallow water (1.50m

depth) the sheet pile wall is a cantilever while at greater depth it is reinforced with a horizontal anchor. The sheet piles rise 2.35 – 5.25m above sea bottom. Driving depth varies from 3.5 to 5.5m. The void behind the quay wall is filled with quarry stone mass. A concrete cap with dimensions 90/60cm is cast on top of the wall. The cap is part of the quay platform road construction. The roadway is a 20cm thick concrete plate which lies on a bed of compacted rock material (fraction 0 – 63mm) with thickness 40cm.

From the tip of the existing groyne another 241 meters of length are added to the facility which makes its total length amount to 392m, measured on the inner side.

The dimensions of the Northern quay-mole are given in Drawing 3.

8.3 Steel sheet pile wall design

The dimensioning of the steel sheet pile wall using the software DeepXcav is included in the detailed design of Fishing Harbor Sarafovo. Three cross sections along the breakwater length are examined - sections 2-2, 3-3 and 8-8 (Drawing 5). The wall is driven in three different depths – 400cm, 500cm and 550cm. In the latter two sections an anchor is used to reduce the drive depth of the wall - 3φ25 reinforcement steel B500B, equipped with a left- and right-threaded sleeve.

The next pages of the present Master’s Thesis present an example of the design procedure of section 8-8 located in the deepest harbor section and hence bearing the maximum load.

8.3.1 Static system, loads and dimensions

The static system of the wall is an anchored wall. The anchor is modeled as a horizontal tieback located 0.5m from the wall crown. The wall is driven 4.5m into silty clay with an undrained shear strength $S_u=50$ kPa. Due to this high value of S_u , the wall can be considered as fixed at the footing.

The loads acting on the sheet pile wall are soil pressure, water pressure, as well as surcharge loads – strip load of 10 kPa and a footing representing the wave turning wall and its foundation – 350 kN.

The basic dimensions are as shown in Figure 57.

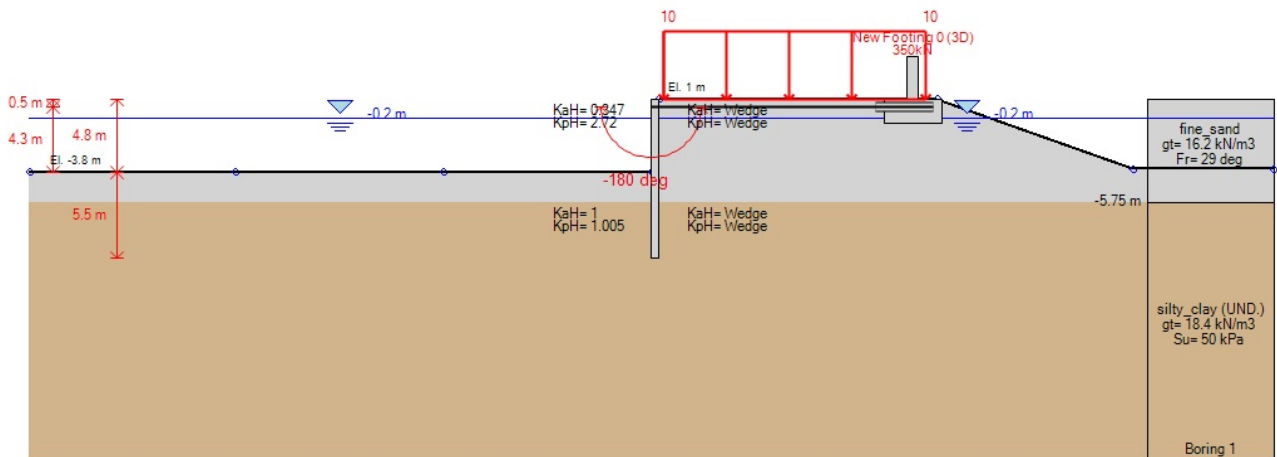


Figure 57: Sheet pile wall model in DeepXcav

The soil parameters used for the calculation are given in Table 36. The tables in this chapter are copied from the calculation report extracted from DeepXcav.

SOIL DATA

Name	g tot (kN/m ³)	g dry (kN/m ³)	Frict (deg)	C' (kPa)	Su (kPa)	Eload (MPa)	Eur (MPa)	kAp NL	kPp NL	kAcv NL	kPcv NL	Vary	Spring Model	Color
fine_sand	16.2	29	29	0	N/A	60	90	0.35	2.88	N/A	N/A	True	Linear	
Silty_clay	18.4	18.4	21	32	50	12	60	0.5	2	0.36	2.77	True	Linear	

Name	Poisson v	Min Ka (clays)	Min sh (clays)	ko.NC -	nOCR -	aH.EXP (0 to 1)	aV.EXP (0 to 1)	qSkin (kPa)	qNails (kPa)	kS.nails (kN/m ³)
fine_sand	0.45	-	-	0.515	0.5	-	-	700	466.67	31430.45
Silty_clay	0.5	0	5	0.531	0.5	-	-	125	83.33	4714.57

gtot = total soil specific weight

gdry = dry weight of the soil

Frict = friction angle

C' = effective cohesion

Su = Undrained shear strength

Eur = unloading/reloading elastic modulus

Kap = Peak active thrust coefficient

Kpp = Peak passive thrust coefficient (initial value, may be modified on each stage according to analysis settings).

Kacv = Constant volume active thrust coeff (only for clays, initial value)

Kpcv = Constant volume passive thrust coeff (only for clays, initial value).

Spring models= spring model (LIN= constant E over the soil layer height

EXP: Exponential, SUB: Modulus of Subgrade Reaction

SIMC= Simplified Clay mode

8.3.2 Steel sheet pile cross sectional properties

The dimensions and other properties of the Larssen 603 steel sheet piles are presented below.

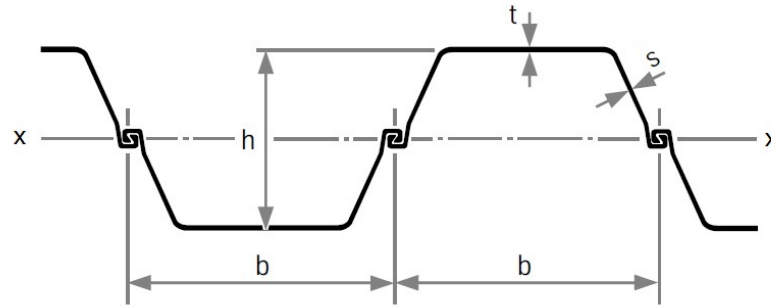


Figure 58: Steel sheet pile wall Larssen 603 – dimension labeling in cross section. Source: [29]

Steel Sheet Pile Cross Sectional Properties

DES	Shape	W	A	h	t	b	s	I _{xx}	S _{xx}
		(kN/m)	(cm ² /m)	(cm)	(cm)	(cm)	(cm)	(cm ⁴ /m)	(cm ³ /m)
L603	U	0.6	138.01	31.01	0.82	60.046	0.97	18599	1198.9

DES=shape (Z or U)

W=width per unit of length

A=area

h=height

t=horiz part thickness

b=width of the single sheet pile part

s=inclined part thickness

I_{xx}=strong axis inertia (per unit of length)

S_{xx}=strong axis section modulus (per unit of length)

Hor. wall spacing: 1

Wall thickness = 0.31

Passive width below exc: 1

Active width below exc: 1

Concrete

fc' = 20

Rebar Fy = 410

E_{conc} = 29962

Concrete tension F_{cT} = 10% of Fc'

Steel members fy = 235 E_{steel} = 206000

8.3.3 Results

Extended Summary

	Calculation Result		Wall Displaceme	Settlement	Wall Moment	Wall Moment
			(cm)	(cm)	(kN-m/m)	(kN-m)
Limit Equilibrium Analysis	Calculation successful		1	2.04	87.82	87.82

	Wall Shear	Wall Shear	STR Combined	STR Moment	STR Shear	Wall Concrete Serv
	(kN/m)	(kN)	Wall Ratio	Wall Ratio	Wall Ratio	Stress Ratio FIC
Limit Equilibrium Analysis	45.47	45.47	0.658	0.658	0.069	N/A

	Wall Reinforcem	Max Support	Max Support	Critical	STR Support	Support Geotech	FS
	Stress Ratio FIS	Reaction (kN/m)	Reaction (kN)	Support Check	Ratio	Capacity Ratio (p	Basal
Limit Equilibrium	N/A	48.09	48.09	0.086	0.02	0.086	3.096

	Toe FS	Toe FS	Toe FS	Zcut	FS Mobilized	FS	Hydraulic
	Passive	Rotation	Length	(Paratie)	Passive	True/Active	Heave FS
Limit Equilibrium	N/A	6.572	2.384	N/A	N/A	N/A	N/A

Forces (Res. F, M/Drive F, M)

	FS1 Passive	FS2 Rotation	FS3 Length	FS4 Mobilized Passive	FS5 Actual Drive	Fh EQ Soil	Fh EQ Water
	(FxResist/FxDrive)	(Mresist/Mdrive)	(Embedment/ToeFS=1)	(FxPassive/FxPas_Mobili	/ Theory Active		
Stage #0	N/A	3840.04/584.87	5.5/2.31	N/A	N/A	0	7.346

Used Soil Strength Parameters for Each Stage on Driving Side (Uphill)

	Layer	Drained/U	Method Description	Used Wall	Used Soil	Used c'	Used Su	Used	Used
				Delta (deg)	Friction (deg)	(kPa)	(kPa)	KaH	KpH
0: Stage 1	fine_sand	Drained	*KaUH=[Coulomb_Kah(deg FR=29 DFR=0,Asur=10.329)]=0.315	0	29	0	0	0.347	3.72
0: Stage 1	Silty_Clay	Undrained	Clay model: Default Kp (from soil	0	0	0	50	0.499	2.002

Used Soil Strength Parameters for Each Stage on Resisting Side (Downhill)

	Layer	Drained/U	Method Description	Used Wall	Used Soil	Used c'	Used Su	Used	Used
				Delta (deg)	Friction (de	(kPa)	(kPa)	KaH	KpH
0: Stage 1	fine_sand	Drained	* KpDH= Coulomb_Kph(deg FR=29 DFR=0,Asur=0, Ax=0.1g)=2.725	0	29	0	0	0.315	1.926
0: Stage 1	Silty_clayC	Undrained	Clay model: Default Ka (from soil ty	0	0	0	50	0.499	2.002

Summary of Wall Moments and Toe Requirements

Top Wall	Wall	L-Wall	H-Exc.	Max+M/Cap	Max-M/Cap	FS Toe	FS Toe	FS Toe	FS 1 Toe EL.	Slope
(m)	Section	(m)	(m)	(kN-m/m)	(kN-m/m)	Passive	Rotation	Embedment	(m)	Stab. FS
1	Wall 1	10.3	4.8	0.59/133.48	87.82/133.48	No.Calc	6.572	2.384	-6.11	N/A

The results are displayed graphically in Figure 59, Figure 60, Figure 61, Figure 62 and Figure 63.

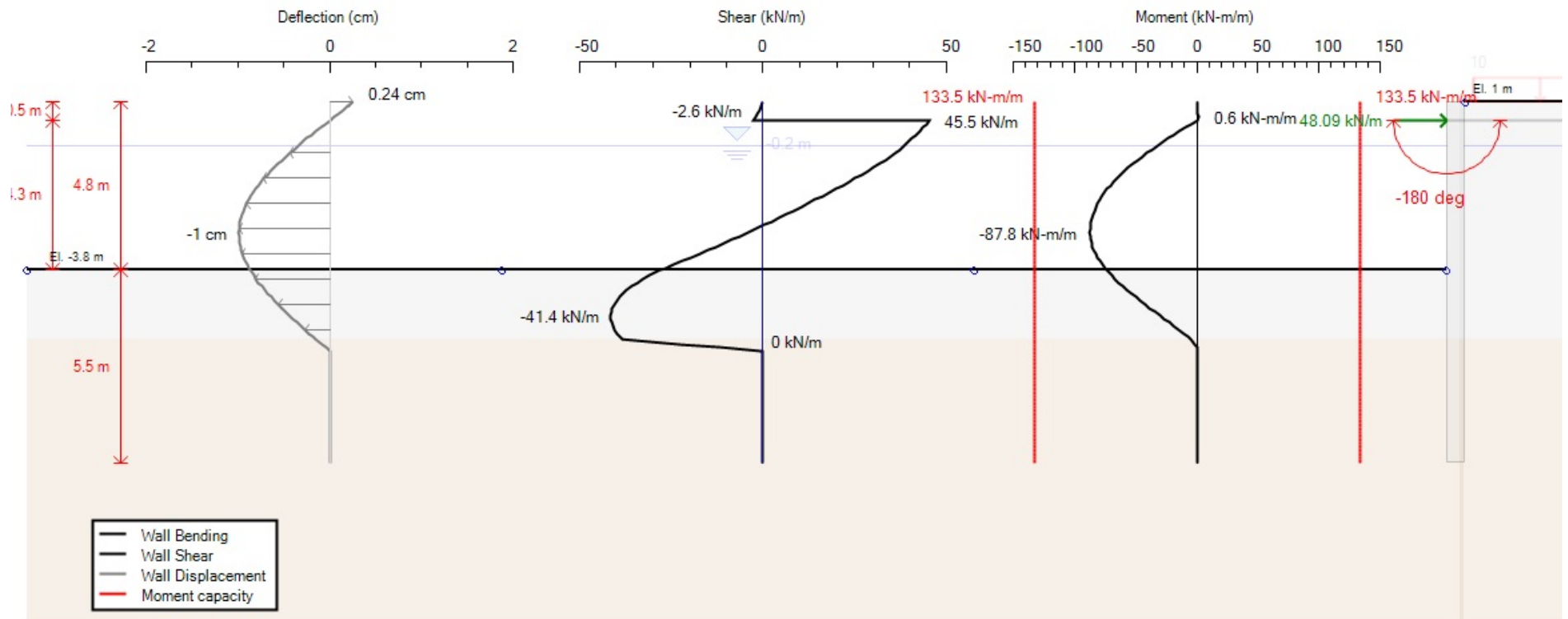


Figure 59: Results from Limit Equilibrium analysis for steel sheet pile wall performed in DeepXcav: Bending moment, Shear force, Displacement and Support reactions

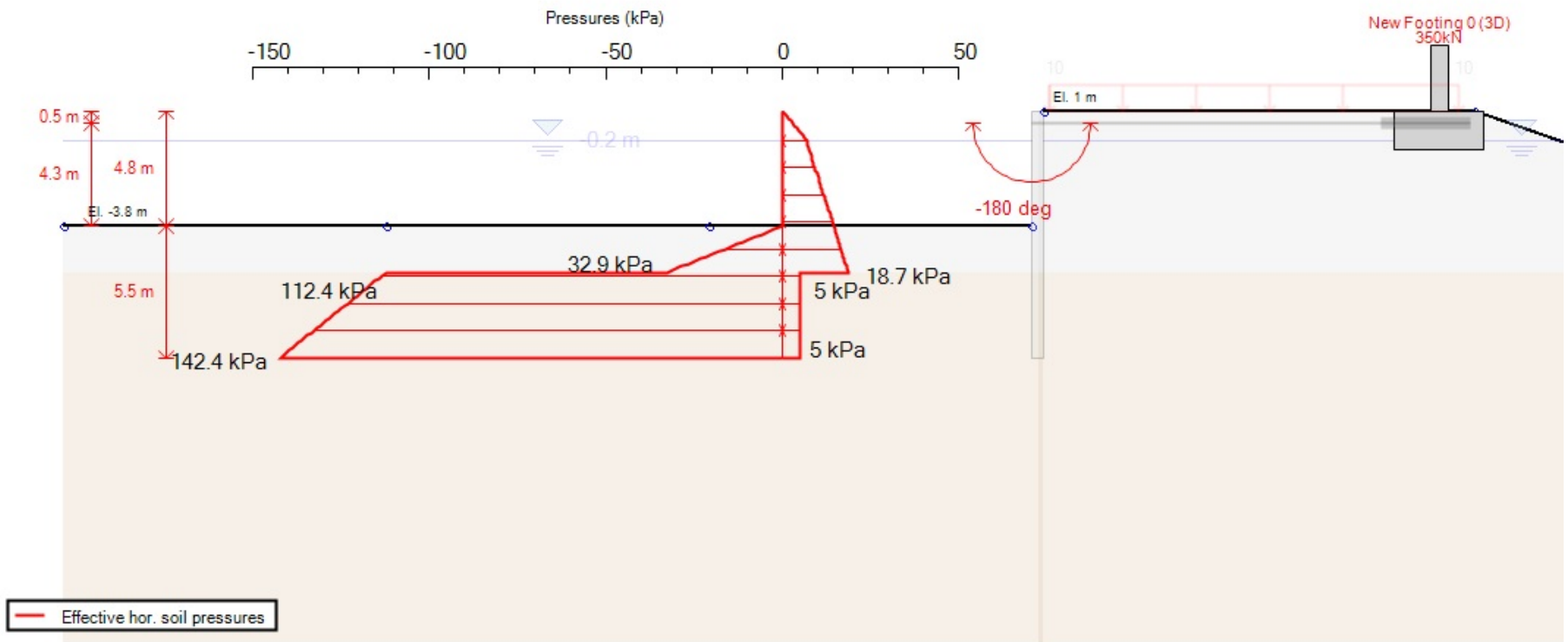


Figure 60: Results from Limit Equilibrium analysis for steel sheet pile wall performed in DeepXcav: Effective horizontal soil pressures

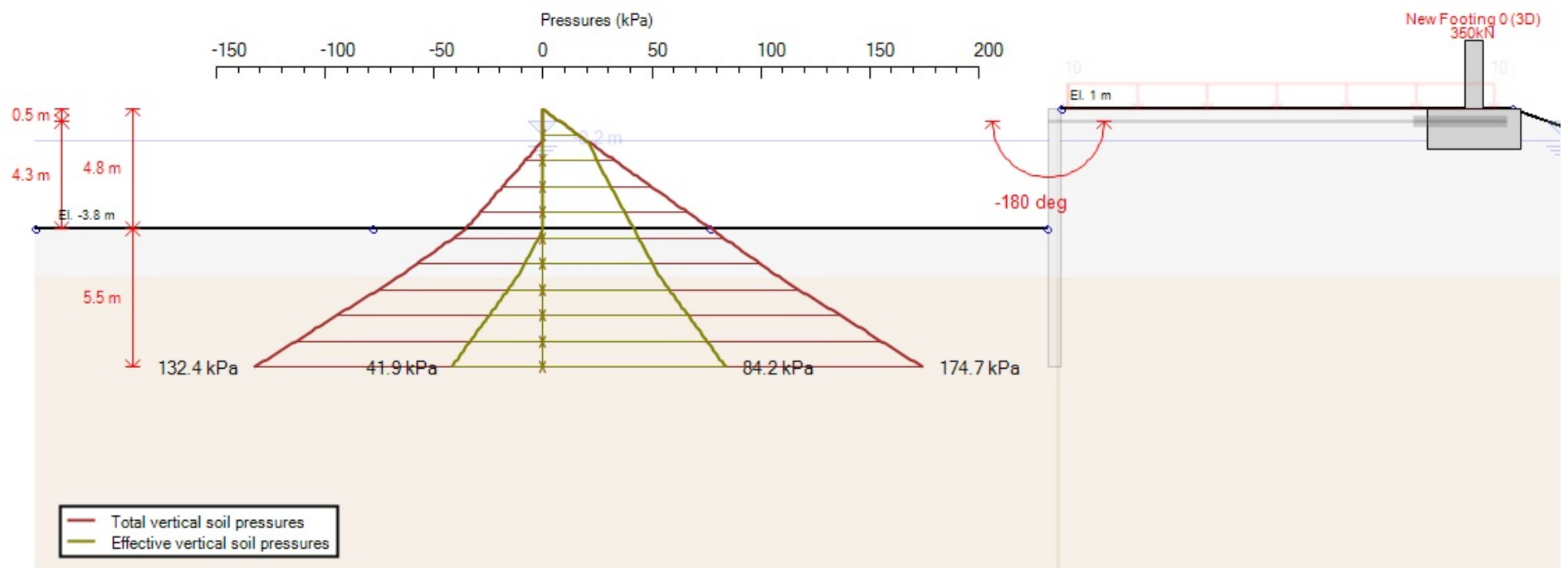


Figure 61: Results from Limit Equilibrium analysis for steel sheet pile wall performed in DeepXcav: Total and effective vertical soil pressures

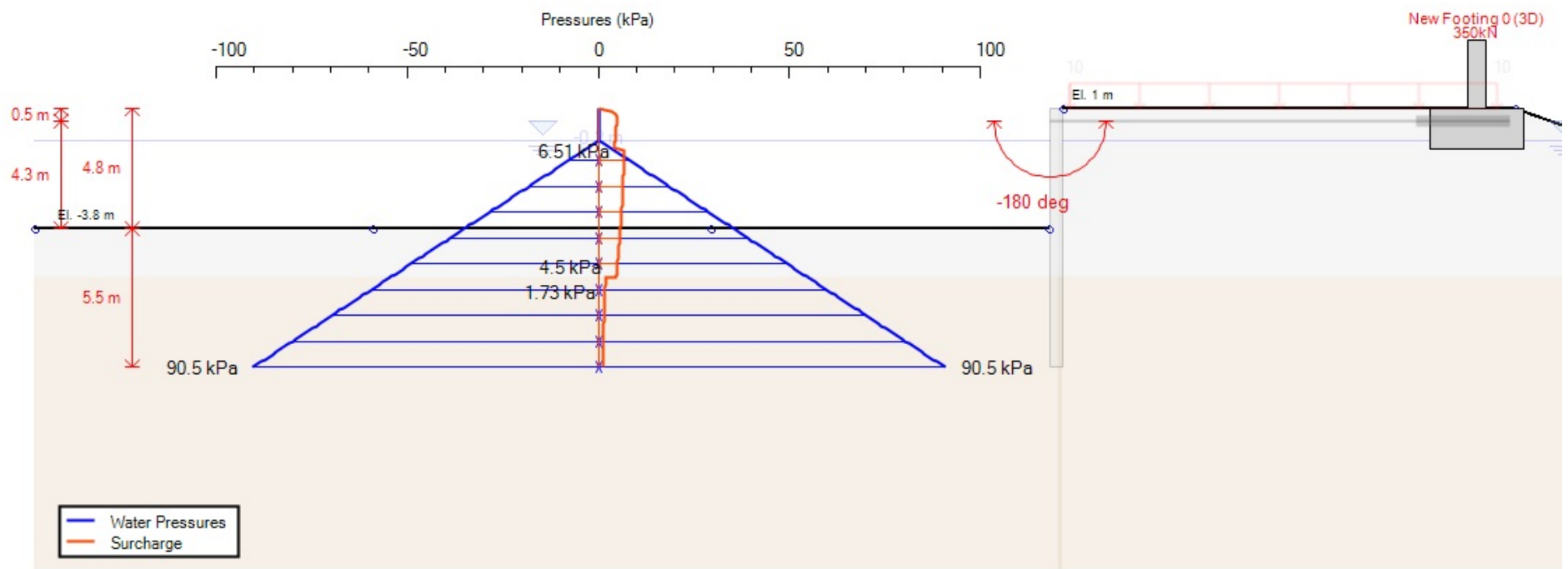


Figure 62: Results from Limit Equilibrium analysis for steel sheet pile wall performed in DeepXcav: Water pressures and Surcharge pressures

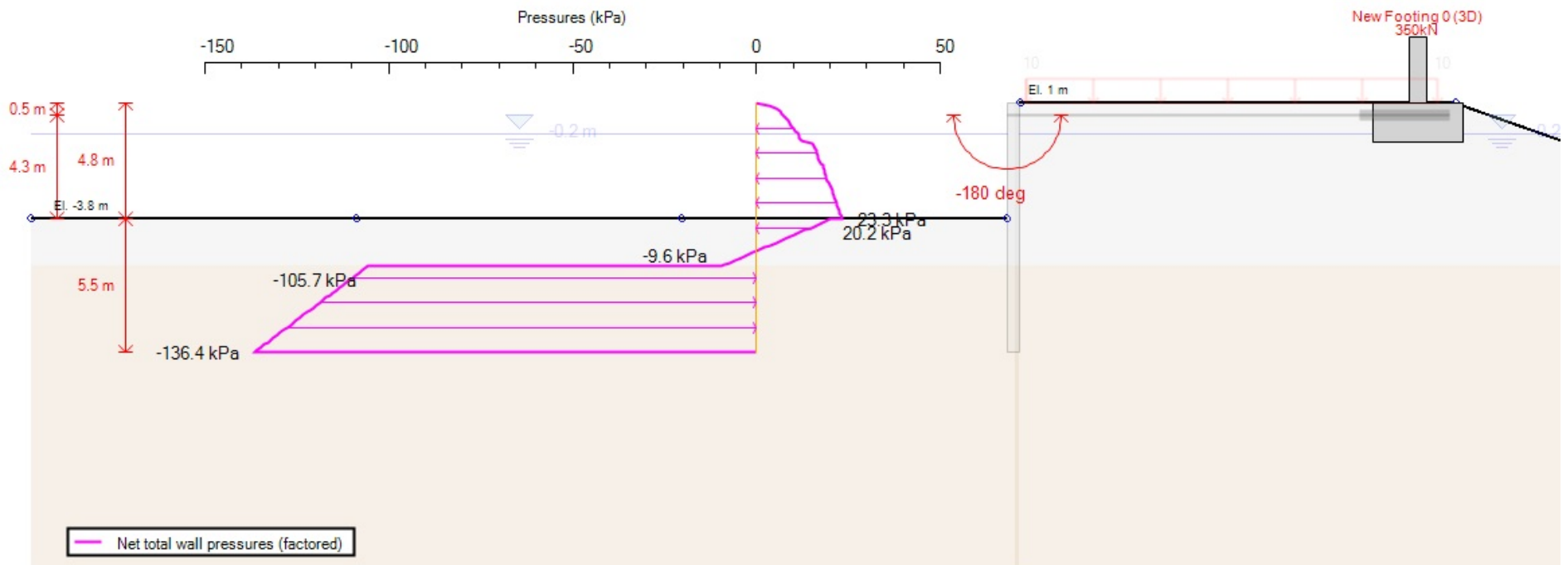


Figure 63: Results from Limit Equilibrium analysis for steel sheet pile wall: Net total wall pressures

9 Stability check of the wave protective structure

9.1 Calculating the weight of the armor units on the breakwater slope

In order to achieve limit equilibrium of the separate embankment structure layers, the minimum required armour unit weight in each of the three wave impact zones is calculated. The calculations are presented in the following pages.

9.1.1 Armour unit weight in zone 1

- According to “Standards for loads and impacts on hydraulic structures by waves, ice and vessels” [2] Section V art. 64

$$G = \frac{\mu_{\phi} \cdot \gamma_c \cdot h^2 \cdot \lambda}{\left(\frac{\gamma_c}{\gamma_w} - 1\right)^3 \sqrt{1+m^3}}, \text{ where} \quad (9.1)$$

μ_{ϕ} – roughness coefficient. For arranged tetrapods it is read in Table 37 that $\mu_{\phi} = 0.0058$,

$\gamma_c = 2.35 \text{ t/m}^3$ – armor units volume density,

$\gamma_w = 1.02 \text{ t/m}^3$ – Black Sea water volume density,

$m = \cotg \varphi = 2$ – armor layer slope,

$h = 2.2 \text{ m}$ – height of the wave reaching the breakwater in zone 1,

$\lambda = 42.7 \text{ m}$ – length of the wave in front of the breakwater (acc. to Table 35).

Table 37 Coefficient μ_{ϕ} for different armour units; Source: [2]

Armour unit type	Coefficient μ_{ϕ} after placement method:	
	Dumping	Placing
Quarry stone	0.025	-
Regular concrete blocks	0.021	-
Tetrapods	0.008	0.0058
Dipods	0.0057	0.0049
Tribars	0.0057	0.0034
Pentapods	0.0042	0.0034

$$G = \frac{0.0058 \times 2.35 \times 2.2^2 \times 42.7}{2.22 \sqrt{1 + 2^3}} = 0.42 \text{ t}$$

- According to the Hudson laboratory formula

$$W = \frac{\gamma_c \cdot h^3}{K_D \left(\frac{\gamma_c}{\gamma_w} - 1\right)^3} \text{ m} \quad (9.2)$$

K_D – stability coefficient, depending on the type and the condition of the armor units; defined empirically. For tetrapods arranged along the structure trunk $\rightarrow K_D = 7.2$ [26].

Table 38 Determining the stability coefficient K_D ; Source: [26]

type of block	number of layers (N)	structure trunk		structure head	
		K_D		K_D	
		breaking wave	non breaking wave	breaking wave	non breaking wave
rough angular quarry stone	1	**	2.9	**	2.3
rough angular quarry stone	2	3.5	4.0	2.5*	2.8*
rough angular quarry stone	3	3.9	4.5	3.7*	4.2*
tetrapod	2	7.2	8.3	5.5*	6.1*
dolos	2	22.0	25.0	15.0	16.5*
cube	2	6.8	7.8		5.0

$$W = \frac{2.35 \times 2.2^3}{7.2 \times 2.22 \times 2} = 0.78 \text{ t}$$

9.1.2 Armour unit weight in zone 2

- According to “Standards for loads and impacts on hydraulic structures by waves, ice and vessels” [2] Section V art. 64

$$G = \frac{\mu_\phi \cdot \gamma_c \cdot h^2 \cdot \lambda}{\left(\frac{\gamma_c}{\gamma_w} - 1\right)^3 \sqrt{1+m^3}}, \text{ where} \quad (9.3)$$

μ_ϕ – roughness coefficient. For arranged tetrapods it is read in Table 37 that $\mu_\phi = 0.0058$

$\gamma_c = 2.35 \text{ t/m}^3$ – armor units volume density

$\gamma_w = 1.02 \text{ t/m}^3$ – Black Sea water volume density

$m = \cotg \varphi = 2$ – armor layer slope

$h = 3.5 \text{ m}$ – height of the wave reaching the breakwater in zone 2

$\lambda = 56.6 \text{ m}$ – length of the wave in front of the breakwater (acc. to Table 35)

$$G = \frac{0.0058 \times 2.35 \times 3.5^2 \times 56.6}{2.22 \sqrt{1+2^3}} = 1.58 \text{ t}$$

- According to the Hudson laboratory formula

$$W = \frac{\gamma_c \cdot h^3}{K_D \left(\frac{\gamma_c}{\gamma_w} - 1\right)^3} \text{ m} \quad (9.4)$$

K_D – stability coefficient, depending on the type and the condition of the armor units; defined empirically. For tetrapods arranged along the structure trunk $\rightarrow K_D = 7.2$.

$$W = \frac{2.35 \times 3.5^3}{7.2 \times 2.22 \times 2} = 3.95 \text{ t}$$

9.1.3 Armour unit weight in zone 3

- According to “Standards for loads and impacts on hydraulic structures by waves, ice and vessels” [2] Section V art. 64

$$G = \frac{\mu_{\phi} \cdot \gamma_c \cdot h^2 \cdot \lambda}{\left(\frac{\gamma_c}{\gamma_w} - 1\right)^3 \sqrt{1+m^3}}, \text{ where} \quad (9.5)$$

μ_{ϕ} – roughness coefficient. For arranged tetrapods it is read in Table 37 that $\mu_{\phi} = 0.0058$,

$\gamma_c = 2.35 \text{ t/m}^3$ – armor units volume density,

$\gamma_w = 1.02 \text{ t/m}^3$ – Black Sea water volume density,

$m = \cotg \varphi = 2$ – armor layer slope,

$h = 4.3 \text{ m}$ – height of the wave reaching the breakwater in zone 3,

$\lambda = 62.3 \text{ m}$ – length of the wave in front of the breakwater (acc. to Table 35).

$$G = \frac{0.0058 \times 2.35 \times 2.2^2 \times 42.7}{2.22 \sqrt{1 + 2^3}} = 2.39 \text{ t}$$

- According to the Hudson laboratory formula

$$W = \frac{\gamma_c \cdot h^3}{K_D \left(\frac{\gamma_c}{\gamma_w} - 1\right)^3} \text{ m} \quad (9.6)$$

K_D – stability coefficient, depending on the type and the condition of the armor units; defined empirically. For tetrapods arranged along the structure trunk $\rightarrow K_D = 7.2$ and for tetrapods around the structure head $\rightarrow K_D = 5.5$.

$$W = \frac{2.35 \times 4.3^3}{7.2 \times 2.22 \times 2} = 5.9 \text{ t along the structure trunk}$$

$$W = \frac{2.35 \times 4.3^3}{5.5 \times 2.22 \times 2} = 7.7 \text{ t around the structure head.}$$

9.1.4 Results summary

Table 39 Calculation results of the armour unit weight on the structure sea slope

Wave impact zone	Wave height	Calculated weight [t]	
	h [m]	“Standards” [2]	Hudson
Zone 1	2.2	0.42	0.78
Zone 2	3.5	1.58	2.89
Zone 3	4.3	2.39	7.66

With these results in mind and with view of the available tetrapods with a weight of 4t on site – around the head and the trunk of the existing groyne 8. for zones 1 and 2 will be used 4t tetrapods and for zone 3 (breakwater head) the armour layer will be fortified with 2 layers of 8t tetrapods.

9.2 Calculation of the wave run-up on the breakwater slope according to the "Standards for loads and impacts of hydraulic structures by waves, ice and vessels" [2] Section V art. 57

The waves from East with probability of exceedance 1% have already broken when they reach the breakwater.

9.2.1 Wave run-up height in zone 1

$$h_{n,i} = k_{\Delta} \cdot k_p \cdot k_c \cdot k_{run} \cdot k_{\beta} \cdot k_{in} \cdot h_i, \text{ where} \quad (9.7)$$

k_{Δ} - slope roughness coefficient; depends on the armour type

The typical roughness Δ in meters is accepted equal to the average size of the concrete armor units. In the given case for tetrapods weighing 4t, $\Delta = 2\text{m}$.

k_p – slope permeability coefficient

Table 40 Values for k_{Δ} and k_p in relation to slope cover type and relative roughness; Source: [2]

Slope cover type	Relative roughness $\frac{\Delta}{h_{1\%}}$	k_{Δ}	k_p
Continuous watertight cover – asphalt concrete	-	1.0	1.0
Concrete and reinforced concrete slabs	-	1.0	0.9
Water permeable cover of sand, gravel, stone and concrete blocks and units	<0.002	1.0	0.9
	0.005 - 0.01	0.95	0.85
	0.02	0.9	0.8
	0.05	0.8	0.7
	0.1	0.75	0.6
	>0.2	0.7	0.5

For $\frac{\Delta}{h_{1\%}} = \frac{2}{2.2} = 0.9$ the values are read from Table 40 as follows: $k_{\Delta} = 0.7$; $k_p = 0.5$

k_c – coefficient depending on the slope m_{α} and the wind speed v

Table 41 Values for coef. k_c ; Source: [2]

m_{α}		0.4	0.4 - 2	3 - 5	> 5
k_c	$v \geq 20\text{m/s}$	1.3	1.4	1.5	1.6
	$v \leq 10\text{m/s}$	1.1	1.1	1.1	1.2

$v > 20\text{m/s}$; $m_\alpha = 2.0$, therefore from Table 41 it is read $k_c = 1.4$

k_{run} is a coefficient depending again on the slope (m_α) and the ratio $\frac{\bar{\lambda}_d}{h_{deep}^{1\%}} = \frac{132}{11.85} = 11.1$

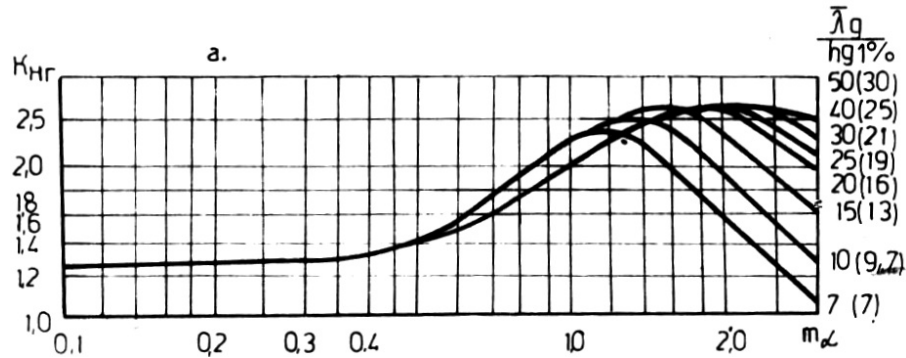


Figure 64: Values for coef. $K_{run}(1)$; Source: [2]

Since the water depth in front of the facility is smaller than the wave height in zone 1 multiplied by 2 ($d < 2h_{1\%}$), the coefficient k_{run} has to be read from Figure 64 or Figure 65 for the wave slope ($\frac{\bar{\lambda}_d}{h_{deep}^{1\%}}$) values in brackets and for depth $d = 2h_{1\%}$. $k_{run} = 2.1$.

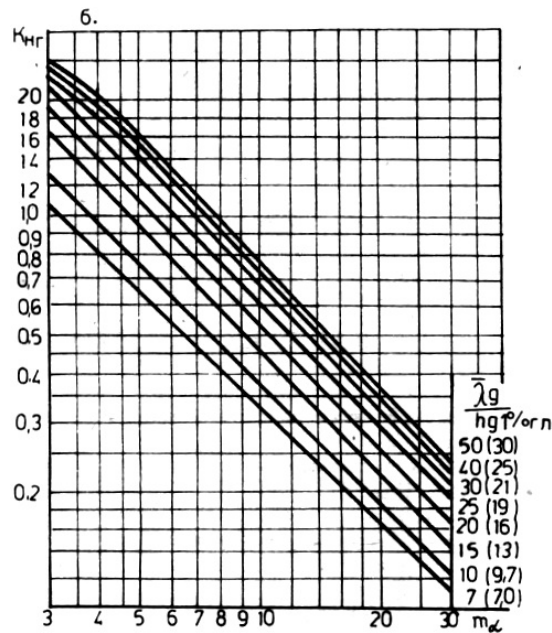


Figure 65: Values for coef. $K_{run}(2)$; Source: [2]

k_β depends on the angle β [°] between the wave front and the breakwater axis . It is defined in Table 42. In this case the E wave front meets the breakwater at an angle $\beta = 70^\circ$ in zone 1. Thus it is read $k_\beta = 0.76$

Table 42 Values for coef. k_β ; Source: [2]

β [°]	0	10	20	30	40	50	60
k_β	1	0.98	0.96	0.92	0.87	0.82	0.76

k_{in} is a coefficient for the probability of exceedance. When determining the crest elevation of hydrotechnical facilities, the probability of exceedance is accepted $i=1\%$. From Table 43 it is read $k_{in} = 1$.

Table 43 Values for coef. k_{in} ; Source: [2]

Wave run-up probability of exceedance i [%]	0.1	1	2	5	10	30	50
k_{in}	1.1	1.0	0.96	0.91	0.86	0.76	0.68

h_i [m] is the wave height with probability of exceedance $i=1\%$. For zone 1 $h_i = 2.2m$ (Table 39)

$$h_{n,1\%} = k_{\Delta} \cdot k_n \cdot k_c \cdot k_{run} \cdot k_{\beta} \cdot k_{in} \cdot h_{1\%} = 0.7 \times 0.5 \times 1.4 \times 2.1 \times 0.76 \times 1.0 \times 2.2 = 1.72m$$

9.2.2 Wave run-up height in zone 2

$$h_{n,i} = k_{\Delta} \cdot k_p \cdot k_c \cdot k_{run} \cdot k_{\beta} \cdot k_{in} \cdot h_i, \text{ where} \quad (9.8)$$

k_{Δ} - slope roughness coefficient; depends on the armour type

The typical roughness Δ in meters is accepted equal to the average size of the concrete armor units. In the given case for tetrapods weighing 4t, $\Delta = 2m$.

k_p – slope permeability coefficient

For $\frac{\Delta}{h_{1\%}} = \frac{2}{2.2} = 0.9$ the values are read from Table 40 as follows: $k_{\Delta} = 0.7$; $k_p = 0.5$

k_c – coefficient depending on the slope m_{α} and the wind speed v

$v > 20m/s$; $m_{\alpha} = 2.0$, therefore from Table 41 it is read $k_c = 1.4$

k_{run} is a coefficient depending again on the slope (m_{α}) and the ratio $\frac{\bar{\lambda}_d}{h_{deep}^{1\%}} = \frac{132}{11.85} = 11.1$

Since the water depth in front of the facility is smaller than the wave height in zone 1 multiplied by 2 ($d < 2h_{1\%}$), the coefficient k_{run} has to be read from Figure 64 or Figure 65 for the wave slope $(\frac{\bar{\lambda}_d}{h_{deep}^{1\%}})$ values in brackets and for depth $d = 2h_{1\%}$.

$k_{run} = 2.1$.

k_{β} depends on the angle β [°] between the wave front and the breakwater axis . It is defined in Table 42. In this case the E wave front meets the breakwater at an angle $\beta = 10^\circ$ in zone 2. Thus it is read $k_{\beta} = 0.98$

k_{in} is a coefficient for the probability of exceedance. When determining the crest elevation of hydrotechnical facilities, the probability of exceedance is accepted $i=1\%$. From Table 43 it is read $k_{in} = 1$.

h_i [m] is the wave height with probability of exceedance $i=1\%$. For zone 2 $h_i = 3.5m$ (Table 39)

$$h_{n,1\%} = k_{\Delta} \cdot k_n \cdot k_c \cdot k_{run} \cdot k_{\beta} \cdot k_{in} \cdot h_{1\%} = 0.7 \times 0.5 \times 1.4 \times 2.1 \times 0.98 \times 1.0 \times 3.5 = 3.43m$$

9.2.3 Wave run-up height in zone 3

$$h_{n,i} = k_{\Delta} \cdot k_p \cdot k_c \cdot k_{run} \cdot k_{\beta} \cdot k_{in} \cdot h_i, \text{ where} \quad (9.9)$$

k_{Δ} - slope roughness coefficient; depends on the armour type

The typical roughness Δ in meters is accepted equal to the average size of the concrete armor units. In the given case for tetrapods weighing 8t, $\Delta = 2.3\text{m}$.

k_p – slope permeability coefficient

For $\frac{\Delta}{h_{1\%}} = \frac{2.3}{4.3} = 0.53$ the values are read from Table 40 as follows: $k_{\Delta} = 0.7$; $k_p = 0.5$

k_c – coefficient depending on the slope m_{α} and the wind speed v

$v > 20\text{m/s}$; $m_{\alpha} = 2.0$, therefore from Table 41 it is read $k_c = 1.4$

k_{run} is a coefficient depending again on the slope (m_{α}) and the ratio $\frac{\bar{\lambda}_d}{h_{deep}^{1\%}} = \frac{132}{11.85} = 11.1$

Since the water depth in front of the facility is smaller than the wave height in zone 1 multiplied by 2 ($d < 2h_{1\%}$), the coefficient k_{run} has to be read from Figure 64 or Figure 65 for the wave slope $\left(\frac{\bar{\lambda}_d}{h_{deep}^{1\%}}\right)$ values in brackets and for depth $d = 2h_{1\%}$.

$k_{run} = 2.1$.

k_{β} depends on the angle β [°] between the wave front and the breakwater axis . It is defined in Table 42. In this case the E wave front meets the breakwater at an angle $\beta = 0^\circ$ in zone 3. Thus it is read $k_{\beta} = 1.0$

k_{in} is a coefficient for the probability of exceedance. When determining the crest elevation of hydrotechnical facilities, the probability of exceedance is accepted $i=1\%$. From Table 43 it is read $k_{in} = 1$.

h_i [m] is the wave height with probability of exceedance $i=1\%$. For zone 3 $h_i = 4.3\text{m}$ (Table 39)

$$h_{n,1\%} = k_{\Delta} \cdot k_p \cdot k_c \cdot k_{run} \cdot k_{\beta} \cdot k_{in} \cdot h_{1\%} = 0.7 \times 0.5 \times 1.4 \times 2.1 \times 1.0 \times 1.0 \times 4.3 = 4.43\text{m}$$

9.2.4 Summary of the results

The wave run-up height on the breakwater slope in the three wave impact zones are presented in Table 44.

Table 44 Wave run-up height on the breakwater slope

Zone	1	2	3
Wave height $h_{1\%}$ [m]	2.2	3.5	4.3
Run-up height [m]	1.72	3.43	4.43

The results show that the wave run-up height in zone 1 is smaller than the initial wave height, while in zone 2 it is bigger with merely 3 cm, and in zone 3 – with 13 cm. Therefore the conclusion can be made that the design slope and the type and size of the armour units are adequately chosen.

10 Technological sequence of operations in the construction of the Northern mole-quay

The technological sequence of operations in the construction of the mole-quay is displayed on drawing 5 by stages as follows:

Stage 1:

Delivery, spreading and compaction of rock padding(100-500kg) with a thickness of 1.0 m

Stage 2:

Delivery, spreading and compaction of exploded rock mass layers for the core of the embankment. Every layer is with a thickness of 30-40 cm and is compacted with 6-8 passings of a 10-ton road roller seawards from the tip of the existing groyne.

Stage3:

Rockfill embankment layer (500 – 1500 kg) for padding under the tetrapod layer

Stage 4:

Delivery and placing of 4t and 8t tetrapods from the sea with a floating crane

Stage 5:

Casing, reinforcement and concrete laying for the wave turning wall base

Stage 6:

Delivery, installment and grouting of the wave turning wall sections.

Stage 7:

Placing of the top tetrapod layer closest to the wave turning wall

Stage 8:

Delivery and driving of the quay wall steel sheet piles

Stage 9:

Delivery, installment and grouting of the anchors

Stage 10:

Delivery, spreading and compaction of exploded rock mass backfill behind the steel sheet pile wall. Every layer is with a thickness of 30-40 cm and is compacted with 6-8 passings of a 10-ton road roller

Stage 11:

Casing, reinforcement and concrete laying for the sheet pile wall grouting cap

Stage 12:

Works on the road surface

11 List of Figures

Figure 1: Aerial maps of Black Sea (left) and Bulgarian Black Sea coast (right); Source: Google Maps 4/10/2013	
Figure 2: Aerial map of Bourgas Bay; Source: Google Maps 4/10/2013.....	5
Figure 3: Location of Fishing Harbor Sarafovo; Source: Google Maps 4/10/2013	6
Figure 4: Navigation plan of the harbor	7
Figure 5: Basic parameters of ocean waves; Source: [34].....	9
Figure 6: Wave front and wave ray (orthogonal); Source: [34]	10
Figure 7: Qualitative wave power spectrum; Source: [33].....	11
Figure 8: Water particle orbits in deep and in shallow water; Source: [34].....	12
Figure 9: Approximate regions of validity of analytical wave theories; Source: [40]	13
Figure 10: Limits of application of the Stokes and Cnoidal wave theories, together with proposed demarcation line between both theories, adapted from Fenton 1990; Source: T.S. Hedges, 1995 [40]	14
Figure 11: Thin boundary layer scheme; Source: [34].....	14
Figure 12: Wind fetch; Source: Brooks/Cole – Thomson (2005).....	15
Figure 13: Bottom friction caused by wave action; Source: [34].....	15
Figure 14: Refraction.....	16
Figure 15: Diffraction.....	16
Figure 16: Reflection.....	16
Figure 17: Transmission; Source: [34]	16
Figure 18: Wave shoaling; Source: [34].....	16
Figure 19: Breaker type classification; Source: [30]	17
Figure 20: Shoaling, refraction, diffraction and reflection of waves in a nearshore region; Source: [34]	18
Figure 21: Aerial photo of Port of Bourgas; Source: Google Earth 06/15/2012	19
Figure 22: Kaliakra Cape; Source: inews.bg, author: Zdravko Doychev	20
Figure 23: Rip currents; Source: [34]	22
Figure 24: Meteorological observation stations in the Bourgas Bay region; Source Google Maps 4/10/2013.....	24
Figure 25: Wind velocity estimation; Source: [6]	32
Figure 26: Mean wave height [cm] from NE for deep water; Source: [1].....	33
Figure 27: Mean wave height [cm] from E for deep water; Source: [1]	34
Figure 28: Mean wave height [cm] from SE for deep water; Source: [1]	35
Figure 29: Mean wave height [cm] from S for deep water; Source: [1].....	36
Figure 30: Wind fetch – direction S; Source: Google Maps 4/10/2013	44
Figure 31: Graph for determining wave parameters period and wave height from the wind properties velocity, fetch and duration; Source: [3].....	45
Figure 32: Graph for determining the coefficient k_i ; Source: [3]	46
Figure 33: Graph for determining the value of λ in shallow water and λ_{sur} in the surf zone; Source: [3].....	47

Figure 34: Bathymetric map of Bourgas Bay	50
Figure 35: Harbor layout	50
Figure 36: Computational grid – direction E.....	52
Figure 37: Computational grid – direction SE.....	61
Figure 38: Computational grid – direction S	70
Figure 39: Scheme of characteristic points for computation analysis	77
Figure 40: Wave load zones along the Northern breakwater	78
Figure 41: Nomogram for determining refraction in shallow water; Source: [3].....	80
Figure 42: Graph for determining kt ; Source: [3].....	83
Figure 43: Graph for determining kl ; Source: [3]	84
Figure 44: Graph for determining ku ; Source: [3]	84
Figure 45: Graph for the estimation of h_{sur} ; Source: [3].....	85
Figure 46: Graph for determining λ_{sur} ; Source: [3].....	85
Figure 47: Wave height from E (case E02)	89
Figure 48: Wave height from SE (case SE02).....	89
Figure 49: Wave height from S (case S02).....	90
Figure 50: Diffraction coefficient in the shadow region	91
Figure 51: Diffracted wave height in the shadow region (direction S)	92
Figure 52: Aerial view of groyne 7. Source: Google Earth.....	95
Figure 53: Graph for determining the maximum possible wave height, Wiegel 1972; Source: [6].....	96
Figure 54: Aerial photo of Landslide Sarafovo; Source: Google Earth 19/9/2013	97
Figure 55: Typical cross section of the Northern quay-mole	99
Figure 56: Cross section of the Northern quay-mole showing the existing groyne contour	100
Figure 57: Sheet pile wall model in DeepXcav	101
Figure 58: Steel sheet pile wall Larssen 603 – dimension labeling in cross section. Source: [29]	103
Figure 59: Results from Limit Equilibrium analysis for steel sheet pile wall performed in DeepXcav: Bending moment, Shear force, Displacement and Support reactions	105
Figure 60: Results from Limit Equilibrium analysis for steel sheet pile wall performed in DeepXcav: Effective horizontal soil pressures	106
Figure 61: Results from Limit Equilibrium analysis for steel sheet pile wall performed in DeepXcav: Total and effective vertical soil pressures.....	107
Figure 62: Results from Limit Equilibrium analysis for steel sheet pile wall performed in DeepXcav: Water pressures and Surcharge pressures	108
Figure 63: Results from Limit Equilibrium analysis for steel sheet pile wall: Net total wall pressures	109
Figure 64: Values for coef. $K_{run}(1)$; Source: [2]	114
Figure 65: Values for coef. $K_{run}(2)$; Source: [2]	114

12 List of Tables

Table 1 Wave classification according to their period; Source: [34].....	10
Table 2 Mean monthly and annual wind velocity [m/s]; Source: [7]	26
Table 3 Mean monthly and annual wind velocity [m/s] by direction for station Pomorie [15].....	26
Table 4 Relative wind frequency [%] by velocity gradient for station Pomorie [15].....	26
Table 5 Relative frequency [%] for wind with $V > 5$ m/s for station Emine [20]	27
Table 6 Relative frequency [%] for wind with $V > 5$ m/s for station Bourgas [18]	27
Table 7 Relative frequency [%] for wind with $V > 5$ m/s for station Sozopol [21]	27
Table 8 Maximum wind velocity [m/s] of different probability of exceedance – station Emine; Source: [7].....	28
Table 9 Maximum wind velocity [m/s] of different probability of exceedance – station Bourgas; Source: [7].....	28
Table 10 Maximum wind velocity [m/s] of different probability of exceedance – station Sozopol; Source: [7].....	28
Table 11 Maximum wind velocity [m/s] from all directions of different probability of exceedance – station Pomorie; Source: [7]	29
Table 12 Frequency of the prevailing wind (% of the number of cases with wind) by direction - station Pomorie; Source: [7]	29
Table 13 Comparison of the study results with probability of exceedance curves for V_{max} published by P. Ivanov	29
Table 14 Duration of the strong winds for station Burgas; Source: [7].....	30
Table 15 Monthly distribution of wave heights in deep water from NE; Source: [1]	33
Table 16 Monthly distribution of wave heights in deep water from E; Source: [1]	34
Table 17 Monthly distribution of wave heights in deep water from SE; Source: [1]	35
Table 18 Monthly distribution of wave heights in deep water from S; Source: [1]	36
Table 19 Maximum rise and decline from the average multiannual water level for the Black Sea west coast; Source: [17]	39
Table 20 Wave properties in deep water – E; Source: [18]	41
Table 21 Wave properties in deep water - SE; Source: [18].....	41
Table 22 Wave properties with direction E at depth 35m; Source: [18].....	43
Table 23 Wave properties with direction SE at depth 35m; Source: [18]	43
Table 24 Wave properties with direction E at depth 12m; Source: [1].....	43
Table 25 Wave properties with direction SE at depth 12m; Source: [1]	43
Table 26 Wave properties at depth 35m – direction E; Source: Table 22	51
Table 27 Wave properties at depth 35m – direction SE; Source: Table 23	51

Table 28 Wave properties at depth 35m – direction S; Source: Chapter 3.5	51
Table 29: Computed wave heights (from chapter 4.3).....	77
Table 30 Plan of wave refraction for direction E.....	81
Table 31 Plan of wave refraction for direction SE.....	82
Table 32 Wave properties at depth 5.5m for waves from E and SE.....	88
Table 33 Wave height comparison at the harbor entrance – directions E and SE	93
Table 34 Wave height comparison at harbor entrance – direction S	93
Table 35 Wave properties and water depth in the three wave impact zones along the mole-quay	96
Table 36 Mechanical properties of the geological strata; Source: [1]	98
Table 37 Coefficient μ_{ϕ} for different armour units; Source: [2]	110
Table 38 Determining the stability coefficient K_D ; Source: [26].....	111
Table 39 Calculation results of the armour unit weight on the structure sea slope	112
Table 40 Values for k_{Δ} and k_p in relation to slope cover type and relative roughness; Source: [2].....	113
Table 41 Values for coef. k_c ; Source: [2]	113
Table 42 Values for coef. k_{β} ; Source: [2].....	114
Table 43 Values for coef. k_{irr} ; Source: [2].....	115
Table 44 Wave run-up height on the breakwater slope	116

13 List of Drawings

Appendix 1 to the Master's Assignment – Topographic and bathymetric map of the harbor range

Drawing 1 – Layout (general plan) of Fishing Harbor Sarafovo

Drawing 2 – Wave refraction plan (E, SE)

Drawing 3 – Northern quay-mole - Layout – tracing and wave impact zones

Drawing 4 – Northern quay-mole - Longitudinal profile

Drawing 5 – Northern quay-mole - Cross sections, Construction stages

Drawing 6 – Wave turning wall, Precast reinforced concrete cassettes - Detailed drawings – Formwork and reinforcement plan

Drawing 7 – Fender, Bollard – Detailed drawings

14 Sources of reference

- [1] Hydrodynamic, lithodynamic survey and engineering-geological properties of project – Fishing Harbor Sarafovo – Bourgas: <http://www.burgas.bg/uploads/40fcd5033fb5dead30fe9c5eff632ffa.pdf>
- [2] Standards for loads and impacts on hydraulic structures by waves, ice and vessels. Sofia, (1989)
- [3] СНИП 2.06.04-82*. Нагрузки и воздействия на ГТС, 1986. p. 31, §7; § 10/1
- [4] Anguelov, K, 1997. Engineering Geodynamics. Sofia. p. 237
- [5] Antonov, Hr., Danchev, D. 1980 Groundwater in Bulgaria Sofia. pub. Technika.
- [6] Shore Protection Manual, 1984, 4th ed, II vol. US Army Engineer Waterways Experiment Station, Coastal Engineering Research Center, US Government Printing Office, Washington DC
- [7] NIMH – BAS Climate Reference Book 1982 – vol. IV – Wind
- [8] Standards for design of hydrotechnical structures. Basic principles BBA 11, Sofia, 1985;
- [9] Ordinance № 9 dated 29 July 2005 for the serviceability of ports and harbors (Official Gazette. 65 of 9 August 2005. amend. OG. 103 of 7 December)
- [10] Demireva, D., Peychev, V.2010. Sea level fluctuations in Bourgas Bay. Pub. by USB Varna.
- [11] Kostichkova, D., Peychev, V. and others 1985. Hydrodynamic and lithodynamic conditions in the coastal zone of Sarafovo site.
- [12] Peychev, V. 2004. Morphodynamic and lithodynamic processes in the coastal zone. Pub. Slavena, Varna, p. 231.
- [13] Project: Oil Pipeline “Bourgas – Alexandroupolis”, Marine terminal in Port Bourgas –Natural conditions data, ILF COSULTING ENGINEERS, 1999
- [14] Gergov, G., Dynamics and sediment impact on the coastal beach line, Coastal protection and long-term stabilization of the Black Sea coast slopes,BAS, 1998;
- [15] Daskalov, Kr., Modev, St., Lissev, N., Tachev, S.,Coastal protection facility and boat quay – Pomorie. Numerical modeling of the wave regime, 2005;
- [16] Давидана, И. Н., Теоретические основы и методы расчета ветрового волнения, Л. Гидрометеиздат, 1988
- [17] German, V. H., 1971. Investigation and estimation of probability characteristics of extreme sea levels. 1971 Proceedings of SOI, Vol. 107, p. 149
- [18] Daskalov, K., Lissev, N. :Port “Burgas” –Master Plan, Extention and reconstruction, Vol 2, Ch. 2.2, 1995
- [19] Minkov, V., Port Construction, Pub.“Technika” 1971. Tabl. 2.26-B ,p. 52
- [20] Belberov, Z., Kostichkova, D., Cherneva, Zh.,Rabi, A., Valchev, N. Wind and wave climate in the Bourgas Bay region, Works of the Institute of Oceanology, vol. 5. Varna 2004, Bulgarian Academy of Science.
- [21] Kostichkova, D., Cherneva, Zh., Velcheva, A. Wind waves climate in the Western Black Sea. Work of the IV International Conference for Ocean Engineering and Marine Technology (Black Sea’97), May 1997, Varna.

- [22] Kostichkova, D., Belberov, Z., Trifonova, E., Grudeva, D. Maximum water levels in the Bourgas Bay. Works of the Institute of Oceanology, vol. 3. Varna 2001, Bulgarian Academy of Science.
- [23] Kostichkova, D., Belberov, Z., Analysis of maximum water levels along the Bulgarian Black Sea coast. 1985, Oceanology, 14, 3-8.
- [24] Cherneva, Zh., Valchev, N., Petrova, P., Andreeva, N., Valcheva, N. Distribution of deepwater properties of wind waves in the Bulgarian Black Sea sector. Works of the Institute of Oceanology, vol. 4. Varna 2003, Bulgarian Academy of Science.
- [25] Keremedchiev, S., Morpho-hydrographical analysis of the Bulgarian Black Sea coastal area, Works of the Institute of Oceanology, vol. 3. Varna 2001, Bulgarian Academy of Science.
- [26] Hydraulic Structures 4th edition P. Novak, A.I.B. Moffat, C. Nalluri, R. Narayanan table 15.3. p. 649
- [27] S.F. Dotsenko, A. K. Tsunami waves in the Black Sea in 1927: observations and numerical modeling.
- [28] Carl A. Thoresen „Port Designer's Handbook: Recommendations And Guidelines” (2003) p. 127 Table 4.3
- [29] http://www.spundwand.de/fileadmin/HSP/Downloads/pdf/larssen/Larssen_603_2013.pdf
- [30] <http://hmf.enseiht.fr/travaux/CD9900/travaux/optsee/bei/info/deavague/rapport.htm>
- [31] Law on Maritime Spaces, Inland Waterways and Ports of the Republic of Bulgaria (Official Gazette. 12 of 11 February 2000. amend. OG. 23 of 22 March 2011)
- [32] Zhelev, Zh., Filipov, K., Stoev, D. Engineering geological study for project “Reconstruction and modernization of Fishing Harbor Sarafovo - Bourgas (2012).
- [33] www.tidesandcurrents.noaa.gov
- [34] Lissev, N. Marine Hydrodynamics (lectures) UACEG, Sofia
- [35] Sorensen, R. M., (1993), Basic Wave Mechanics for Coastal and Ocean engineers. John Wiley & Sons
- [36] Dean, R. G. & Dalrymple R. A. (1984), Water Wave Mechanics for Engineers and Scientists, Prentice-Hall, Englewood Cliffs.
- [37] Ilov, G 2006 Soil Mechanics. Pub. „Era”. p. 196
- [38] Inman, D. L., and Brush, B.M., 1973. The Coastal Challenge. Science, 181, 20-32
- [39] Fenton, J. D. Nonlinear Wave Theories (1990) from *The Sea – Volume 9: Ocean Engineering Science, Part A*, edited by Le Méhauté, B. and Hanes, D.M.
- [40] Hedges, T. S. Regions of Validity of Analytical Wave Theories (1995)



Preliminary Design of the Northern Breakwater-Quay from the Project: “Reconstruction and Modernization of Fishing Harbor Sarafovo”

MASTER’S THESIS

DRAWINGS

submitted for the degree of
“MASTER OF SCIENCE”

Master’s programme

Infrastructure Planning and Management

submitted by

Stefina Dimitrova

Matriculation number 0927914

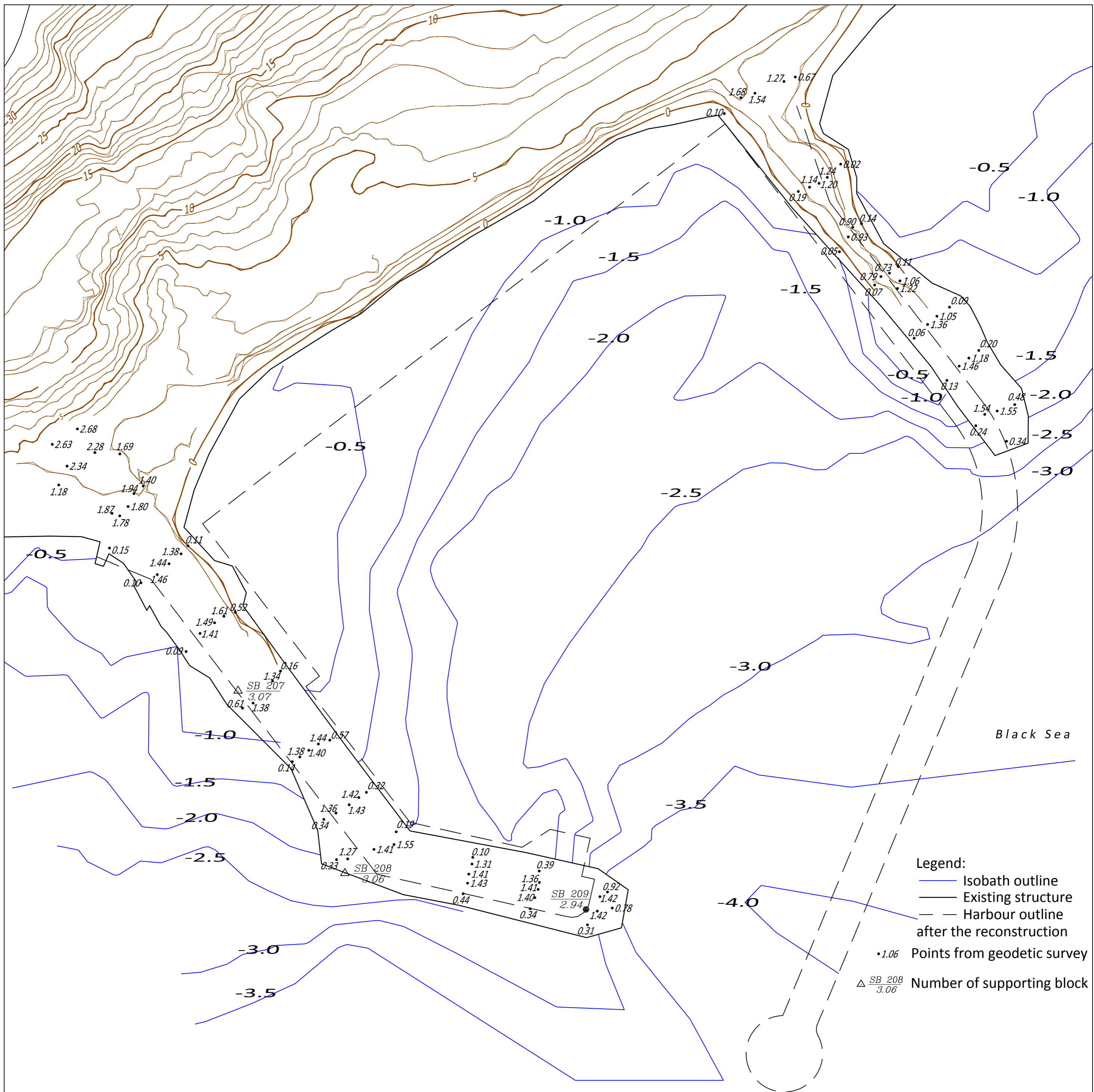
under the supervision of

Prof. John Fenton

Ao.Univ.Prof. Dipl.-Ing. Dr.techn. Norbert Krouzecky

Assoc. Prof. Dr. Eng. Ignat Ignatov

Sofia, October 2014



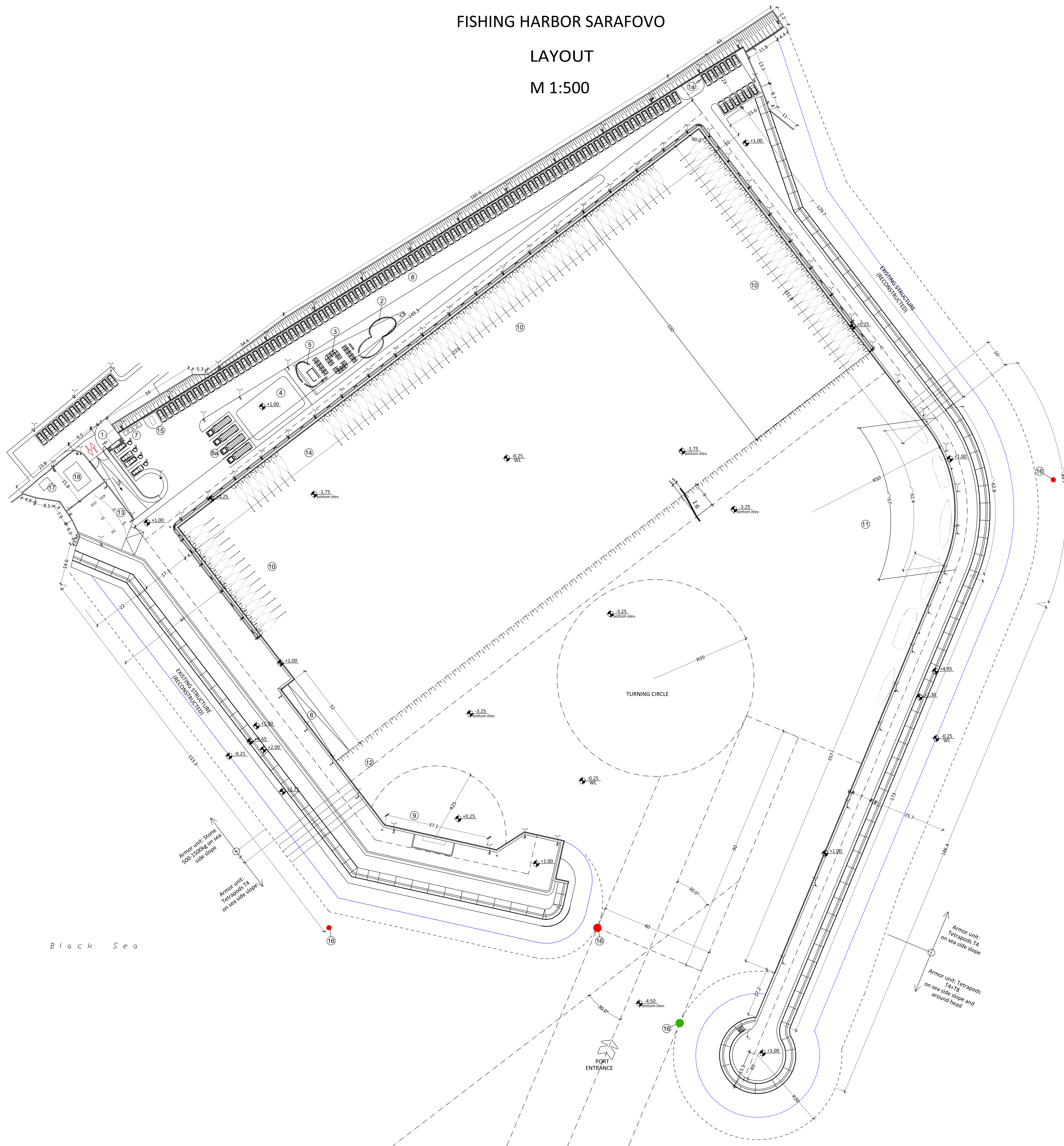
- Legend:**
- Isobath outline
 - Existing structure
 - Harbour outline after the reconstruction
 - 1.06 Points from geodetic survey
 - △ $\frac{SB\ 208}{3.06}$ Number of supporting block

University for Architecture, Civil Engineering and Geodesy - Sofia Vienna University of Technology			
Chair	Hydraulic Engineering		
Project	Reconstruction and modernization of Fishing Harbor "Sarafovo"		
Drawing	App. 1	Topographic and bathymetric map of the harbor range	M 1:1000
Graduate	Stefina Dimitrova	Nr. 0927914	Nr. 689
Supervisors	Prof. J. FENTON Ao.Univ.Prof. Dipl.-Ing. Dr.techn. N. KROUZECKY Assoc. Prof. Dr. Eng. I. IGNATOV		

FISHING HARBOR SARAFOVO

LAYOUT

M 1:500



KEY:

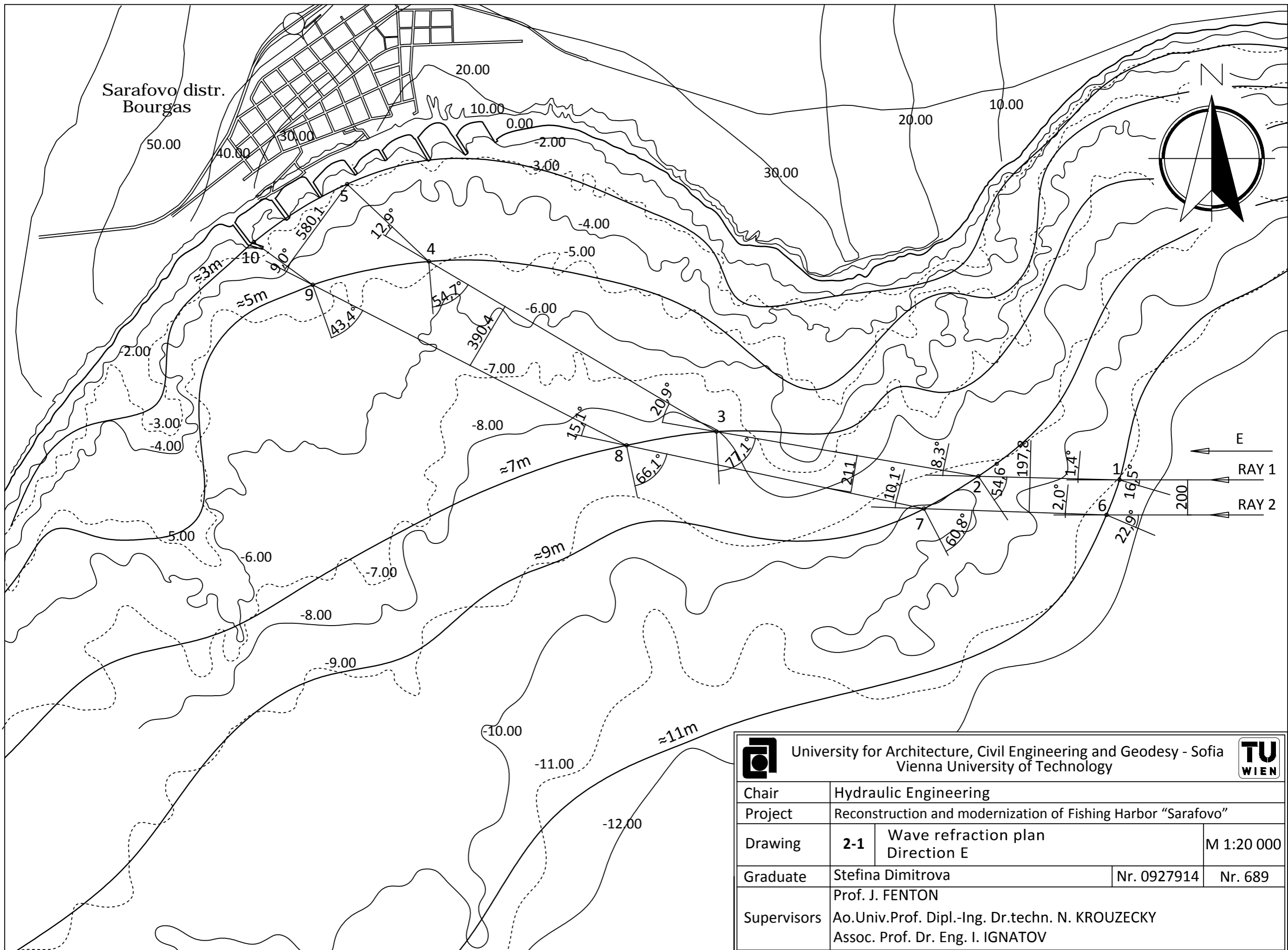
1. Checkpoint, Security and video surveillance
- 1a. Security and video surveillance
2. Building for domestic purposes and administration - II Stage
3. Covered market-place /fish market/ - II Stage
4. Platform for loading, sorting and primary draught processing
5. Warehouses for draught, wrapping and equipment - II Stage
6. Covered berth
7. Area for port reception facilities /secured zone with constant video surveillance and guard/
8. Parking - 103 parking spaces for vehicles (incl. 4 for disabled)
- 8a. Parking - 4 parking spaces for heavy trucks
9. Bunker area
10. Berthing and mooring area for vessels up to 8m in length; number of spaces: 104
11. Berthing and mooring area for fishing ships up to 20m in length; number of spaces: 6
12. Draught unloading area for ships up to 20m in length
13. Open-air repair site for vessels
14. Draught unloading area for ships up to 8m in length
15. Generator for electricity
16. Anchor with buoy
17. Power substation
18. Pumping station



Entrance/Exit to the construction site

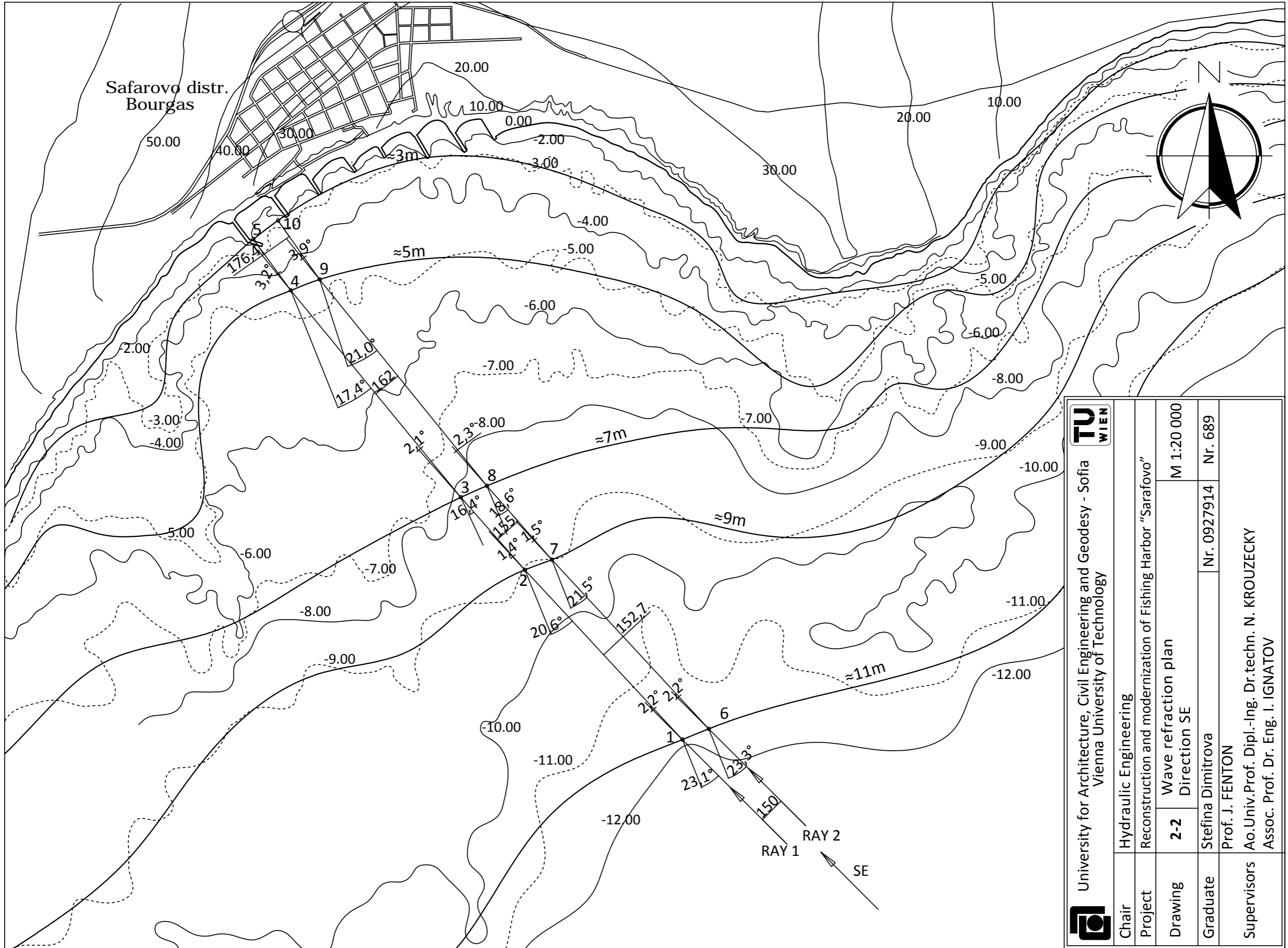
Entrance/Exit Port

Altitude system: Baltic

University for Architecture, Civil Engineering and Geodesy - Sofia Vienna University of Technology			
Chair	Hydraulic Engineering		
Project	Reconstruction and modernization of Fishing Harbor "Sarafovo"		
Drawing	1	Layout of Fishing Harbor Sarafovo	M 1:500
Graduate	Stefina Dimitrova	Nr. 0927914	Nr. 689
Supervisors	Prof. J. FENTON Ao.Univ.Prof. Dipl.-Ing. Dr.techn. N. KROUZECKY Assoc. Prof. Dr. Eng. I. IGNATOV		



 University for Architecture, Civil Engineering and Geodesy - Sofia Vienna University of Technology			
Chair	Hydraulic Engineering		
Project	Reconstruction and modernization of Fishing Harbor "Sarafovo"		
Drawing	2-1	Wave refraction plan Direction E	M 1:20 000
Graduate	Stefina Dimitrova	Nr. 0927914	Nr. 689
Supervisors	Prof. J. FENTON Ao.Univ.Prof. Dipl.-Ing. Dr.techn. N. KROUZECKY Assoc. Prof. Dr. Eng. I. IGNATOV		

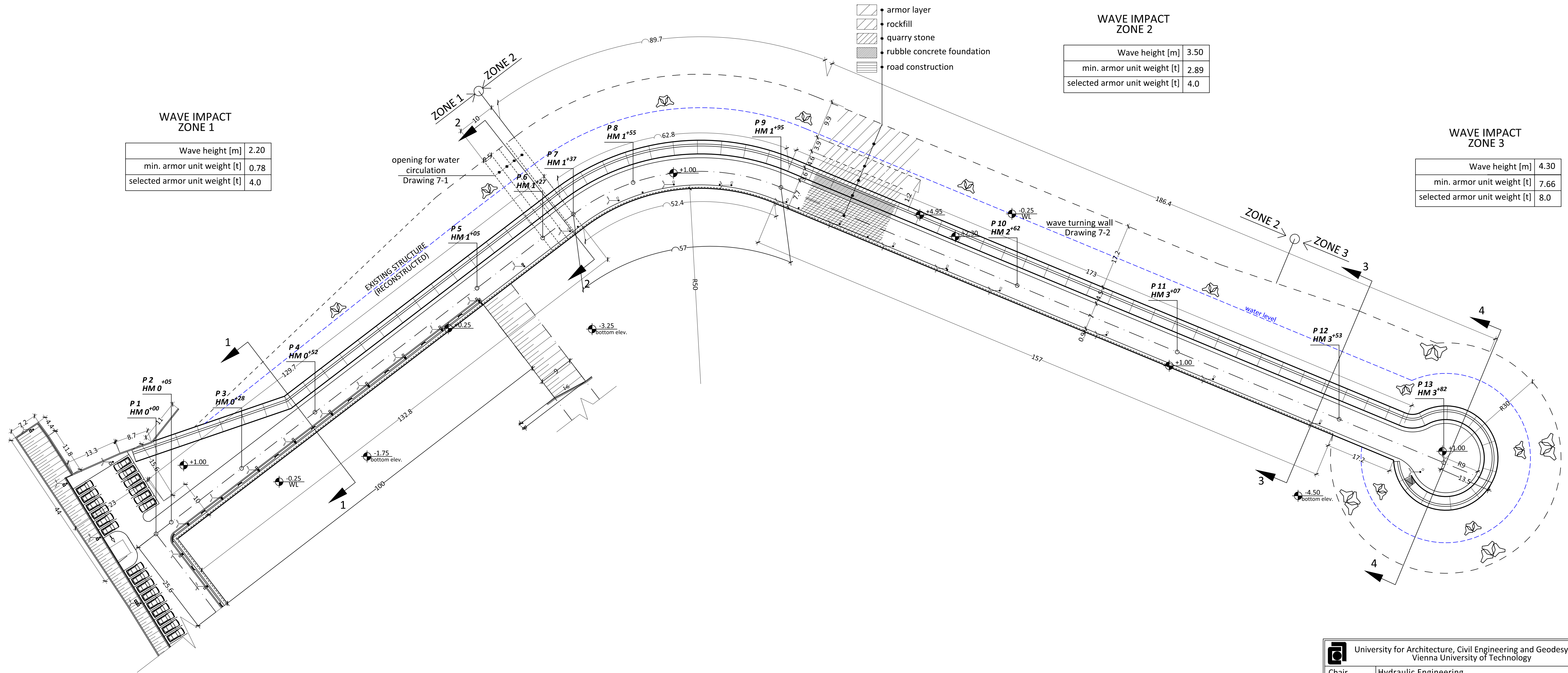


University for Architecture, Civil Engineering and Geodesy - Sofia
Vienna University of Technology



Chair	Hydraulic Engineering		
Project	Reconstruction and modernization of Fishing Harbor "Sarafovo"		
Drawing	2-2	Wave refraction plan Direction SE	M 1:20 000
Graduate	Stefina Dimitrova	Nr. 0927914	Nr. 689
Supervisors	Prof. J. FENTON Ao.Univ.Prof. Dipl.-Ing. Dr.techn. N. KROUZECKY Assoc. Prof. Dr. Eng. I. IGNATOV		

NORTHERN QUAY-MOLE TRACING AND WAVE IMPACT ZONES



WAVE IMPACT ZONE 1

Wave height [m]	2.20
min. armor unit weight [t]	0.78
selected armor unit weight [t]	4.0

WAVE IMPACT ZONE 2

Wave height [m]	3.50
min. armor unit weight [t]	2.89
selected armor unit weight [t]	4.0

WAVE IMPACT ZONE 3

Wave height [m]	4.30
min. armor unit weight [t]	7.66
selected armor unit weight [t]	8.0

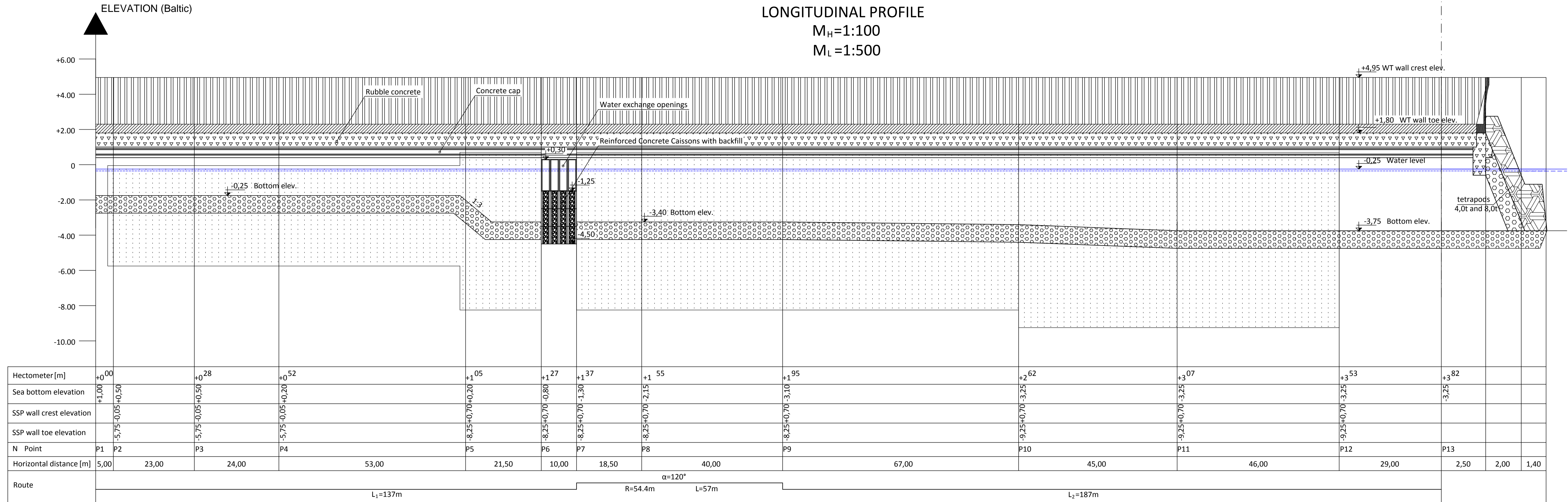
University for Architecture, Civil Engineering and Geodesy - Sofia Vienna University of Technology			
Chair	Hydraulic Engineering		
Project	Reconstruction and modernization of Fishing Harbor "Sarafovo"		
Drawing	3	Northern Quay-mole Layout - tracing and wave impact zones	M 1:500
Graduate	Stefina Dimitrova	Nr. 0927914	Nr. 689
Supervisors	Prof. J. FENTON Ao.Univ.Prof. Dipl.-Ing. Dr.techn. N. KROUZECKY Assoc. Prof. Dr. Eng. I. IGNATOV		


NORTHERN BREAKWATER-QUAY

LONGITUDINAL PROFILE

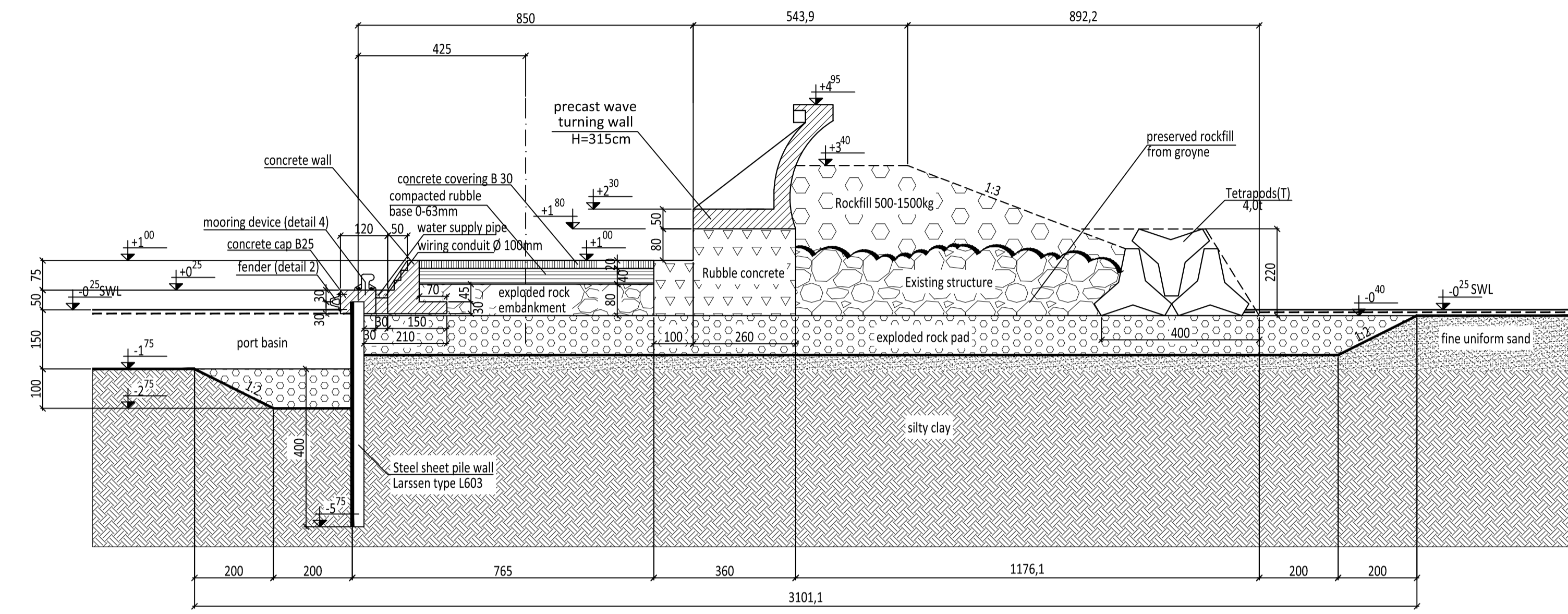
$M_H=1:100$

$M_L=1:500$

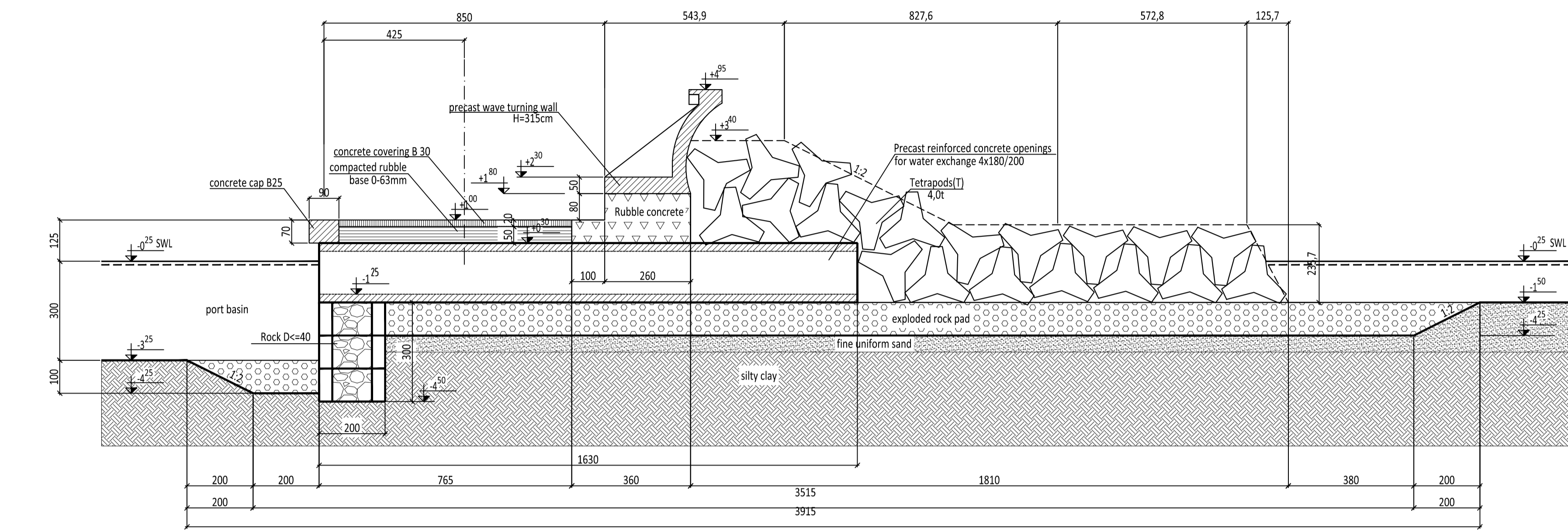


 University for Architecture, Civil Engineering and Geodesy - Sofia Vienna University of Technology			
Chair	Hydraulic Engineering		
Project	Reconstruction and modernization of Fishing Harbor "Sarafovo"		
Drawing	4	Northern quay-mole - Longitudinal profile	M 1:100 M 1:500
Graduate	Stefina Dimitrova	Nr. 0927914	Nr. 689
Supervisors	Prof. J. FENTON Ao.Univ.Prof. Dipl.-Ing. Dr.techn. N. KROUZECKY Assoc. Prof. Dr. Eng. I. IGNATOV		

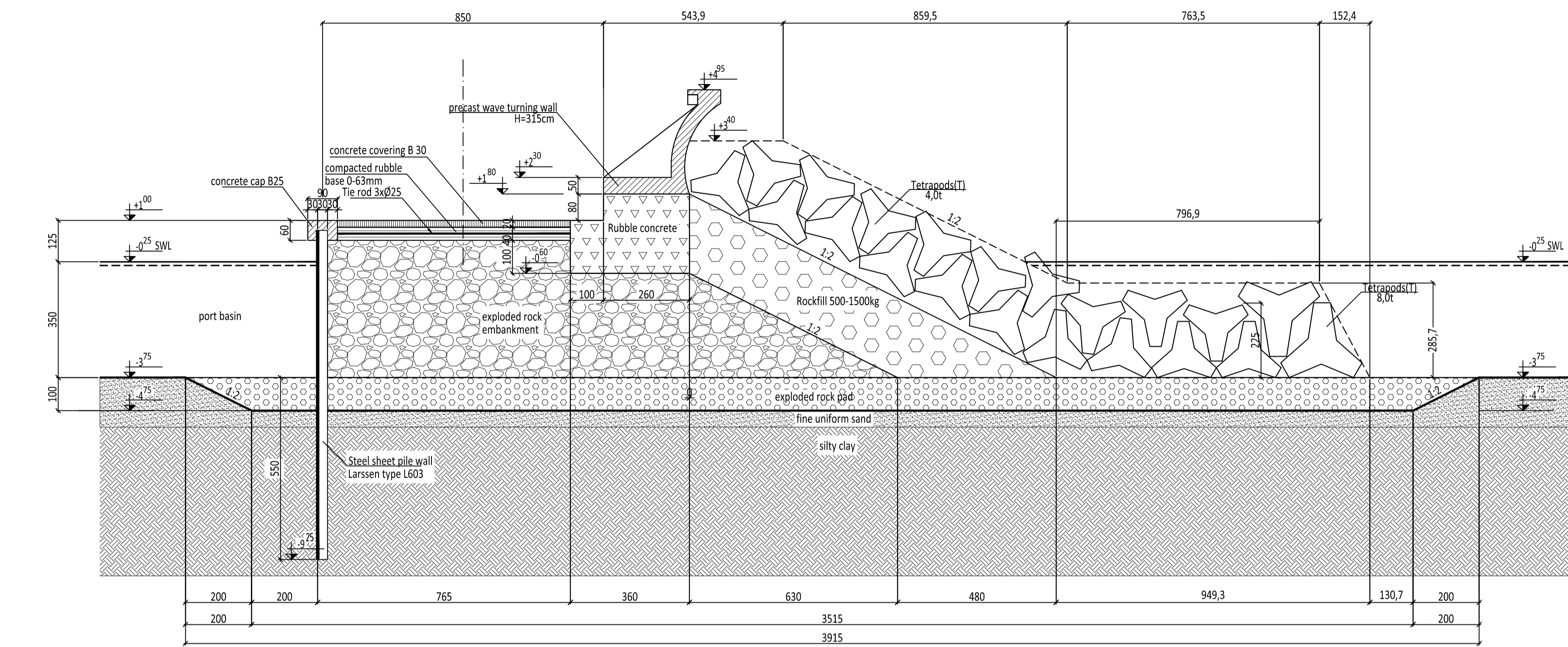
SECTION 1 - 1



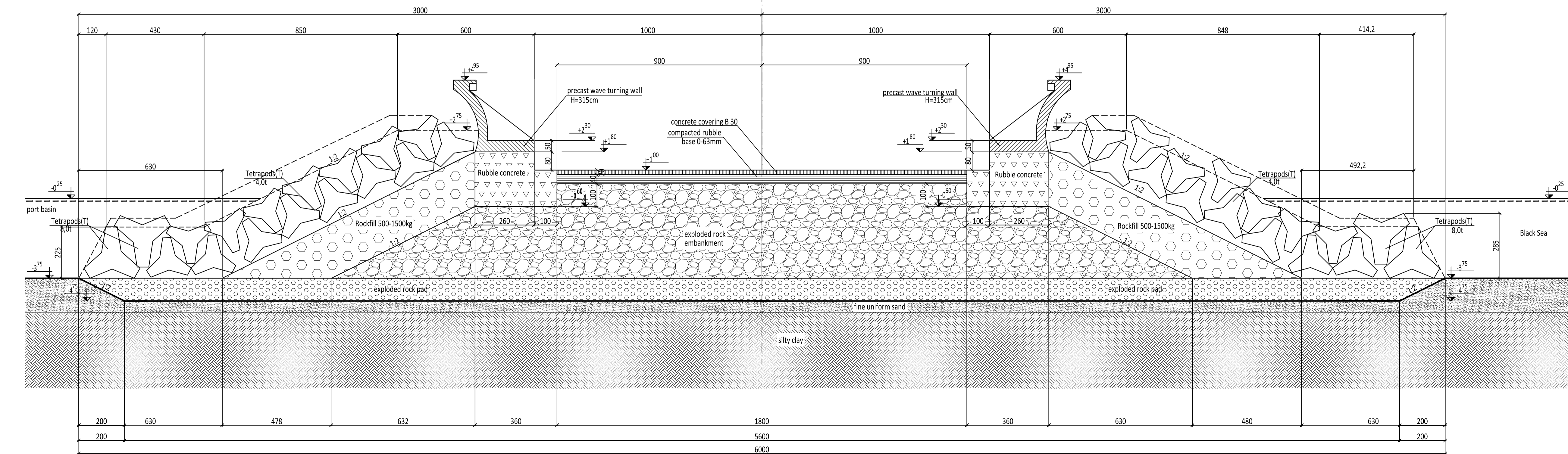
SECTION 2 - 2



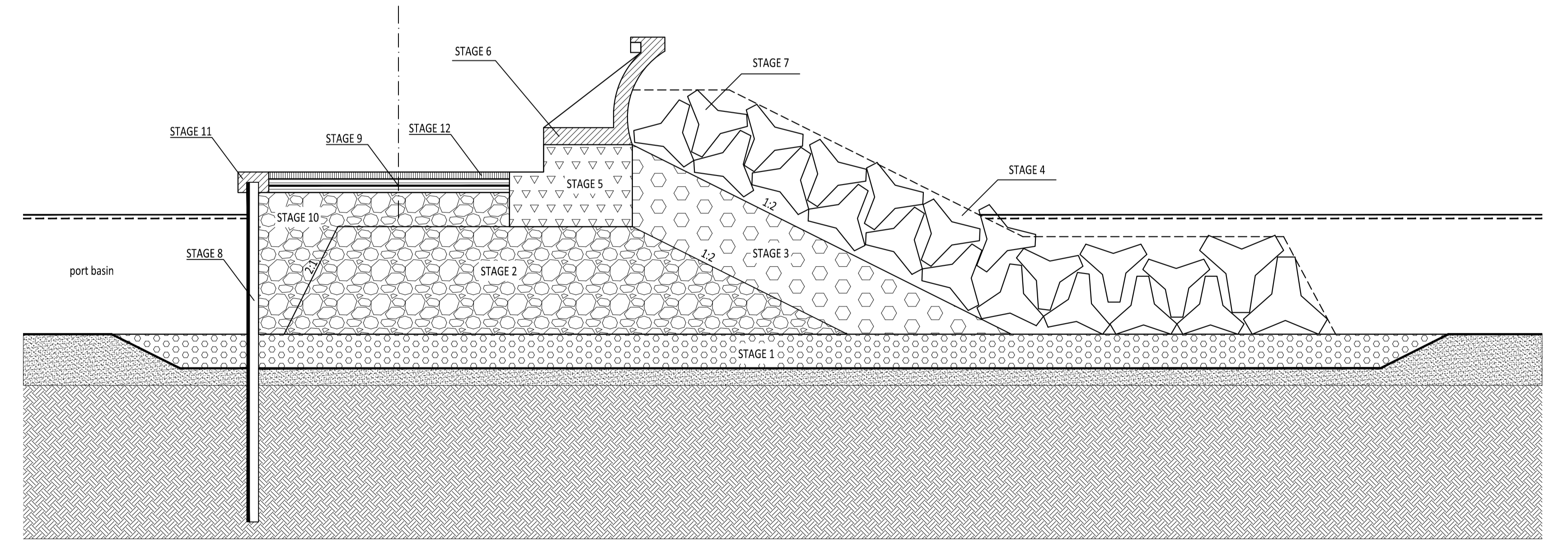
SECTION 3 - 3



SECTION 4 - 4



CONSTRUCTION STAGES

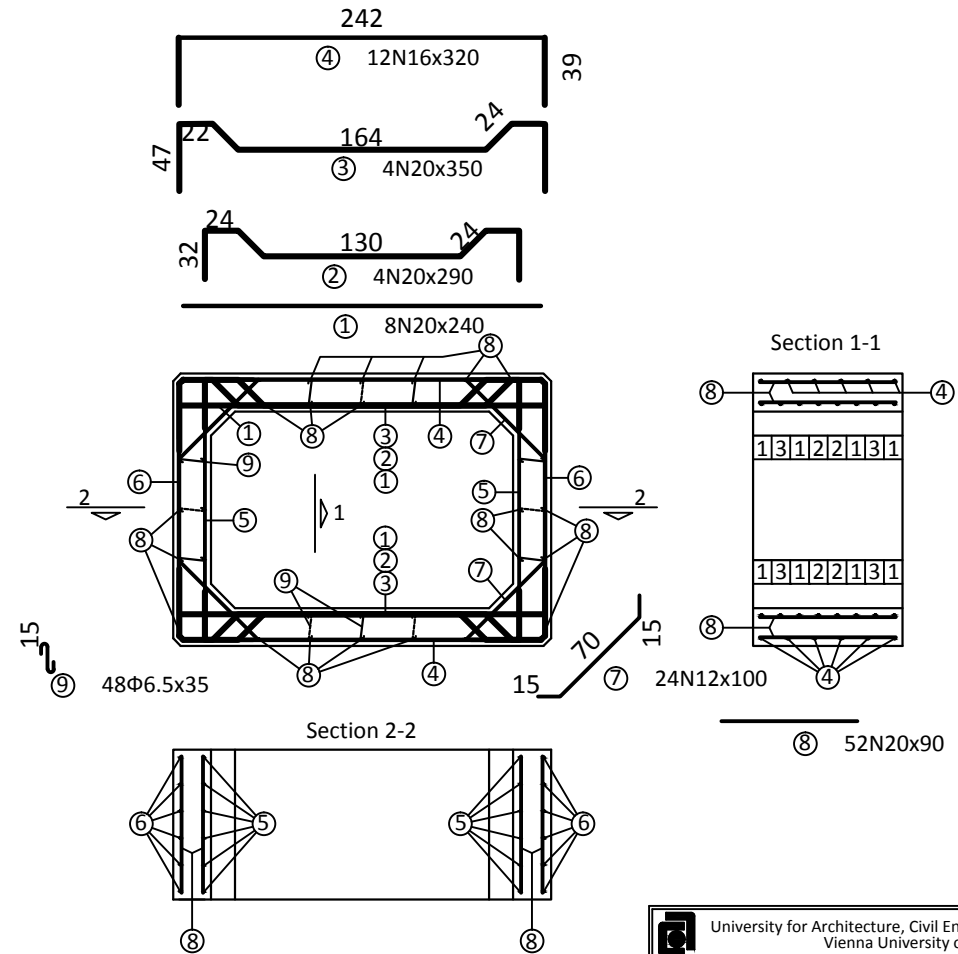
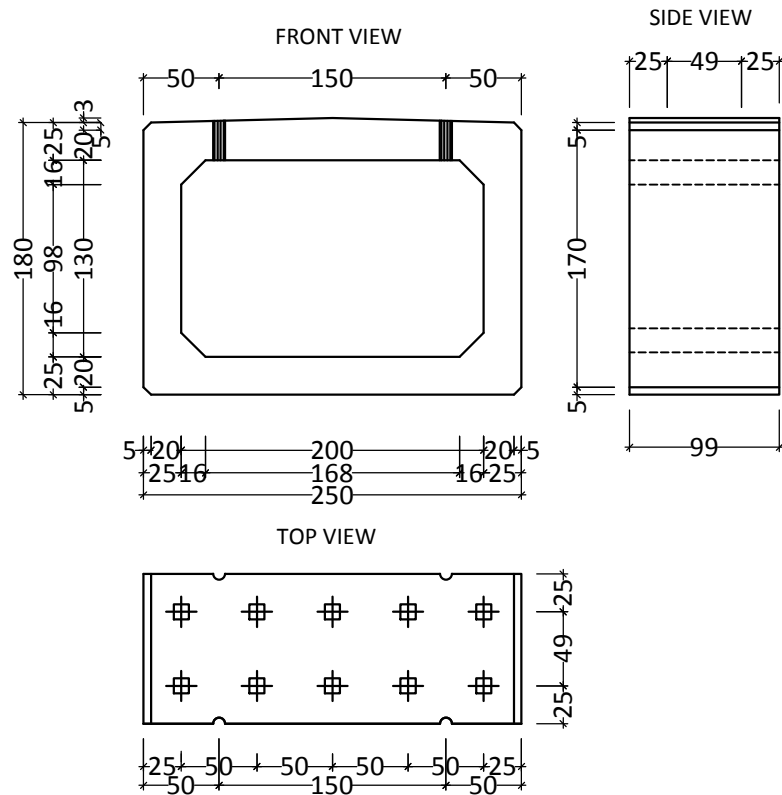



University for Architecture, Civil Engineering and Geodesy - Sofia Vienna University of Technology			
Chair	Hydraulic Engineering		
Project	Reconstruction and modernization of Fishing Harbor "Sarafovo"		
Drawing	5	Northern quay-mole - Cross sections, Construction stages	M 1:100
Graduate	Stefina Dimitrova	Nr. 0927914	Nr. 689
Supervisors	Prof. J. FENTON Ao.Univ.Prof. Dipl.-Ing. Dr.techn. N. KROUZECKY Assoc. Prof. Dr. Eng. I. IGNATOV		

Precast concrete cassette

Reinforcement plan
1:25

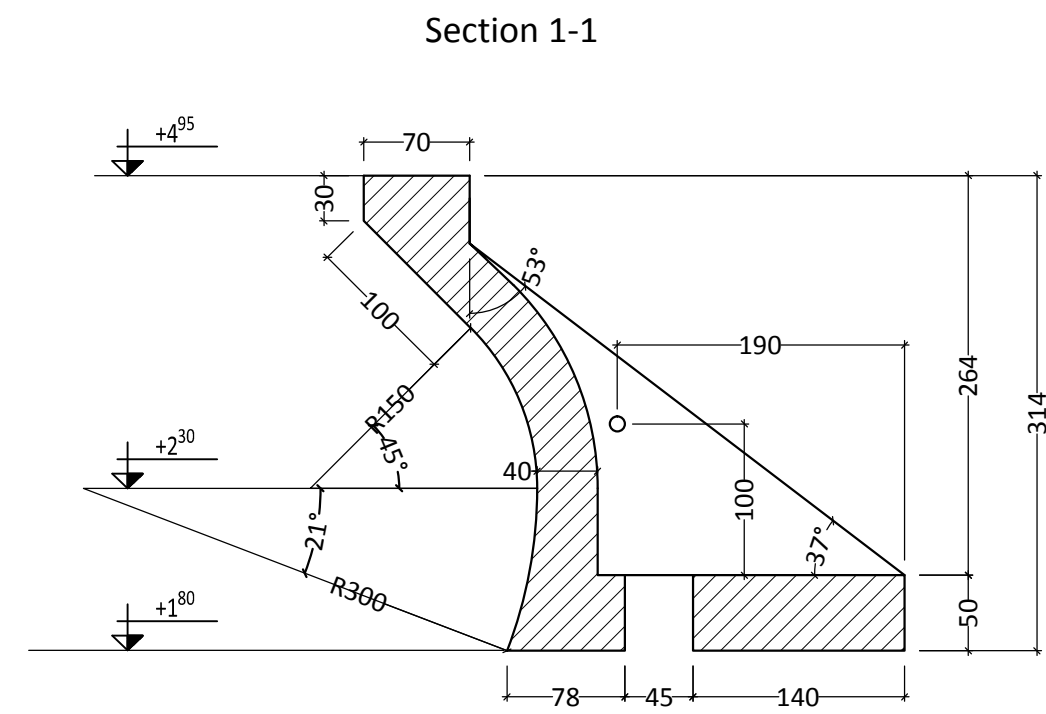
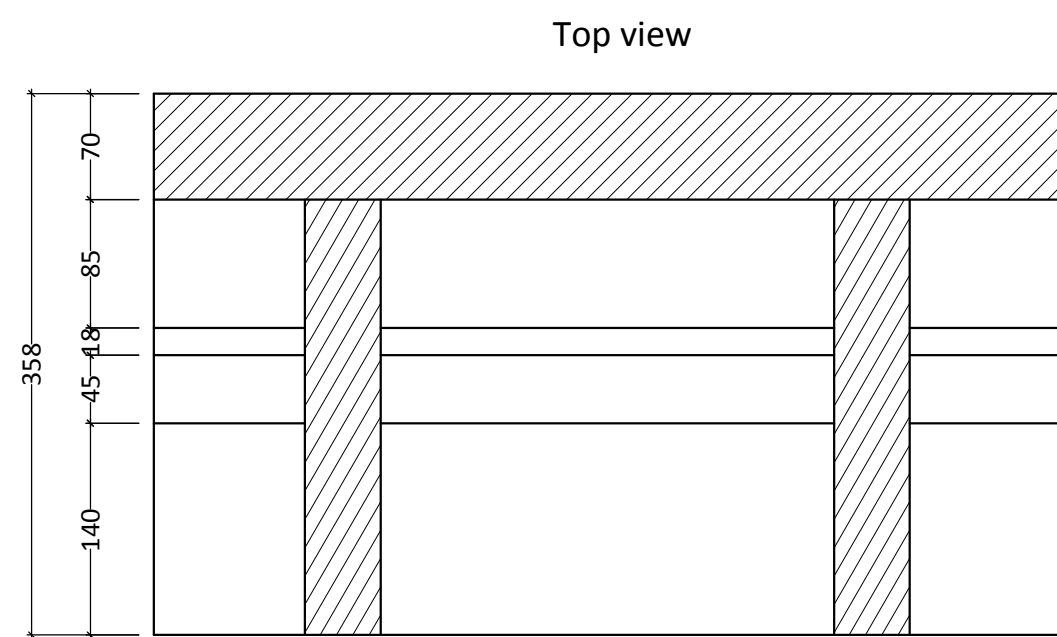
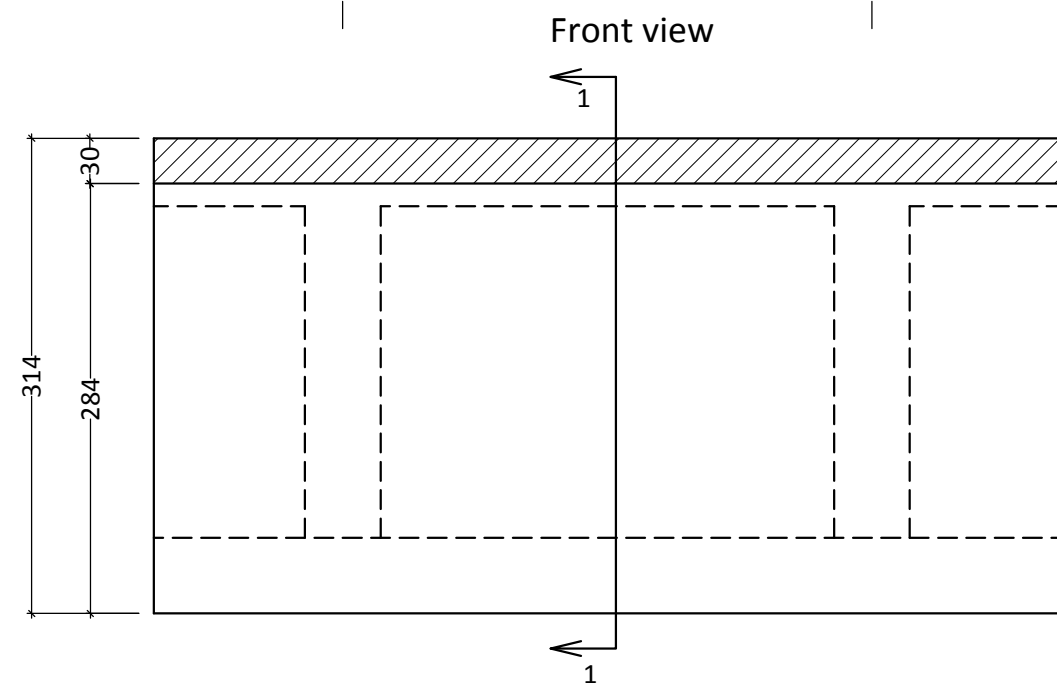
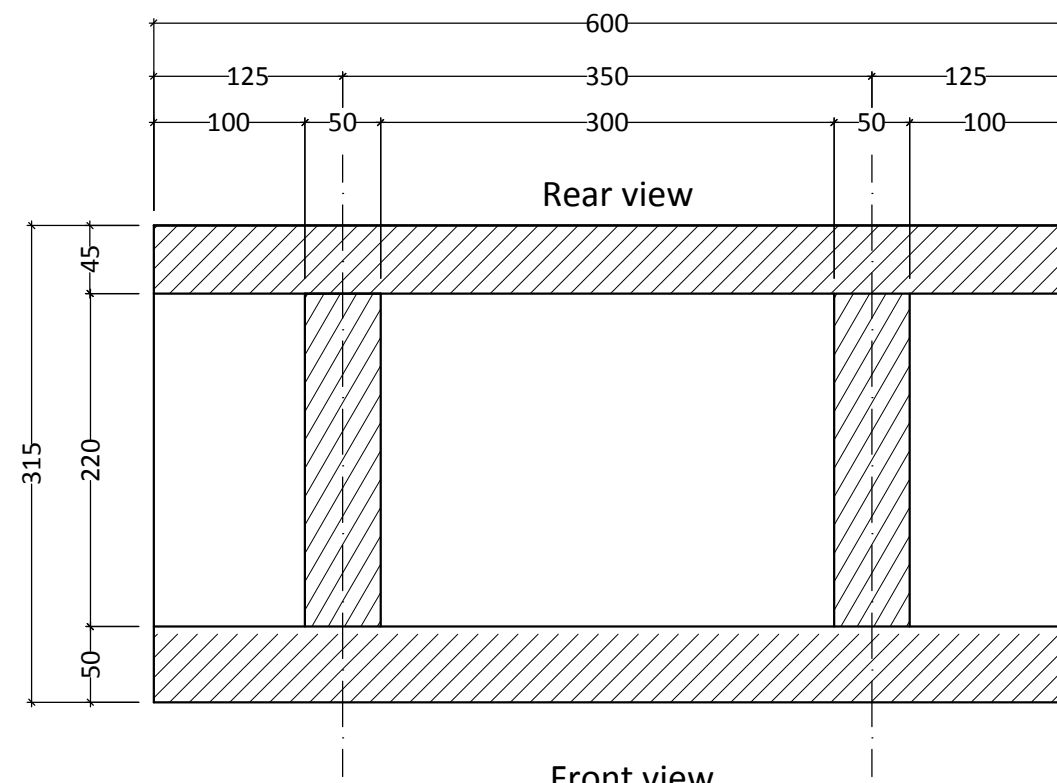
Formwork Plan
1:25



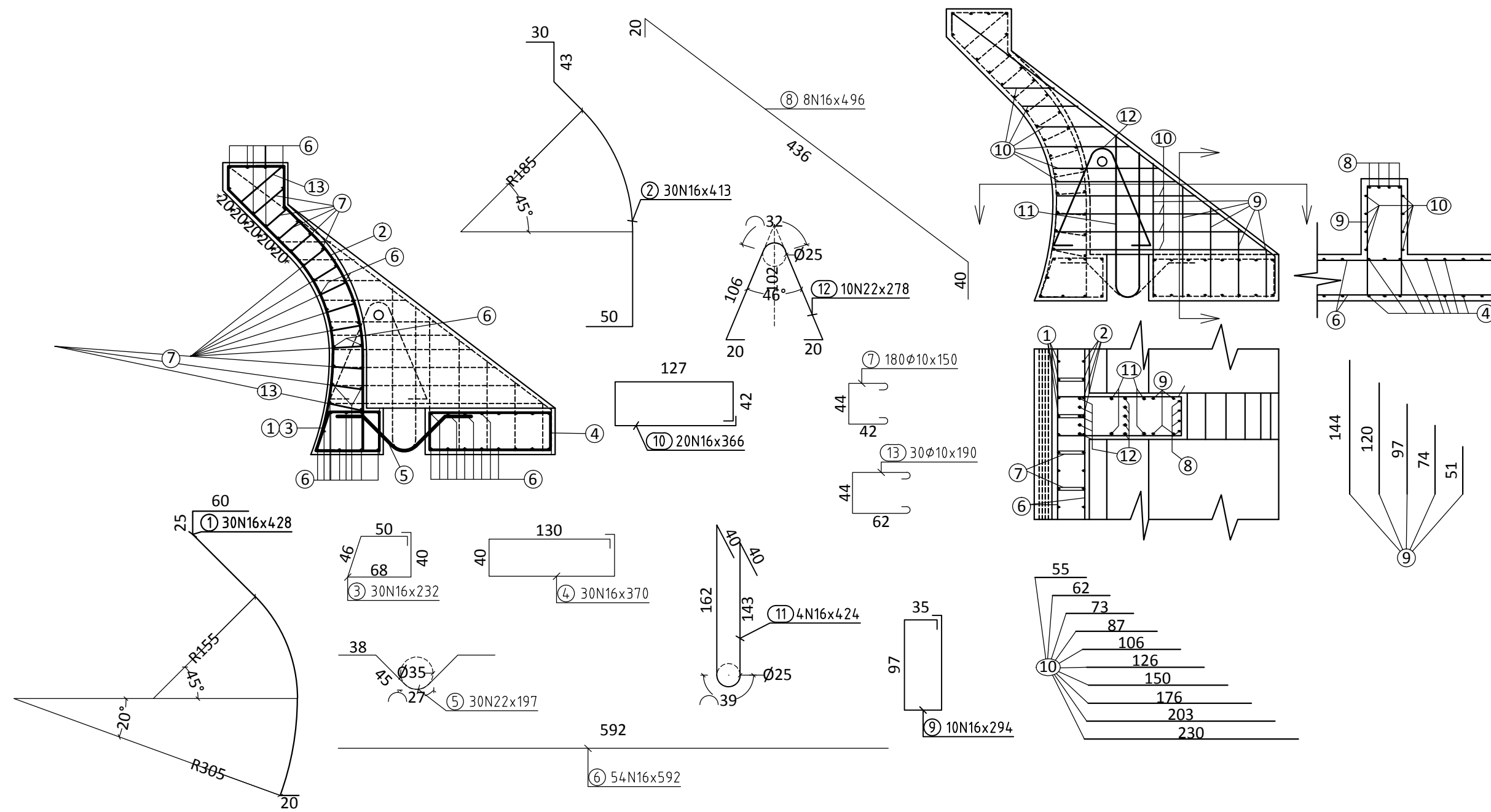
 University for Architecture, Civil Engineering and Geodesy - Sofia Vienna University of Technology			
Chair	Hydraulic Engineering		
Project	Reconstruction and modernization of Fishing Harbor "Sarafovo"		
Drawing	7-1	Reinforced concrete cassette - Formwork plan, Reinforcement plan	M 1:25
Graduate	Stefina Dimitrova	Nr. 0927914	Nr. 689
Supervisors	Prof. J. FENTON Ao.Univ.Prof. Dipl.-Ing. Dr.techn. N. KROUZECKY Assoc. Prof. Dr. Eng. I. IGNATOV		

Formwork Plan M 1:50

Precast wave turning wall section

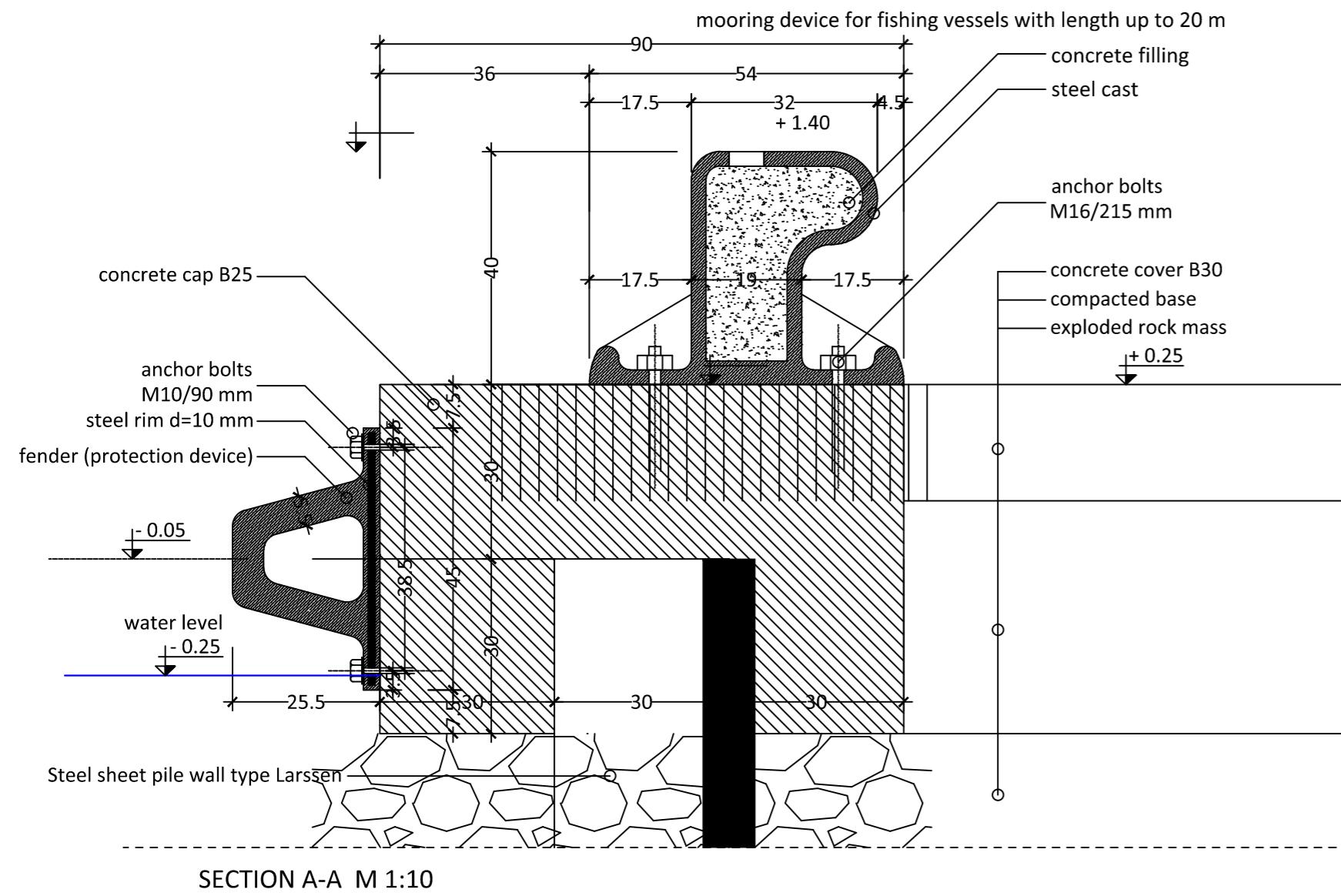
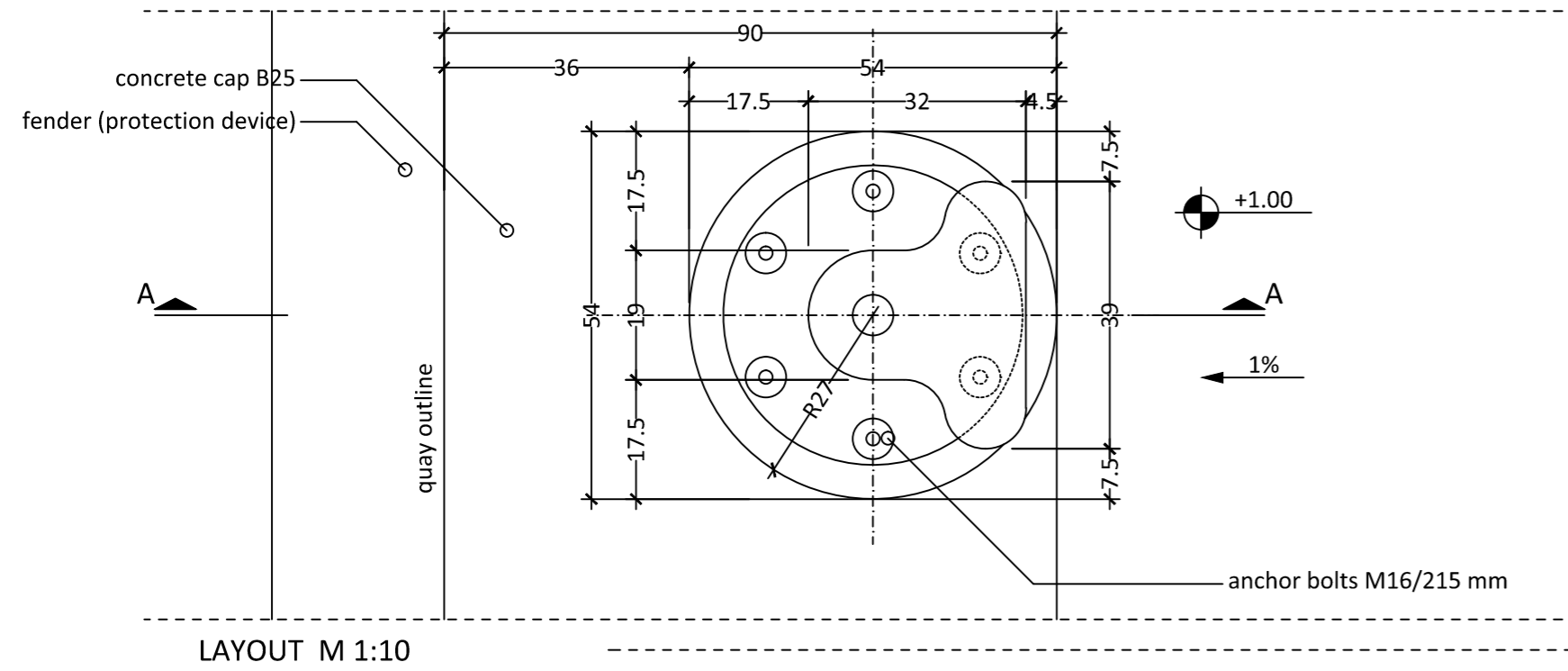


Reinforcement Plan M 1:50

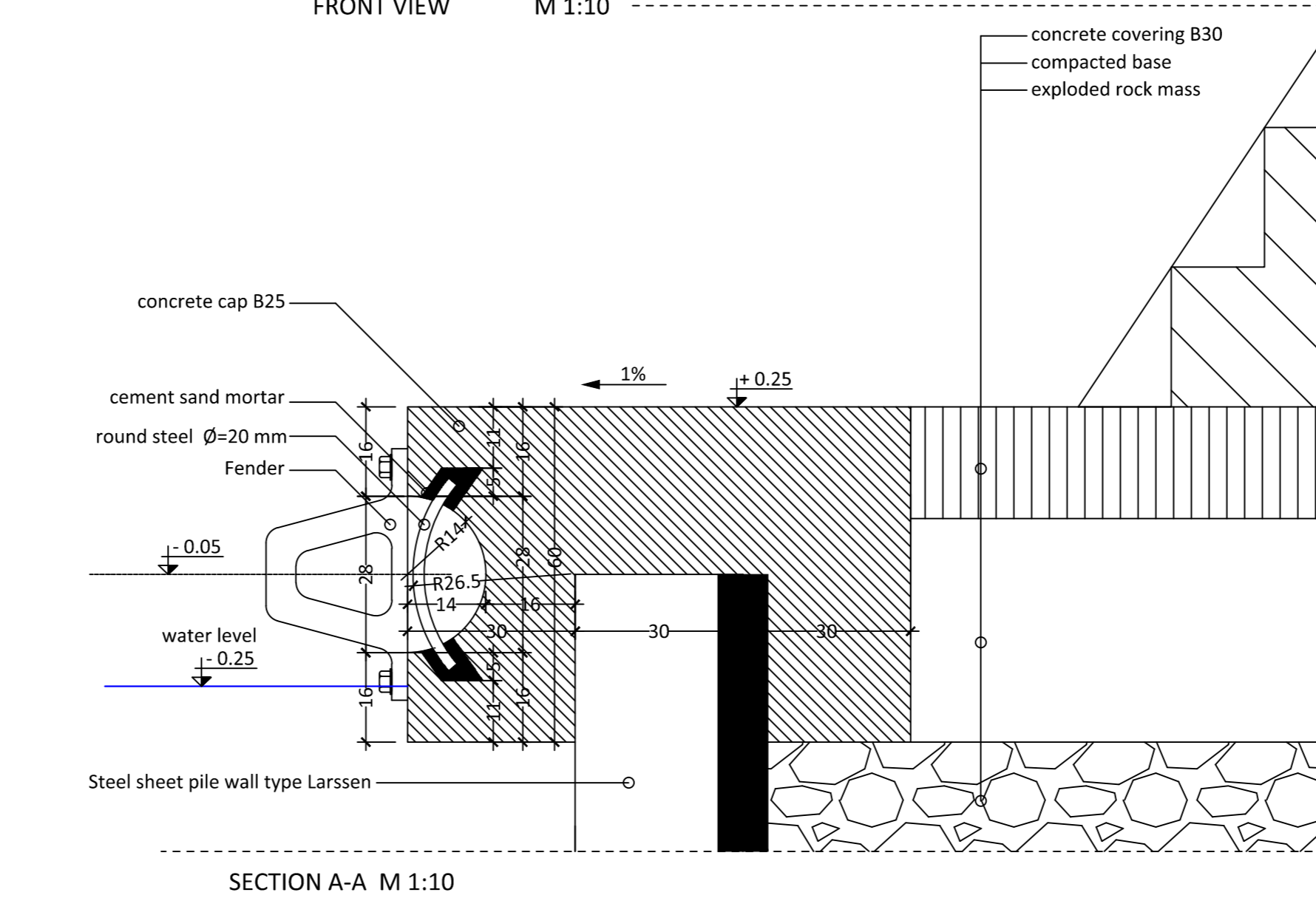
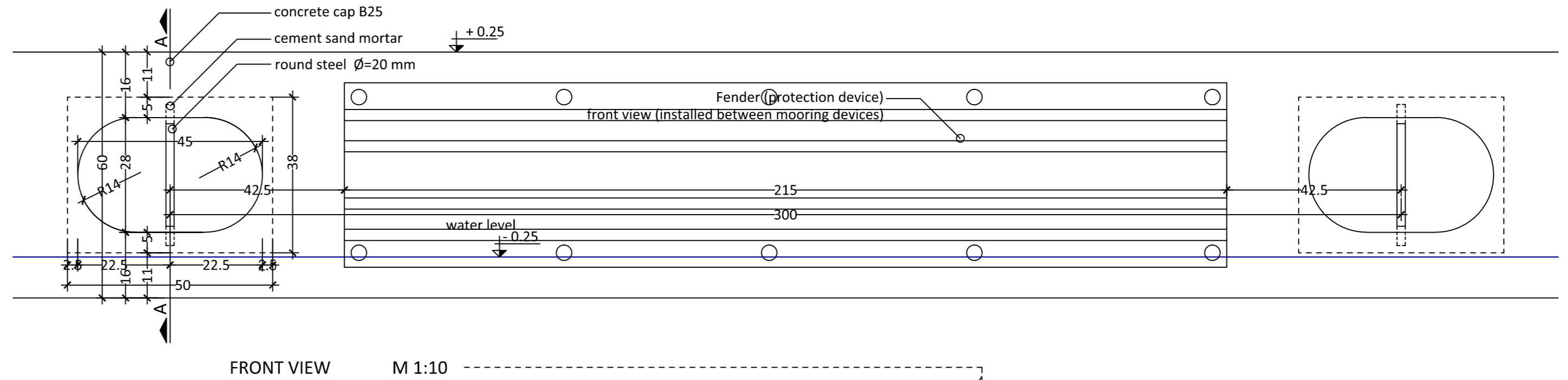



University for Architecture, Civil Engineering and Geodesy - Sofia Vienna University of Technology			
Chair	Hydraulic Engineering		
Project	Reconstruction and modernization of Fishing Harbor "Sarafovo"		
Drawing	7-2	Precast turning wall section - Formwork plan, Reinforcement plan	M 1:50
Graduate	Stefina Dimitrova	Nr. 0927914	Nr. 689
Supervisors	Prof. J. FENTON Ao.Univ.Prof. Dipl.-Ing. Dr.techn. N. KROUZECKY Assoc. Prof. Dr. Eng. I. IGNATOV		

DETAIL 1: BOLLARD



DETAIL 2: FENDER



 University for Architecture, Civil Engineering and Geodesy - Sofia Vienna University of Technology			
Chair	Hydraulic Engineering		
Project	Reconstruction and modernization of Fishing Harbor Sarafovo		
Drawing	7	Bollard, Fender - Detailed drawings	M 1:10
Graduate	Stefina Dimitrova	Nr. 0927914	Nr. 689
Supervisors	Prof. J. FENTON Ao.Univ.Prof. Dipl.-Ing. Dr.techn. N. KROUZECKY Assoc. Prof. Dr. Eng. I. IGNATOV		